UNCLASSIFIED

AD NUMBER

ADB238349

NEW LIMITATION CHANGE

TO

Approved for public release, distribution unlimited

FROM

Distribution authorized to U.S. Gov't. agencies only; Proprietary Info.; Jul 98. Other requests shall be referred to U.S. Army Medical Research and Materiel Comd., Fort Detrick, MD 21702-5012.

AUTHORITY

19990406 - Ms Phylis M. Rhinehart, DCS/Info Mgmt, MCMR-RMI-S [70-1y], Mar 24, 1999.

THIS PAGE IS UNCLASSIFIED

AD_____

CONTRACT NUMBER DAMD17-96-C-6074

TITLE: Perform Initial Measurements to Investigate Microwave Detection for Location of Hemorrhage Sites Within the Body

PRINCIPAL INVESTIGATOR: Ronald G. Riechers, Ph.D.

CONTRACTING ORGANIZATION: Spectra Research, Incorporated
Kettering, Ohio 45420-1173

REPORT DATE: August 1998

TYPE OF REPORT: Final

PREPARED FOR: U.S. Army Medical Research and Materiel Command
Fort Detrick, Maryland 21702-5012

DISTRIBUTION STATEMENT: Distribution authorized to U.S. Government agencies only (proprietary information, Jul 98). Other requests for this document shall be referred to U.S. Army Medical Research and Materiel Command, 504 Scott Street, Fort Detrick, Maryland 21702-5012.

The views, opinions and/or findings contained in this report are those of the author(s) and should not be construed as an official Department of the Army position, policy or decision unless so designated by other documentation.

REPORT DOCUMENTATION PAGE

Form Approved
OMB No. 0704-0188

Public reporting burden for this collection of information is estimated to average 1 hour per response, including the time for reviewing instructions, searching existing data sources, gathering and maintaining the data needed, and completing and reviewing the collection of information. Send comments regarding this burden estimate or any other aspect of this collection of information, including suggestions for reducing this burden, to Washington Headquarters Services, Directorate for Information Operations and Reports, 1215 Jefferson Davis Highway, Suite 1204, Arlington, VA 22202-4302, and to the Office of Management and Budget, Paperwork Reduction Project (0704-0188), Washington, DC 20503.

1. AGENCY USE ONLY *(Leave blank)*	2. REPORT DATE	3. REPORT TYPE AND DATES COVERED
	August 1998	Final (1Jun 96 - 1 Jul 98)

4. TITLE AND SUBTITLE
Perform Initial Measurements to Investigate Microwave Detection for Location of Hemorrhage Sites Within the Body

5. FUNDING NUMBERS
DAMD17-96-C-6074

6. AUTHOR(S)
Riechers, Ronald, G., Ph.D.

7. PERFORMING ORGANIZATION NAME(S) AND ADDRESS(ES)
Spectra Research, Incorporated
Kettering, Ohio 45420-1173

8. PERFORMING ORGANIZATION REPORT NUMBER

9. SPONSORING / MONITORING AGENCY NAME(S) AND ADDRESS(ES)
U.S. Army Medical Research and Materiel Command
Fort Detrick, Maryland 21702-5012

10. SPONSORING / MONITORING AGENCY REPORT NUMBER

11. SUPPLEMENTARY NOTES

12a. DISTRIBUTION / AVAILABILITY STATEMENT
Distribution authorized to U.S. Government agencies only (proprietary information, Jul 98). Other requests for this document shall be referred to U.S. Army Medical Research and Materiel Command, 504 Scott Street, Fort Detrick, Maryland 21702-5012

12b. DISTRIBUTION CODE

13. ABSTRACT *(Maximum 200 words)*

A novel method for location and characterization of discontinuities in biological systems is described. The method uses electromagnetic waves in the RF and microwave region of the spectrum, and a modified signal processing algorithm, previously used for estimation of the angle of arrival of radar signals. Results are presented for the case of a porcine skull section, backed by a porcine brain, and the skull backed by porcine blood and brain.

DTIC QUALITY INSPECTED 1

14. SUBJECT TERMS	15. NUMBER OF PAGES
dielectrics, permituity, hemorrhage, subdermal, epidermal, hematoma, microwave, RF, signature	85
	16. PRICE CODE

17. SECURITY CLASSIFICATION OF REPORT	18. SECURITY CLASSIFICATION OF THIS PAGE	19. SECURITY CLASSIFICATION OF ABSTRACT	20. LIMITATION OF ABSTRACT
Unclassified	Unclassified	Unclassified	Limited

FOREWORD

Opinions, interpretations, conclusions and recommendations are those of the author and are not necessarily endorsed by the U.S. Army.

____ Where copyrighted material is quoted, permission has been obtained to use such material.

____ Where material from documents designated for limited distribution is quoted, permission has been obtained to use the material.

____ Citations of commercial organizations and trade names in this report do not constitute an official Department of Army endorsement or approval of the products or services of these organizations.

__✓__ In conducting research using animals, the investigator(s) adhered to the "Guide for the Care and Use of Laboratory Animals," prepared by the Committee on Care and Use of Laboratory Animals of the Institute of Laboratory Resources, National Research Council (NIH Publication No. 86-23, Revised 1985).

____ For the protection of human subjects, the investigator(s) adhered to policies of applicable Federal Law 45 CFR 46.

____ In conducting research utilizing recombinant DNA technology, the investigator(s) adhered to current guidelines promulgated by the National Institutes of Health.

____ In the conduct of research utilizing recombinant DNA, the investigator(s) adhered to the NIH Guidelines for Research Involving Recombinant DNA Molecules.

____ In the conduct of research involving hazardous organisms, the investigator(s) adhered to the CDC-NIH Guide for Biosafety in Microbiological and Biomedical Laboratories.

Ronald G Rieckhoff July 21, 1998

PI - Signature Date

Table of Contents

LIST OF FIGURES

LIST OF TABLES

1.0 INTRODUCTION

This document reports on research conducted by Spectra Research, Inc. on the ability of electromagnetic waves in the RF and microwave region to detect regions of blood pooling in the body. The purpose is to demonstrate the feasibility of using such interrogating energy in a portable unit for battlefield use. The research included a phantom measurement effort and limited tissue measurements. This research had its origin in a USAF STTR program to apply electromagnetic techniques to the early detection of breast tumors. The following paragraphs describe the problem and the solution proposed Spectra Research, Inc.

1.1 The Problem

A major problem facing medical personnel in military and civilian emergency situations is the need to examine victims quickly, determine the patient's vital signs, diagnose and decide on the treatment alternatives. An important part of the process is location of internal bleeding. Traditional medical imaging systems such as X-ray CT, MRI and ultrasound are not practical as the size and weight of such systems precludes their use on the battlefield or at accident sites. Extensive processing of the measured data reduces the timeliness of the diagnosis, and places the patient out of the sight of the physician for extended periods of time. Hence a system that avoids some or all of these problems is needed.

This report describes the results of initial study pursued under a BAA with the US Army Medical Research and Materiel Command, Combat Casualty Care Research Branch. Initial measurements conducted to verify the applicability of microwaves for locating internal bleeding sites via detection of discontinuities in permittivity in a medium. The technique was originally developed during a USAF funded STTR for early detection of breast cancers using non-ionizing radiation.

Early studies analytically demonstrated the capability of detecting permittivity differences with a contrast ratio of nearly one. Hemorrhage detection is somewhat easier since the presence of hemoglobin in the blood substantially changes the dielectric properties of the target region. Also, since substantially larger volumes are to be detected (up to 50 cc of blood), the problem is less difficult. The situation of concern is shown in Figure 1.

Illustrated is a subdural hematoma of sufficient size so as to compress the brain and cause significant mid-line shift. The injury causing the bleed has not fractured the skull so until the victim presents symptoms that indicate the presence of the hematoma, the physician is uncertain as to the diagnosis. Patients in a trauma center can be examined by CT or MRI and steps taken to alleviate the condition. However, if the patient is not in such a facility, then no diagnostic imaging tool will be available. Such is the case in most situations in which the "first responder," such as the medic on the battlefield must perform triage and evacuate the most serious cases first. A portable diagnostic tool that would identify such bleeds would reduce the number of incorrectly diagnosed casualties and provide for more efficient evacuation.

19980918 033

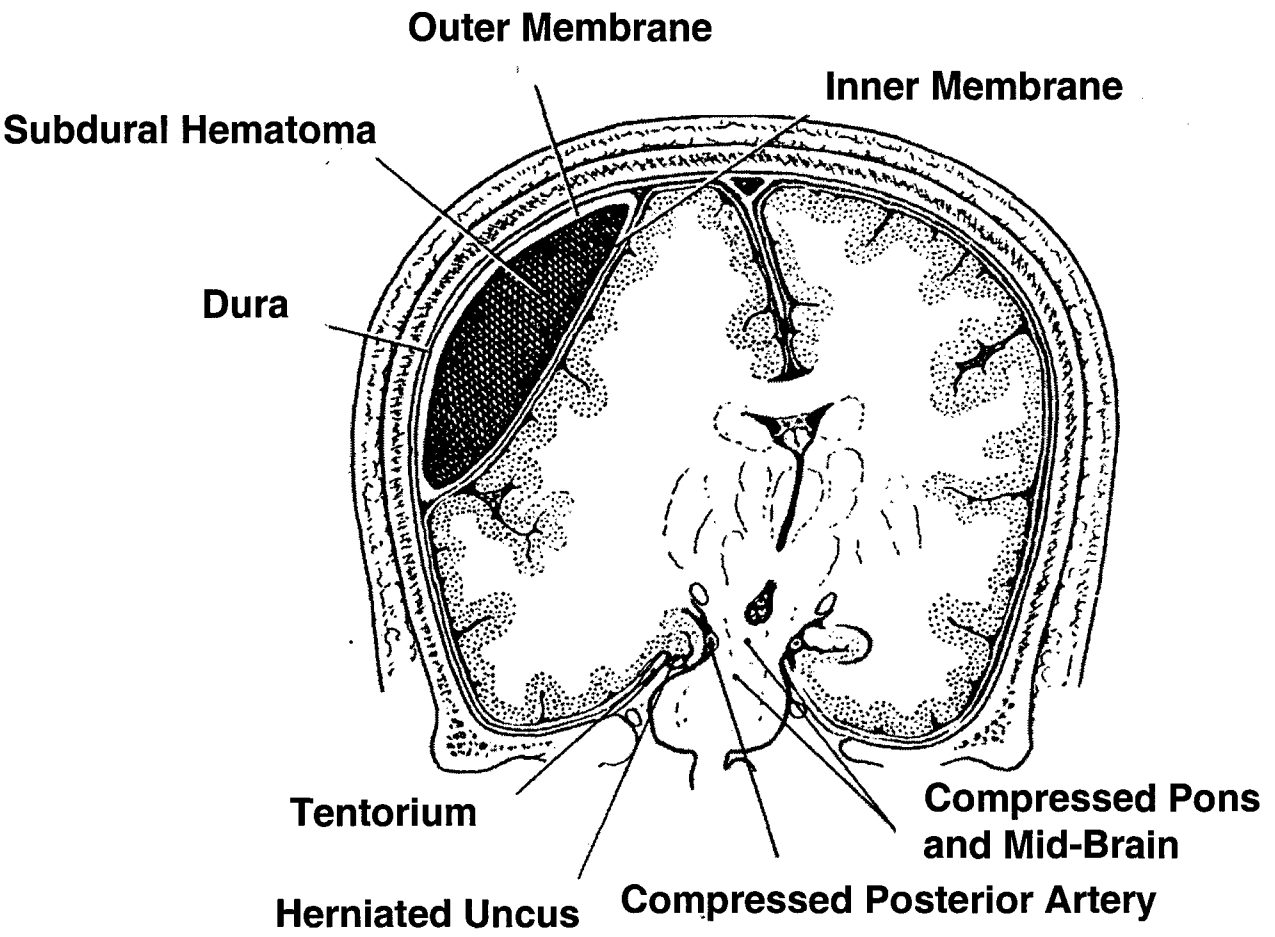

Figure 1. The Problem

1.2 The Solution

Spectra Research conducted the initial research to provide a system to detect, locate and determine the volume of blood in a hematoma. Figure 2 illustrates a concept for the final system, it should be noted that this system does not exist, but represents a concept only. The initial research was directed at demonstrating the ability of electromagnetic waves to perform diagnostic, functional imaging.

An HDS will consist of the following subsystems, 1) an antenna/applicator to launch energy into the examination volume, 2) an RF generation unit to produce the necessary wideband electromagnetic energy, 3) a signal processing unit to perform the computations required to diagnose, and 4) a display unit to present the results to the physician.

The theory of operation of the system will be presented in the following chapter. This will include the electromagnetics and the signal processing used in detecting blood in the body.

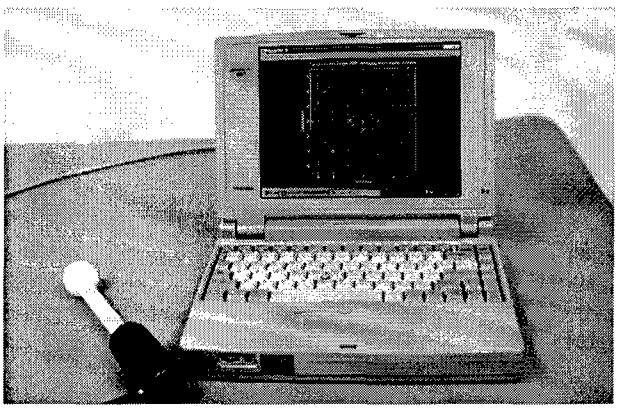

Figure 2. Conceptual Design for a Hemorrhage Detection System (HDS).

2.0 MEDICAL ISSUES

Intracranial hemorrhage can present itself in many different contexts, from the 85 year old woman on anticoagulation to the infant shaken brutally by a frustrated parent, in both cases, the injury may be the same (subdural hematoma) but the clinical presentation and the management strategies distinctly different. Injuries such as epidural hematomas can kill an individual without warning to caregivers. Trauma, however is not the only etiology for intracranial bleeds. Individuals with high blood pressure, atherosclerotic disease, atrial fibrillation, and a myriad other medical conditions are at risk for having a stroke. Whether the hemorrhage occurs during the natural progression of the infarct or iatrogenically following interventional radiology (tPA) hemorrhage following infarction increases the morbidity and mortality of the initial insult.

The care of patients who possibly have suffered an intracranial bleed involves many members of the medical community, including paramedics on site, emergency room physicians, neurologists, radiologists, and neurosurgeons. All individuals presently rely upon techniques that are time consuming and sometimes suspect. The clinical evaluation is user dependent and often of limited value, the radiologic techniques are often conclusive but require time that could be crucial to the patient's survival. The concept of a hand held imaging unit to detect hemorrhage is attractive due to its many advantages. It could be used in many settings, by many different health care professionals, and could provide advance warning in trauma cases or provide a monitoring option cheaper and less involved than CT or MRI. HDS provides this option. To truly understand the value of HDS we must look at what it could be used for, how these injuries occur, how frequently they occur, what else is out there, and where HDS fits into the process.

2.1 ANATOMY

Before we discuss the different types of intracranial bleeds, we must first take a brief look at the normal anatomy of the cranium. Covering the cranium is the scalp, which is made up of five layers of tissue. The most superficial is the skin, directly below it is the subcutaneous fascia, and deep to this, the galea aponeurosis. These three layers function essentially as a unit and thus are sewed together as such. The vascular supply to the scalp runs deep in the aponeurosis. Frequently these upper three layers provide the only obvious signs of head trauma through

lacerations, swelling, and/or bruising. Below this is the loose areolar connective tissue which acts as a cushion between the scalp and the tightly adherent fibrous pericranium. The loose connective tissue can provide a conduit for infection to spread within the scalp. Directly internal to the scalp is the skull, the bulk of which is made up of seven bones. These include the frontal bone, left and right parietal bones, left and right temporal bones, and the occipital bone. These fit together like a jigsaw puzzle attached at suture lines. These suture lines provide strong points of attachment for the next deeper layer, the dura.

The dura is tough fibrous tissue that not only lines the skull, but also forms venous sinuses that drain the blood from the brain. Between the dura and the skull runs the meningeal arteries, these arteries supply the meninges and as one might expect based on their position, are susceptible to injury following trauma to the skull. Under the dura is the arachnoid mater. The arachnoid is a thinner membrane that serves many anatomic functions, it contains the cerebrospinal fluid that bathes the brain and also covers the veins and arteries that supply the brain itself. Connecting the dura to the arachnoid are bridging veins that traverse the subdural space and drain into the dural venous sinuses. Below the arachnoid and directly adherent to the brain parenchyma is the pia mater. The pia is grossly indistinguishable from the brain tissue. The pia, arachnoid, and dura all make up the meninges of the brain. Below these meninges is the brain, which fills the majority of the cranial vault. The following is a simple cross sectional representation of the layers within the cranium.

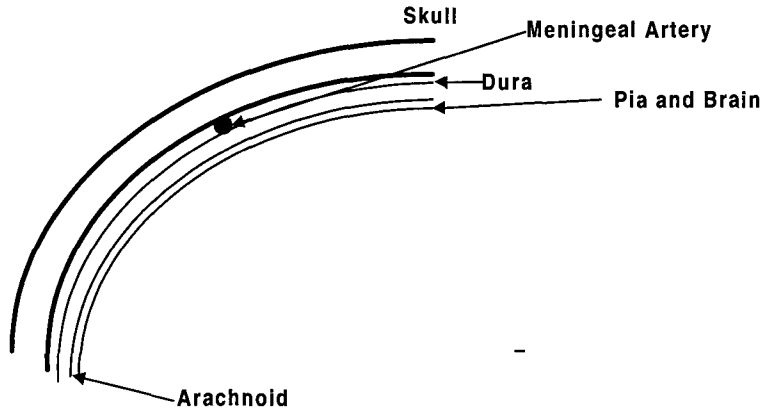

Figure 3. Cranial Anatomy

In addition to understanding the anatomy of the skull, it is essential that one understands the vascular anatomy of the brain when discussing intracranial hemorrhages. The blood supply to the head originates from two sources the vertebral arteries and the carotid arteries. The carotid arteries split into the internal and external carotid arteries, with the external carotids supplying the face, neck, and scalp, and the internal carotids supplying the eye, brain, and part of the scalp. The vertebral arteries combine along the brainstem to form the basilar artery. At the base of the brain, these arteries form a circle, the circle of Willis that gives off the major arteries which supply the regions of the brain. This circle is essential to maintain normal blood flow especially when one of the contributors is narrowed by atherosclerosis, however, its proximity to brain matter and being enclosed within the subarachnoid space allows ample area for collection of

blood following hemorrhage from aneurysm, vasculitis, trauma, etc. These vessels are important also because they are some of the only pain sensitive structures within the cranium. As far as nervous tissue, it is paradoxical that the center of the nervous system lacks any sensory endings itself and therefore does not experience pain. The following is a graphical representation of the Circle of Willis:

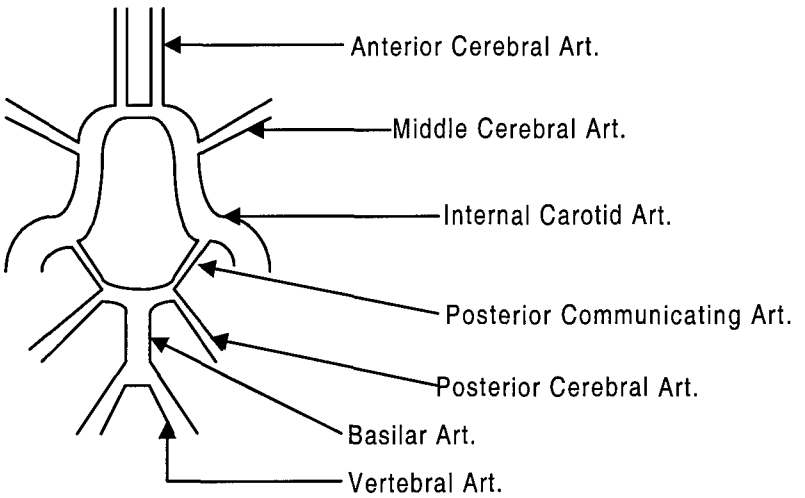

Figure 4. The Circle of Willis

2.2 PATHOLOGY

With a basic understanding of the cranial anatomy, we can now move on to discuss the pathological findings of certain types of intracranial hemorrhages. In general, hemorrhage can either occur from veins, arteries, or venous sinuses, all of which have different aspects. In general, arterial bleeds tend to develop quicker and release more blood due to the pressure within these vessels. Venous sources, on the other hand, tend to develop over a longer period of time and have less blood because they are low flow channels. The first we will discuss is the epidural hematoma. It is the most external of the hemorrhages. In an epidural hematoma, the blood collects within the space between the dura and the calvarium.

Epidural hematomas are almost exclusively related to trauma, most commonly skull fractures. In fact, there is a 75 to 90 percent association between skull fractures and epidural hematomas (Rengachary 1547). The bleeding is most commonly linked to a laceration of the middle meningeal artery, but can also be due to tearing of the dural venous sinuses. Hemorrhage from arterial source, as one might expect, can develop quickly and increase the pressure significantly. The size of these injuries is dependent on a number of factors including: size of artery involved, tightness of the adherence between the dura and the skull, and depth of artery in the skull (Rengachary 1547). The spread of these injuries along the skull, however is typically limited by the sutures of the calvarium. Frequently, epidural hematomas occur in the temporal region of the head but they can also occur in the posterior fossa near the cerebellum. Usually, these hematomas will assume a lens shaped appearance because of the immobility of the skull and the dense fibrous nature of the dura. The blood within these hematomas is normally clotted.

As one would imagine, the presence of an expanding hematoma within the cranium will tend to increase intracranial pressure significantly leading to herniation of areas of the brain and occlusion of arteries supplying certain parts of the brain. Herniation refers to the process by which increased intracranial pressure leads to the shift of more pliable brain tissue through the foramen magnum. This brain tissue will compress the brain stem leading to a number of clinical signs and symptoms such as visual deficits, loss of consciousness, paralysis and loss of sensation. This is a common theme when discussing intracranial hemorrhages because of the accumulation of blood within a closed system. Due to this rapid accumulation of blood, the hematoma tends to develop within six hours.

Clinically, patients with epidural hematomas typically have a "lucid interval", i.e. a period of time following their initial injury during which they have no symptoms or signs of brain injury but they quickly lose consciousness and often die. This interval is an essential period during which the physician must act because it can mean the difference between life and death for the patient. In addition to the epidural hematoma, these patients frequently have other injuries to the brain including other types of hemorrhage, cerebral contusions, and diffuse axonal injury. The mortality of epidural hematomas quoted by one study was 10-12 percent (Hacke 705). In another study, 24 percent of those with epidural hematomas died, were in a vegetative state, or were severely disabled. Also, the mortality rates show some relation to age, younger patients (0-5) tend to have better prognosis, whereas patients over 40 have distinctly higher mortality. The following is a graphical representation of an epidural hematoma:

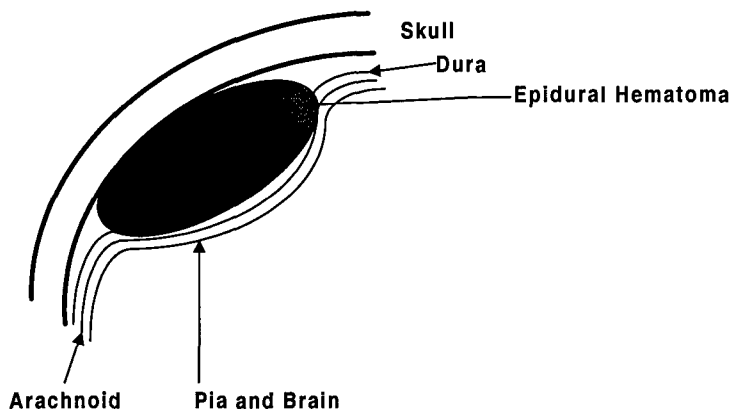

Figure 5. The Epidural Hematoma.

The next type of hemorrhage to be investigated is the subdural hematoma. The subdural hematoma develops in the potential space between the dura mater and the arachnoid membrane. These injuries have been separated into 3 types based on time course: acute, subacute, and chronic. Acute subdural hematomas develop within 48-72 hours of the initial insult and are closely related to traumatic head injuries. These are often from a high velocity impact. This impact can lead to tearing of the bridging veins that connect to the venous sinuses, direct injury to the cortex and the vessels that supply it, or both. As a consequence of their close relation to

impact injuries, other intracranial injuries are present. Also, there is a close association with skull fractures.

The most frequent region in which these develop is the frontotemporal region close to the Sylvian fissure. This location is due to the "dashboard" injury from the brain slamming against the sphenoid wing of the skull base. Subdural hematomas appear crescent shaped on both gross examination and on CT because they are not limited by the arachnoid. Interestingly, subdural hematomas cannot cross the midline but are frequently bilateral in distribution. The blood within these lesions, unlike epidural hematomas, is partially clotted and partially liquid.

The clinical presentation of subdural hematomas is varied and depends upon the size and because they tend to enlarge, the number of deficits will increase with time. Primarily these deficits are altered level of consciousness, pupillary changes, and motor losses. The mortality of these lesions is significantly higher than epidural hematomas with most studies showing a mortality of greater than 50 percent (Rengachary 1658). Similar to epidural hematomas, age does play a role in mortality of these injuries with older individuals showing a higher mortality. Subacute and chronic subdural hematomas are not very different from acute subdurals pathologically, however their differences are in time course, clinical appearance, and individuals at risk. Subacute lesions tend to appear 3 days to 3 weeks following the injury whereas chronic lesions appear from three weeks to several months following the initial injury. These lesions do not share the close association with major trauma as the previous hematomas do and when associated, the trauma is often mild and has since been forgotten by the patient.

Clinically, the subacute label is a very tenous one because subacute subdurals during the first week have signs and symptoms similar to an acute subdural while those presenting more than a week after the injury are more like chronic subdurals. The aforementioned signs and symptoms are frequently diffuse and include altered consciousness and motor deficits. Chronic subdural hematomas are notably more frequent in the elderly, chronic alcoholics, epileptics, and those with coagulation defects. In light of the fact that the symptoms are so diffuse, often including mental status changes, and the elderly are often afflicted, chronic subdural hematomas have been mistaken for dementia. As a result of the slow development of these lesions and the lack of other significant intracranial lesions, the mortality of chronic subdural hematomas is only 10 percent with 75 percent regaining normal function after treatment (Rengachary 1660). The following is a graphical representation of a subdural hematoma.

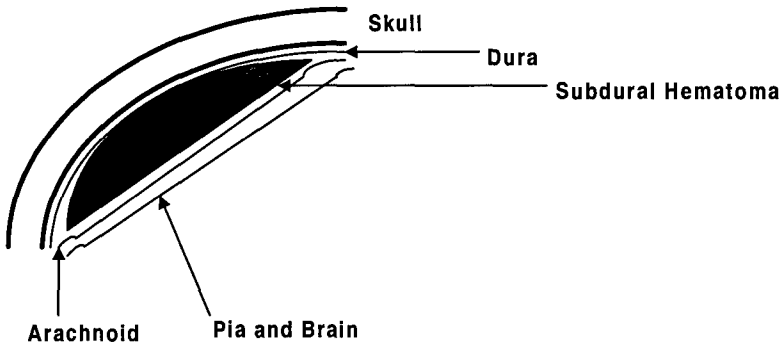

Figure 6. The Subdural Hematoma.

This clearly illustrates one part of the problem, the ability to detect the presence or absence of the dielectric interface at the skull. If the contrast differs between the skull-blood interface and the skull brain interface, then a binary decision can be made.

The remaining part of the problem is the determination of the shape and the volume of the hematoma. This process is critical to the determination of the complete diagnosis, and monitoring the volumetric increase may give the physician a better idea of the progress of the condition and the need for some action and the time lines for this response.

3.0 SYSTEM THEORY

Our initial research, as previously stated, was directed toward resolving the electromagnetic issues of the problem. Once satisfied that the electromagnetics were correct, advanced signal processing techniques were applied to provide the detection and location mechanism. Our proposed research will focus on the development of a measurement system to perform the priority task, the detection and location of a dielectric region having permittivity ε_{blood} embedded in an ambient region of permittivity $\varepsilon_{ambient}$ with minimal error and/or false alarms. The remainder of this section will discuss the remaining electromagnetic issues and signal processing aspects of the problem.

3.1 Electromagnetics of the Problem

The physics and geometry of the problem are shown in Figure 3. Dielectrics present in this case are the skin, bone, and dura that enclose the brain. The parameter of interest in the detection system is the permittivity of the materials in the structure. The anatomy of the region may be well known but the dielectric properties of the materials that compose the region are **not** necessarily known, especially as functions of frequency. This fact becomes a critical issue in the design of the system. If one has available, the necessary information on the permittivity, then a system could be optimally designed to illuminate a region of interest and receive the scattered signals from the various interfaces in the region.

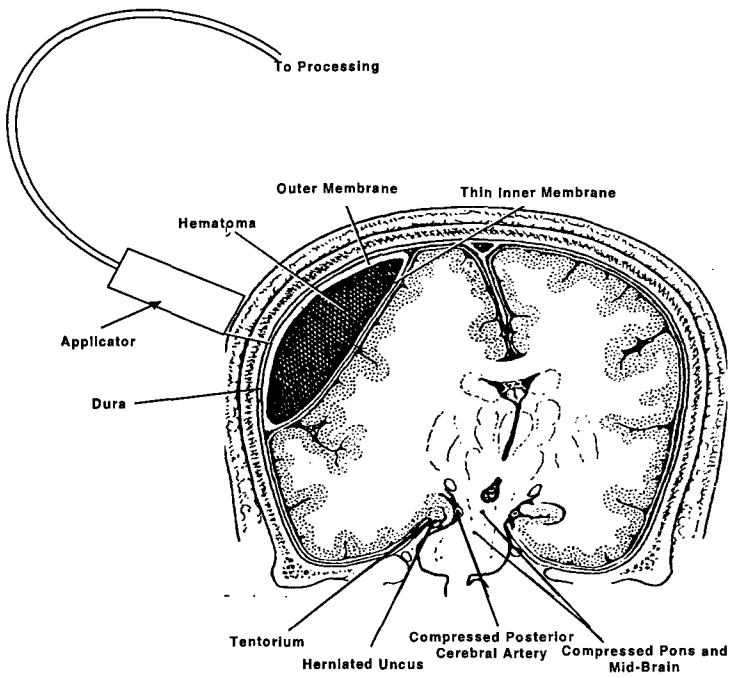

Figure 7. Electromagnetics of the Hemorrhage Detection/Location Problem

The physical basis of the detection /location system is the scattering of electromagnetic waves by any objects located in the path of the wave. Electromagnetic scattering is a result of the fields satisfying the boundary conditions on the surface of the object. Similar boundary conditions on the fields are imposed at the interface between two dielectric media. Boundary conditions are defined for the fields as before, but the conditions are less restrictive since none of the fields are zero on the interface. Thus fields exist on both sides of the interface, an incident field, a reflected field, and a transmitted field. The boundary conditions on the electric and magnetic fields at the interface will determine the field behavior in all regions.

3.2 Tissue Permittivity Characteristics

The permittivity of various tissue types has been measured and reported in the literature, in particular, the permittivity of common biological materials was measured from HF (27 MHz) through X-band (10 GHz) and presented by Johnson and Guy[i]. Measurements have also been made for specific tissue types, at specific frequencies[ii] and presented. A detailed discussion of the physical causes for dielectric properties of biological materials was published by Pethig.[iii] Land and Campbell[iv] presented data for dielectric properties of malignant versus non-malignant tissues at several frequencies, they have also discussed a measurement method for determining the electrical properties at microwave frequencies[v]. An Indian research group has investigated breast

tissue, both malignant and non-malignant and presented measured data[vi]. There is limited data available on the permittivity and conductivity of many biological tissues, blood included. Pethig states that at 37° C and illuminated at a frequency of 2450 MHz, the electrical constitutive parameters of blood and brain tissue are as shown in Table 1.

Table 1. Dielectric Properties of Brain and Blood at 2450 MHz.

Parameter	Brain (Gray Matter)	Blood
Permittivity	43	60
Conductivity	1.43	2.04

Recently, the interest in the possible risks associated with long term exposure to cellular telephone emissions has sparked renewed interest in the measurement of the dielectric properties of biological materials. Table 2 presents data published by Gandhi et. al[vii].

Table 2. Dielectric Constant for Various Tissue Types in the Human Body.

Tissue Type	Dielectric Constant ε_r	Conductivity σ (S/m)
Air	1.0	0.0
Muscle	40.0	4.9
Fat	6.0	0.3
Bone	6.0	0.3
Cartilage	6.0	0.3
Brain	30.0	5.3
Blood	51.0	5.8
Eye	30.0	3.8
CSF	72.0	6.7
Vitreous Humor	63.0	7.2
Sclera/cornea	36.0	4.7
Lens	30.0	3.8
Ear	23.0	2.6

It will be noted that the values presented differ slightly, this is due to the fact that this data is gathered at selected frequencies, usually a frequency of concern and not over a wide frequency band. This also illustrates the critical aspect of this technique, *the variation of the dielectric properties of a particular material with frequency*. It is this property that is exploited in the HDS.

It was noted earlier that the fundamental principle of operation involves the detection of the brain-blood interface. The most convenient way to discuss this idea is by defining a quantity that will quantify the discontinuity between two materials and characterize the interface. A logical choice is to form a ratio between the permittivities of the materials. Let the *contrast ratio* ρ, be defined as,

$$\rho = \varepsilon_{blood} / \varepsilon_{brain},$$

where the larger permittivity is placed in the numerator to ensure that ρ is greater than one.

Contrast, as we have defined it, is a measure of the level of reflected signal one can expect from a dielectric discontinuity. Contrast ratio values that are much greater than one indicate the presence of interfaces that will give rise to large reflected signals that will be easily detected. Contrast values in the range, $1 \leq \rho \leq 2$ will also produce a backscattered signal, but the reflected signal magnitude will be smaller, negatively impacting the system signal to noise ratio (SNR).

3.2.1 Electromagnetic Signature

Backscattered signal is a measure of the reflecting properties of the object and is expressed through the reflection coefficient of the material, Γ. This is a complex quantity, in the mathematical sense, that can be related to the constitutive properties of the scatterer, ε and μ. Γ is directly related to the scattering parameter, S_{11}. Thus, by making a measurement of the reflection coefficient or scattering parameters, one can find indirectly the electromagnetic properties of the scatterer. If data are taken over a wide range of frequencies, then ε and μ are also known over the same frequency range and this behavior can be catalogued.

Scattering is dominated by two properties, 1) the geometry or "characteristic dimension" of the target, and 2) the target composition, defined by its constitutive parameters. The behavior becoming one in which over a wide frequency band, the signature has a resonant behavior, with peaks at well-defined frequencies corresponding to characteristic dimensions on the target. Targets such as blood pools are many times not very well defined geometrical shapes, but have a relatively well defined composition.

Since the dielectric constant of most materials is frequency dependent, one must carefully choose the operating frequency to optimize the detection performance. Previous research has indicated that contrast values as small as $\rho = 1.05$ can be detected using signal processing algorithms. The contrast ratio of the brain-blood discontinuity at a frequency of 2450 MHz is approximately 1.4, so one can expect to achieve good detection performance by interrogating at this frequency.

3.3 Signal Processing Technique

A signal processing technique applicable to hemorrhage detection has been demonstrated that permits the user to detect, classify and identify hemorrhage sites. Our research has demonstrated experimentally and analytically the application of 1) Electromagnetic waves and 2) An existing signal processing technique, modified to improve performance of blood pool detection. This has led to the definition of a wide band electromagnetic signature for biological targets. This signal processing technique, a variation of the *Multiple Signal Classification Algorithm* ***(MUSIC)*** produces signatures that can be used to uniquely characterize biological targets, and such signatures have been measured in the laboratory. The following paragraphs describe the signal processing theory.

3.3.1 Auto-correlation Processing

Use of the Wold decomposition[viii] provides a means of applying methods from random process theory to analyze the performance of systems. Wold proved that any signal can be written in the following form:

$$s = r + \eta,$$

where r is the known signal and η is a Gaussian noise. Angle of Arrival (AOA) estimations are of this kind, except that the known signal has a very specific form. AOA estimation is concerned with two aspects of the problem, 1) Spatial location of the signal source, and 2) Signal identification. Since the sources of signals impinging on an aircraft are from radar, communications and electronic warfare systems, and such systems operate using known frequencies and modulations, the only remaining problem is spatial location, since the other signal properties can be determined by channelizing the receiver, and signal processing. Spatial location can be accomplished using an array of receivers with known properties, located in a known pattern. Another method for accomplishing the same result that offers a possible new electromagnetic imaging technique is to use a single antenna to transmit and receive, and operate the system over a wide band of frequencies. This obviously is not possible in the AOA problem, but for problems that involve the detection, location and identification of passive targets, this is an opportunity to accomplish a task that has significant importance.

A hemorrhage detection system (HDS) should be designed to operate over a relatively wide band of frequencies, stepping in frequency at some frequency step suitable for achieving the desired system performance. The choice of frequency band will be dictated by the physics of the problem, the attenuation properties of the material. For the hemorrhage detection problem, the frequency band will be centered at a frequency that optimizes the desired response with minimal degradation as the band edges are approached from above or below. As an example, for hemorrhage detection, one would likely choose a frequency in the 0.5 - 2 GHz range to obtain the best possible tissue penetration. Using a high frequency such as X-band would be suitable for surface detection, but would have limited brain penetration.

3.3.2 Auto-correlation Matrix for Stepped Frequency Signals

Thus the transformed auto-correlation contains information on which frequencies one would expect to have the greatest concentration of the signal power. This is of particular interest if one is measuring the reflected signals from scatterers. How one can use such information is directly dependent upon the excitation used. Suppose we have a situation where we have M scatterers and illuminate this constellation of scatterers using a source with a signal that is of the form:

$$s(\omega) = e^{j\left(\frac{\omega}{c}\right)x}.$$

Let the radian frequency be $2\pi f$, and the resulting signal is:

$$s(\omega) = e^{j\left(\frac{2\pi f}{c}\right)x} = e^{j2\pi f\left(\frac{x}{c}\right)} = e^{2\pi ft}.$$

Letting the frequency become discrete leads to a set of frequencies that are used to interrogate the region, $\{f_1, f_2, \ldots, f_M\}$.

Each frequency is permitted to exist for a finite duration during which the target region is illuminated. The signal repeats every T seconds, and is of τ seconds in duration. This can be thought of as a set of individual signals, each a CW signal having time harmonic dependence. These signals are used to illuminate the terrain and the return is received and processed.

The reflected signal from the l^{th} scatterer is given by:

$$s_l(\omega) = \Gamma_l e^{j\left(\frac{\omega}{c}\right)x_l} = \Gamma_l e^{j2\pi ft_l},$$

Where f, is the cyclic frequency, and t_l is the two-way travel time from the source to the l^{th} scatterer and back, and Γ_l is the reflection coefficient for the l^{th} scatterer. The total signal is the vector sum of the M reflected signals from the scatterers in the illuminated region. This is just,

$$s_T(\omega) = \sum_{l=1}^{M} s_l(\omega) = \sum_{l=1}^{M} \Gamma_l e^{j2\pi ft_l}$$

We know that there will be additive noise present in the system and this will be frequency dependent also. This will modify the form above to,

$$s_T(f) = \sum_{l=1}^{M} \Gamma_l e^{j2\pi ft_l} + \eta(f)$$

This then is the signal with which the system will have to work. Since the signal is composed of desired and undesired components, we need to have some method of separating these out. A single frequency measurement cannot determine the desired information, more data must be obtained. A spatial measurement uses all of the antennas in the array to increase the information content in the measurement. The extension to the frequency domain case will require that one take data over N frequencies, and then perform some operation on this data to determine scatterer location. The resulting data will be of the form:

$$s_T(f_m) = \sum_{l=1}^{M} \Gamma_l e^{j2\pi f_m t_l} + \eta(f_m)$$

This equation is true for $m = 1,2,3\ldots,N$, and leads to the following set of equations:

$$s_T(f_1) = \sum_{l=1}^{M} \Gamma_l e^{2\pi j f_1 t_l} + \eta(f_1)$$
$$s_T(f_2) = \sum_{l=1}^{M} \Gamma_l e^{2\pi j f_2 t_l} + \eta(f_2)$$
$$\vdots$$
$$s_T(f_N) = \sum_{l=1}^{M} \Gamma_l e^{2\pi j f_N t_l} + \eta(f_N)$$

This is a set of N equations in M unknowns, and the ability to obtain the solution will depend on the relationship between N and M. The system can be written in a matrix form by noting that the left hand side of the equation is a column vector and that the right hand side is the sum of a vector-matrix product (a column vector) and another column vector. This is conveniently written as:

$$\bar{s}_T = \bar{\bar{P}}\bar{\Gamma} + \bar{\eta},$$

where matrix notation has been used to compress the space on the page. How the data is processed is the next question that must be answered. Since we are receiving the signals from a number of discrete sources, we would like some means of "separating" the various contributions. One method of accomplishing this is to investigate the auto-correlation of the backscattered signal. The resulting matrix will have an eigen-structure that will permit the desired information to be obtained. The next section will discuss the method used to accomplish this, the MUSIC algorithm.

3.4 MUSIC Algorithm

The original development of this algorithm was based on the early work of Pisarenko[ix], and extended by Schmidt[xxi] in the early 1980's. Schmidt's work was directed to the angle of arrival estimation problem and used the spatial array method. We propose to use multiple frequencies and measure the reflected signal.

Let there be M measurements made of the reflected signal, at the frequencies, $\{f_1, f_2, \ldots, f_M\}$. The auto-correlation matrix is given by the following expression,

$$\bar{\bar{C}} = E(\bar{s}_T \bar{s}_T^H), \text{ where,}$$

$\bar{s}_T = \bar{\bar{P}}\bar{\Gamma} + \bar{\eta}$,and all other quantities are as previously defined.

This can be expanded using the definition of the total signal, the result, assuming that signals and noise are uncorrelated. This can be expanded in the following manner.

$$\bar{\bar{C}} = E(\bar{s}_d \bar{s}_d^H) + E(\eta\eta^H),$$

We have let the decomposition of the signal be in the form:

$$\bar{s}_d = \bar{\bar{P}}\bar{\Gamma},$$

the matrix contains the array properties, and the vector is the scattering properties of the various interfaces. The second term is the noise auto-correlation and can be treated, for the case of Gaussian noise, as a constant, σ_0^2 . Thus we can write,

$$\bar{\bar{C}} = E(\bar{\bar{P}}\bar{\Gamma}\bar{\Gamma}^H\bar{\bar{P}}^H) + \sigma_0^2\bar{\bar{I}}, \text{ where,}$$

$\bar{\bar{I}}$ is the identity matrix and σ_0^2 is the noise variance in the measurement. This matrix can lead to a significant result, that the measured signal vector space can be decomposed into two orthogonal subspaces. This is seen by simply considering the matrix-vector product,

$$\bar{\bar{C}}\bar{s}_d = E(\bar{\bar{P}}\bar{\Gamma}\bar{\Gamma}^H\bar{\bar{P}}^H)\bar{s}_d + \sigma_0^2\bar{\bar{I}}\bar{s}_d$$

Since the vector $\bar{s}_d$ is written in the following way: $\bar{s}_d = \bar{\bar{P}}\bar{\Gamma}$, using this in the equation above will yield:

$$\bar{\bar{C}}\bar{s}_d = [E((\bar{\Gamma}^H\bar{\Gamma})(\bar{\bar{P}}^H\bar{\bar{P}})) + \sigma_0^2)]\bar{s}_d = \lambda_C\bar{s}_d$$

This is a statement of the eigenvalue problem, a solution to which is easily obtained. The matrix $\bar{\bar{C}}$ has dimension M, thus if the matrix has full rank it will have M eigenvectors and eigenvalues. If it is not of full rank, then there will be some number of degenerate eigenvectors. One can see that the minimum value that λ_C takes occurs when the first term in brackets is zero. Thus there is a set of eigenvectors having as their eigenvalue, σ_0^2. These are the so-called, *noise eigenvectors* of the signal. If there are N signals then there will be N signal eigenvectors if the individual signals are uncorrelated and thus $M - N$ noise eigenvectors. Since a priori knowledge of the actual number of signals in a measurement is not necessarily a known in advance, one can make an educated guess as to the number and then test the quality of the guess by plotting the eigenvalue spectrum. A typical eigenvalue spectrum is shown in Figure 8. The spectrum clearly shows signal eigenvalues monotonically decreasing, followed by a set of noise eigenvalues that are nearly constant.

3.4.1 Decorrelation Technique

Signals used in the interrogation of a region are a sequence of single frequencies with known amplitude and phase relationships. At a frequency f signals are of the form,

$$s(f) = \Gamma_1 e^{j2\pi f t_1} + \ldots + \Gamma_M e^{j2\pi f t_M} + \eta(f).$$

Data are gathered at a number of frequencies and the resulting system of received signals is used to form the correlation matrix. If the signals (frequencies) are uncorrelated then one obtains the previous results and a perfect decomposition into orthogonal subspaces occurs. This procedure is also valid if the signals are partially correlated, the only real difficulty occurs if there is perfect correlation between the signals. Since the signal source for our interrogation is the swept source of the vector network analyzer, coherence of the signals is a problem and one must apply some method to achieve the performance expected from MUSIC. Algorithm performance is greatly improved if the signals are more nearly uncorrelated than for correlated cases, and a method has been developed to "decorrelate" signals[11]. This method we refer to as "averaging" and is an integral part of the signal processing algorithm set. The algorithm subdivides the measurement band into sub-bands and processes each sub-band.

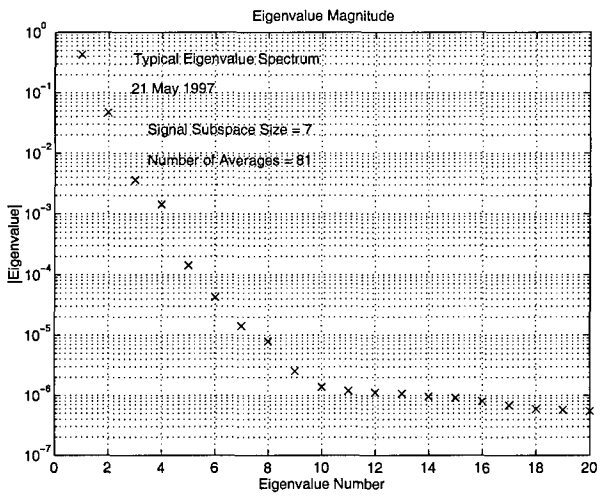

Figure 8. Typical Eigenvalue Spectrum Obtained from MUSIC.

An iterated correlation matrix is formed using each of the vectors from the sub-bands. This leads to the following for the k^{th} correlation matrix, R_k.

$$R_k = E\left[\overline{\overline{A}}\,\overline{\overline{D}}^{k-1}(\overline{\Gamma}\overline{\Gamma}^H)\overline{\overline{D}}^{k-1}\overline{\overline{A}}^H\right] + \sigma^2\overline{\overline{I}}\text{ , where,}$$

E denotes the expectation operator, and the superscript H denotes the hermitian conjugate of the matrix. The matrix $\overline{\overline{D}}$ is diagonal with exponential entries proportional to powers of the form, $e^{2\pi f t_m}$. Finally, the average of the various correlation matrices formed, leading to the result:

$$R_{avg} = \frac{1}{M}\sum_{k=1}^{M} R_k\ .$$

This is used to decorrelate the received signals removing the effects of coherence and producing a new correlation matrix with an eigenstructure having more well-defined signal and noise subspaces. This technique assumes a reasonable guess at the number of signals is available. This

will require skill on the part of the user to estimate the number of signals so as not to overwhelm himself with the interpretation of the results.

3.5 Determination of the Frequency Dependence of the Scatterer.

Scattering by a dielectric is dependent upon the properties of the medium in which the wave is propagating and on the material the wave interacts with. When a wave impinges upon the interface, to satisfy the boundary conditions, a reflected wave is set up. Not all of the energy is reflected. The remainder is transmitted into the second material. Reflected wave properties are characterized by the reflection coefficient, Γ. Reflection coefficients are, in general, complex and thus the amplitude and phase of the reflection coefficient must be determined. The value of the reflection coefficient depends upon the wave impedance in each material. This relationship is,

$$\Gamma = \frac{Z_1 - Z_0}{Z_1 + Z_0}.$$

The wave impedance in turn, depends upon the constitutive parameters of the materials. i.e.

$$Z_k = \sqrt{\frac{\mu_k}{\varepsilon_k}}.$$

This dependence is the basis for the constitutive signature of biological materials. There is a second signature that is of importance, the geometrical signature. This characterizes the geometry of the interface and is used in imaging of the interface. The geometry of the interface can be simple, as in a terminated transmission line or quite complex as presented in Figure 1. The ability to locate the interface and find its signature is fundamental to the system.

3.5.1 Algorithm for Determining Frequency Dependence

We now consider the procedure for the determination of the scattering amplitude response at the p^{th} frequency, of the k^{th} scatterer, $\Gamma_k(f_p)$, $k = 1,2,\cdots L$. Towards this end we consider a band of frequencies of width B_r and centered at f_p. Let there be $(N+1)$ samples of data over this band. The signal model corresponding to this band of frequencies is given by,

$$r_\ell = r(f_\ell) = \sum_{k=1}^{L} \Gamma_k(f_\ell)\, e^{-j2\pi f_\ell t_k}, \quad \ell = p - N/2, \cdots, p + N/2 .$$

Note that the scattering amplitudes are not assumed to be constant, and that the round trip time delays are assumed known and replaced by their estimates, t_k, previously determined. We assume a functional form for the k^{th} scattering amplitude function $\Gamma_k(f)$. These functional forms may be different for different values of k. For instance, it may be a polynomial of order q, as given by,

$$\Gamma_k(f)=\Gamma_{ko}+\Gamma_{k1}f+\Gamma_{k2}f^2+\ldots+\Gamma_{kq}f^q.$$

Another possible functional form is a simple power rule:

$$\Gamma_k(f)=\Gamma_{ko}f^{\alpha}.$$

Biological materials have been measured over selected frequency ranges and the results are available in the literature. Such data has indicated that the dielectric properties are monotonically decreasing functions of frequency, e.g. $\varepsilon(f)=\alpha f^{-m}$. Since the reflection coefficient depends on the media involved in the scattering, we can use this *a priori* information to our advantage.

3.6 Additional Signal Processing Techniques Employed in Hemorrhage Detection

3.6.1 Background Subtraction

S*R has developed a technique we call "background subtraction" that enables us to remove the contribution of scatterers that are in known locations. This technique is similar to that used in the RCS measurement community to remove contributions from known scatterers in an RCS measurement range. This technique dramatically increases the dynamic range of the measurement. We have had the same success in using the technique in our processing.

Background subtraction is accomplished in two steps. First, a measurement is made of the set-up without the target present. As noted, the data collected contains amplitude and phase information for the region without the target present, primarily the response of the absorbing material. These data are stored and the target is placed on the absorber and the data taken and stored again. Once this is completed, the vector difference is taken, and these data are processed. This removes "most," but not all, of the contribution from the background and permits the desired target to be more accurately located by the MUSIC algorithm, increasing the resolution. The process is described in the next paragraph.

We assume the received signal is composed of a linear combination of scattering interfaces, M, in number, and a Gaussian noise contribution. The signal contains amplitude and phase information, stated mathematically,

$$s_{BKGD}(f)=\sum_{m=1}^{M}a_m(f)e^{jk_md_m}+\eta_{BKGD}(f),$$

where the amplitudes are a_m, the propagation constant in each region is k_m, the distance to the scatterer is d_m, and $\eta_{BKGD}(f)$ is a Gaussian noise at frequency f. The amplitude and phase data are stored. The data from the target and background are:

$$s_{BKGD+TGT}(f)=\sum_{m=1}^{M}a_m(f)e^{jk_md_m}+\eta'_{BKGD}(f)+\sum_{l=1}^{P}t_l(f)e^{jk_ld_l}+\eta_{TGT}(f),$$

where the amplitudes of the P scatterers are denoted as t_l, the propagation constants and locations follow the same notation as before. The difference between these expressions is taken and the result is:

$$s_{TGT}(f) = s_{BKGD+TGT}(f) - s_{BKGD}(f) = \sum_{l=1}^{P} t_l(f) e^{jk_l d_l} + \eta_{TGT}(f) + \eta'_{BKGD}(f) - \eta_{BKGD}(f).$$

Processing the data in the above expression produces the locations of the scatterers. Note that the noise term is composed of three contributions and it is this that leads to the statement that "most" of the background is removed. There can be slight configuration differences between measurements and this will preclude the complete removal of the background. Even with this, the success of background subtraction has been remarkable.

3.6.2 Scatterer or Peak Subtraction

A previous paragraph described the process of background subtraction and its application to the location of targets. We have developed an analogous method for application to signature estimation, the process is called *scatterer subtraction*. It is performed after the scatterers in the region have been located. After the location processing, the frequency dependence of the individual scatterers is determined. As noted previously, there are scatterers in the region that are known *a priori*. These can cause confusion in the algorithm leading to false alarms. Hence any method that can remove these will serve to reduce the false alarm rate (FAR). An example is the presence of the skull which will always be present and can be removed from the data to be processed using this technique.

It was explained in the previous section that the contribution to the total received signal is composed of all target signals in the region that meet a user defined selection criterion. Suppose that the processing finds M scatterers. This would imply the signal has the form:

$$s_{proc}(f) = \sum_{s=1}^{M} A_s e^{jkd_s} + \eta(f)$$

The amplitudes A_s have a known frequency dependence (determined by processing) and the phase terms are also known, hence, the contribution from undesired scatterers can be removed simply by subtraction the known contributions. The resulting signal can be processed a second time and additional information can be obtained. This process is used to better locate desired targets and to obtain better approximations to the received signal.

4.0 RESULTS

4.1 Measurement System

A simple system has been developed for measuring the properties of biologically relevant interfaces, such as skull-brain, and skull-blood-brain. If these can be demonstrated to be significantly different, then a simple detection scheme can be developed to detect the presence or

absence of subdural bleeds. The system designed consists of a transmission tunnel structure lined with absorber. Figure 9 illustrates the set-up in an end view. The target is supported by a styrofoam stand having a flat base upon which the target rests. The target is illuminated by a wideband antenna having an operating range of 2 - 18 GHz. This antenna rests on the sheet of flat absorber, and the target is illuminated from below, simulating a coronal interrogation. The reflected signals are received and the Vector Network Analyzer records the amplitude and phase of each signal. This data is stored to 3.5 inch diskette for further processing.

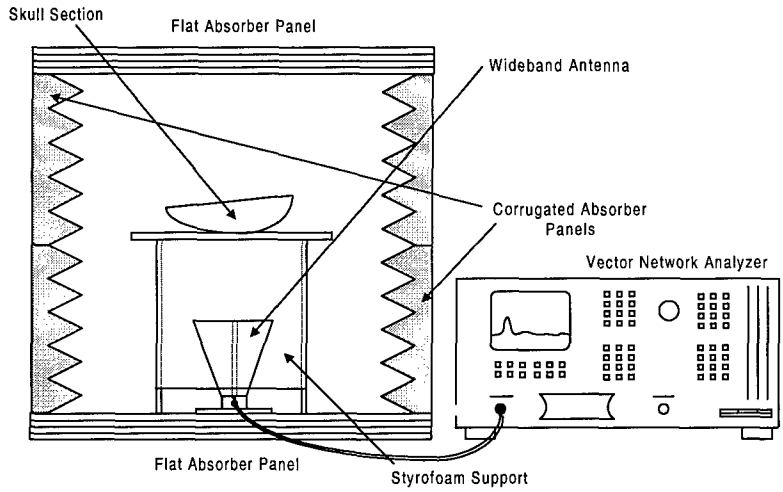

Figure 9. Measurement System.

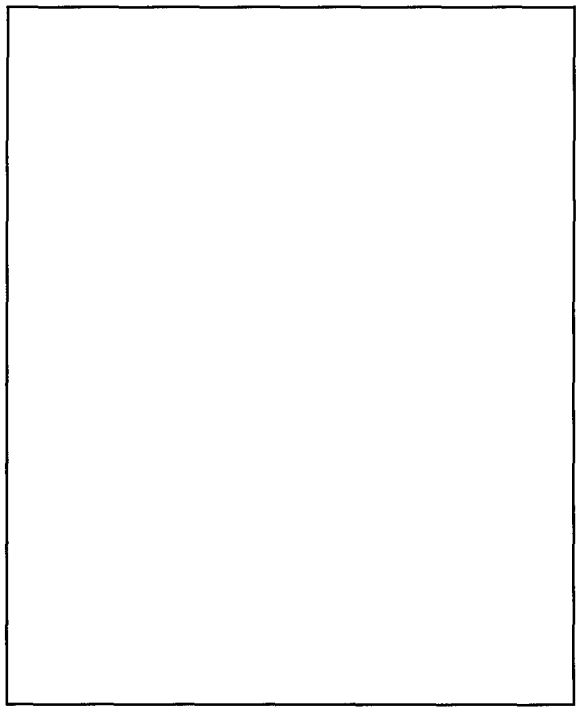

Figure 10. Measurement Set-up Used for Porcine Brain Measurements.

The measurement is made in several steps, for the purposes of better data presentation, all of the spectral results are normalized to those of a metal plate located at the resting point of the target. The first measurement made is to determine the background. It is taken to later be used for background subtraction. Next the reference is taken, using a 8 inch square aluminum panel. Finally, the target is placed on the support and interrogated. This process, in the current configuration, takes approximately 2 minutes, the greatest part of the time spent in data transfer and storage. Once the data is available, it can be processed using any PC having MATLAB™ available. All processing of the data occurs in a single MATLAB m-file, including graphical output of the data.

4.2 Phantom Measurements

4.2.1 Technical Results

The following graphs illustrate data taken by Spectra*Research on a human skull using a Wiltron 37247B Vector Network Analyzer and a horn antenna. Figure 11 depicts the test setup. The horn antenna was aimed at a target, in this case a nylon slab of approximate volume 0.394 in^3 (5.72 cm^3) and data was collected using the network analyzer.

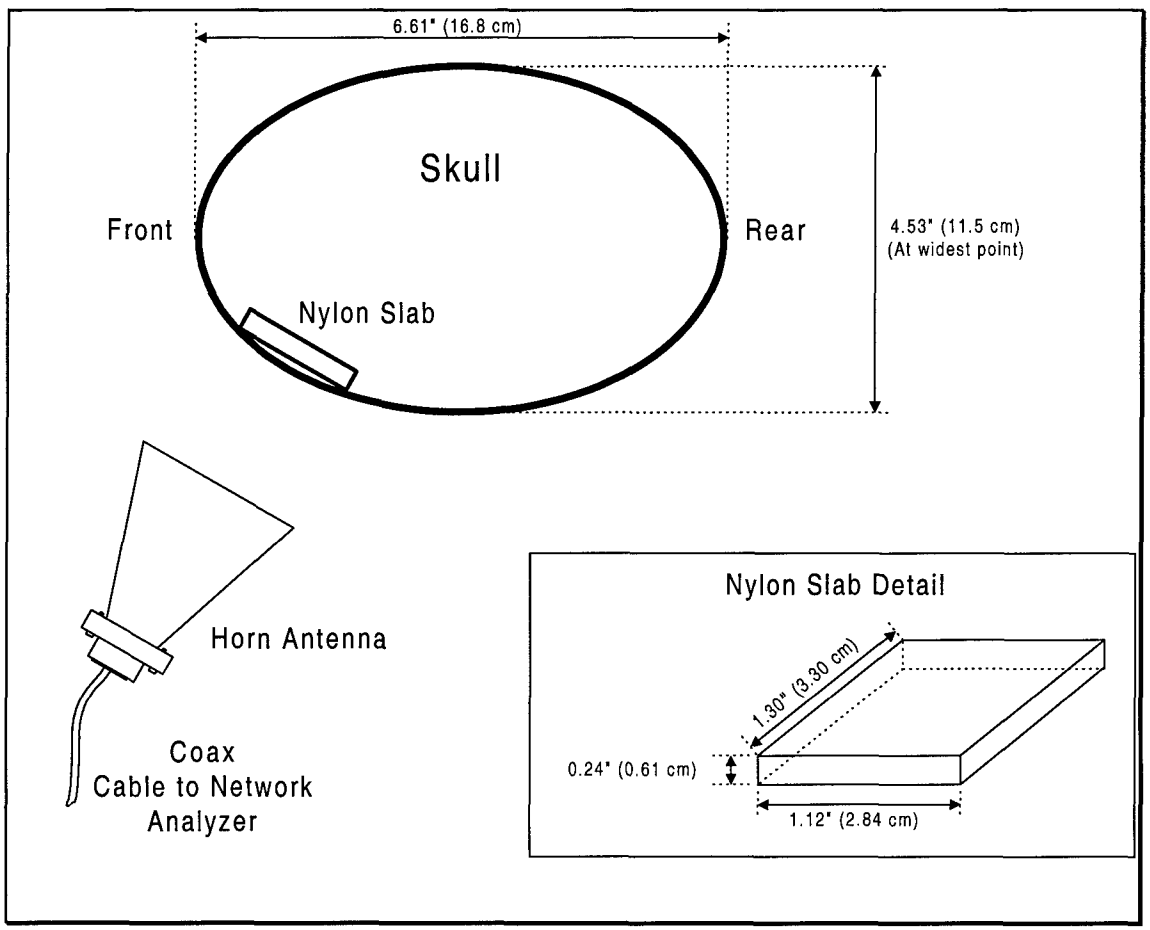

Figure 11: Test Setup

The following results were obtained by processing measured scattering data using the S*R modified MUSIC algorithm.

4.2.2 Skull With Nylon Slab (Temporal, Subdural Model)

This data was obtained using the setup shown in Figure 11. This setup is designed to simulate a subdural hematoma near the thin walls in the proximity of the left temporal area.

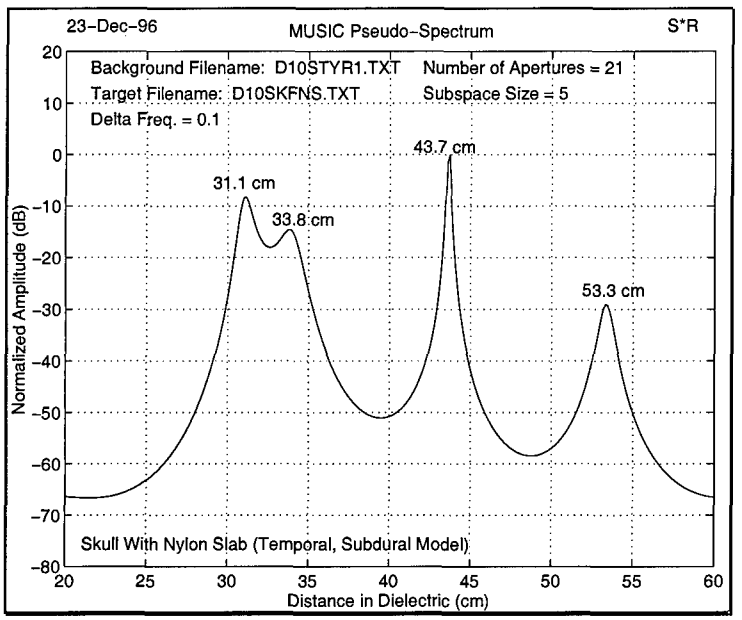

Figure 12: MUSIC Pseudo-Spectrum

Figure 12 shows four distinct peaks. The peak at 31.1 cm is the front skull wall. The peak at 33.8 cm is an interface of the nylon slab. The remaining peaks at 43.7 cm and 55.3 cm are from the back wall of and other structures inside the skull.

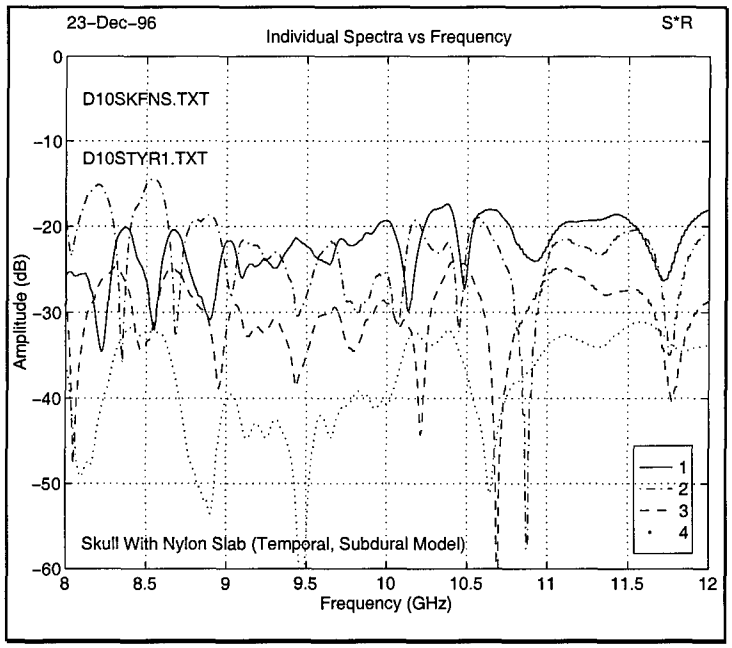

Figure 13: Individual Spectra

Figure 13 shows the spectrum for all four scatterers. As expected, the first scatterer appears generally most prominent.

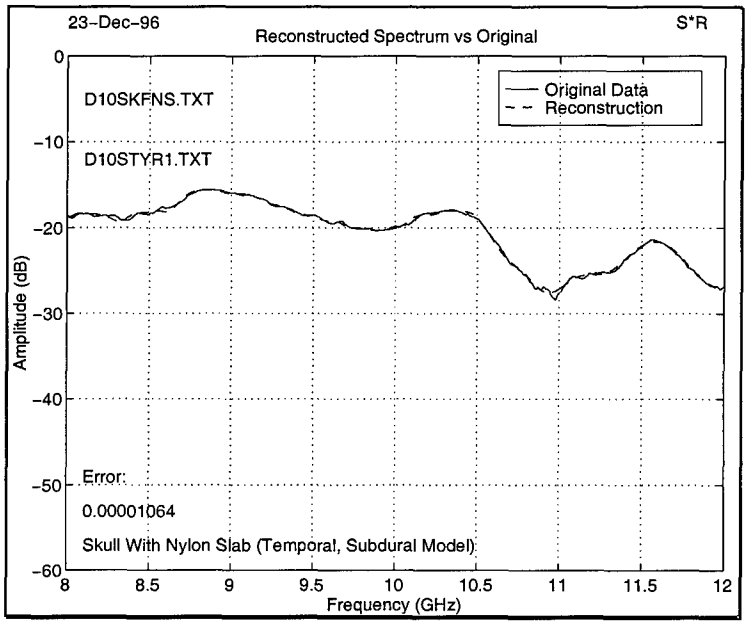

Figure 14: Reconstructed Spectrum vs. Original

4.2.2.1 Skull With Nylon Slab (Temporal, Subdural Model) High Gain Antenna

This data is similar to that of Figures 12, 13 and 14. The difference in the results is due to the use of a higher-gain horn antenna was used, but the measurement was made over the same frequency band.

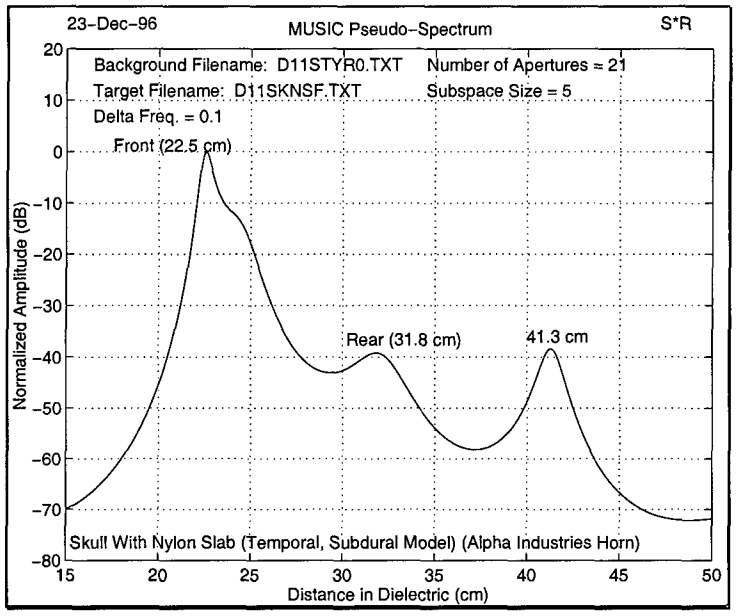

Figure 15: MUSIC Pseudo-Spectrum

Figure 15 shows four distinct peaks. The peak at 22.5 cm is the front of the skull. A noticeable shoulder appears to the right of this peak suggesting the presence of another scatterer that is too close to the first scatterer to be resolved individually. This is due to the limited bandwidth used. The peak at 31.8 cm is the rear wall of the skull.

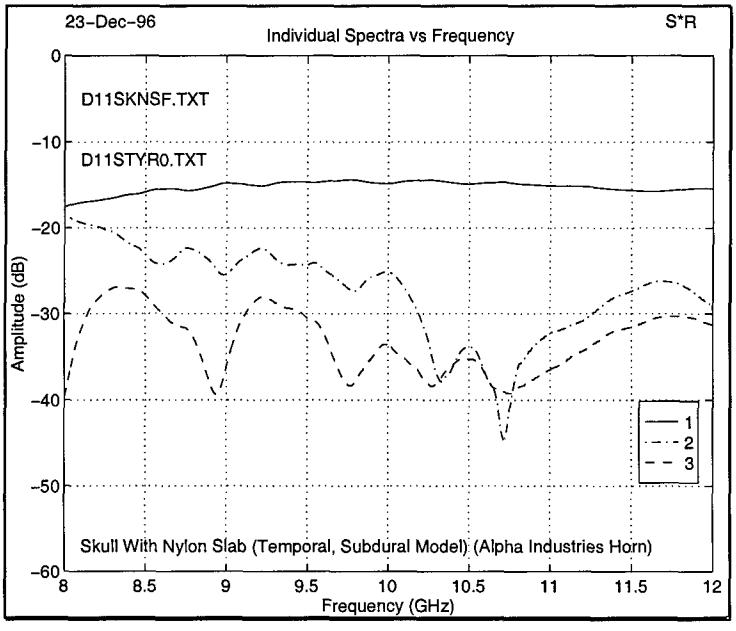

Figure 16: Individual Spectra vs. Frequency

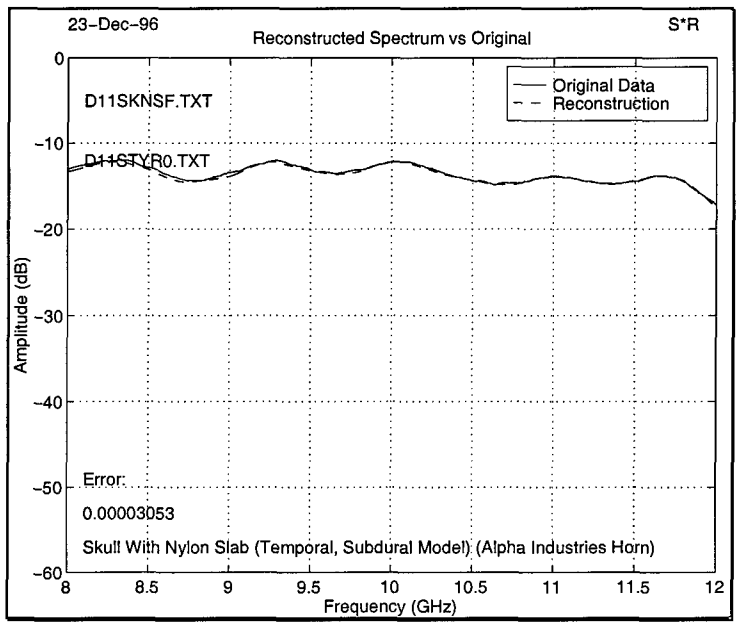

Figure 17: Reconstructed Spectrum vs. Original

Figures 16 and 17 show the spectra for each scatterer and reconstructed spectrum vs. measured S_{11} data respectively. From Figure 16 it is clear that the first scatterer has by far the greatest contribution.

4.2.2.2 Skull With Flat Nylon Slab Model for Temporal Subdural Hematoma

These plots show the same data that was used for Figures 15, 16 and 17. Different processing parameters were used, however.

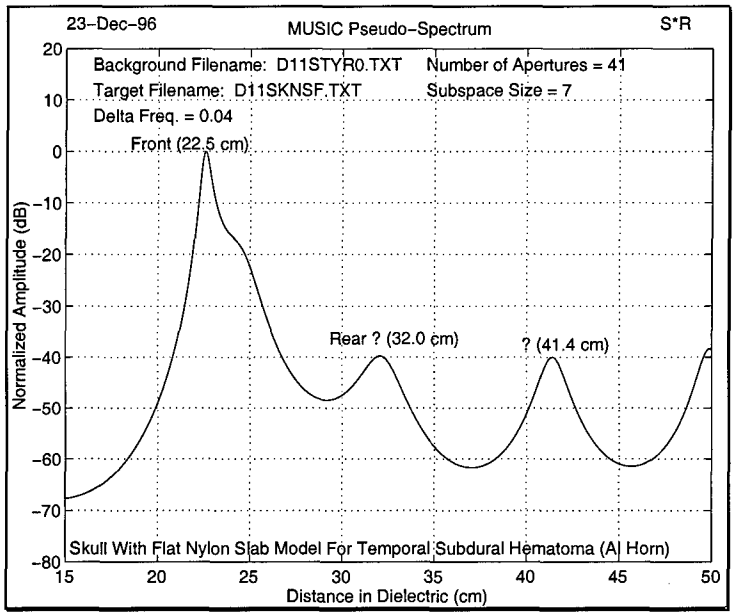

Figure 18: MUSIC Pseudo-Spectrum

Figure 18 shows how the MUSIC Pseudo-Spectrum changes when more averaging (increased number of apertures), greater subspace size and a narrower frequency increment Δf are used. This was an attempt to "pull out" the scattering response from the nylon slab. As can be seen, the first scatterer has become better defined relative to that illustrated in Figure 15. A drawback of increasing the subspace size is that this sometimes results in artifacts being displayed. The peak at approximately 50 cm is an artifact.

Figures 19 and 20 appear very similar to the results presented in Figures 16 and 17 respectively.

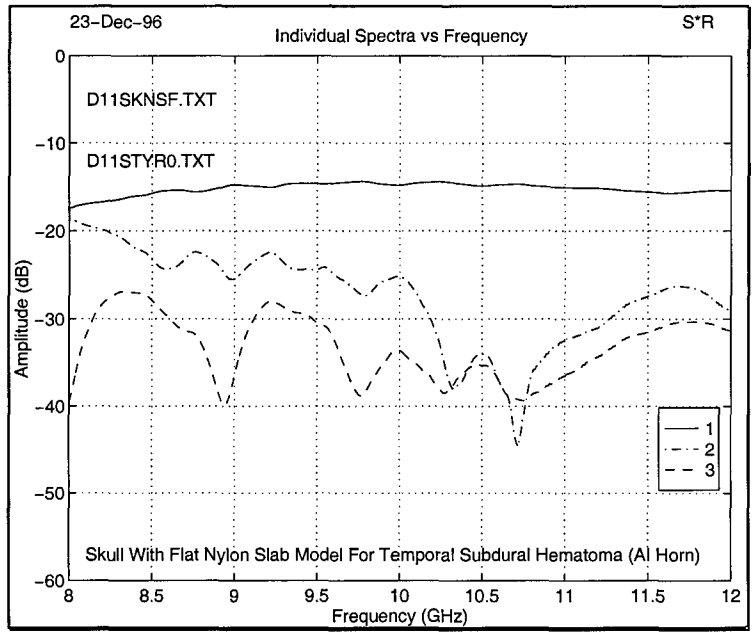

Figure 19: Individual Spectra vs. Frequency

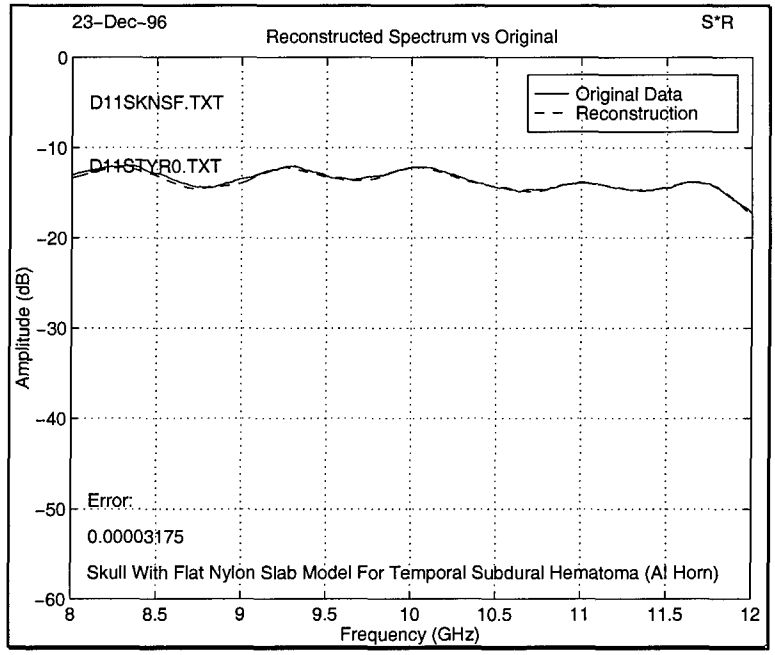

Figure 20: Reconstructed Spectrum vs. Original

4.2.2.3 Skull With Flat Nylon Slab Model of Temporal Subdural Hematoma

These graphs represent the same data from Figures 15 through 20 with different processing parameters used.

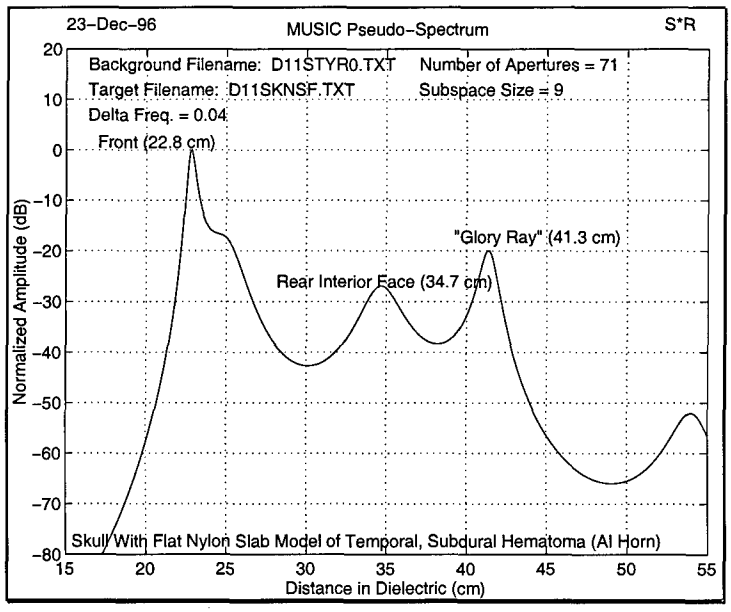

Figure 21: MUSIC Pseudo-Spectrum

Figure 21 shows another effect of using a higher subspace size and number of apertures. The result is a lower overall noise floor and a shift of the peak at 34.7 cm (previously at approximately 32 cm).

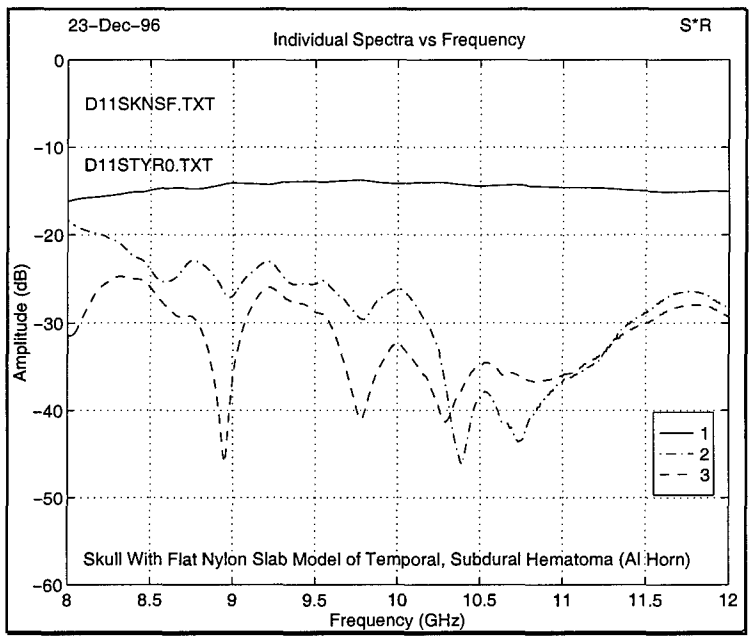

Figure 22: Individual Spectra vs. Original

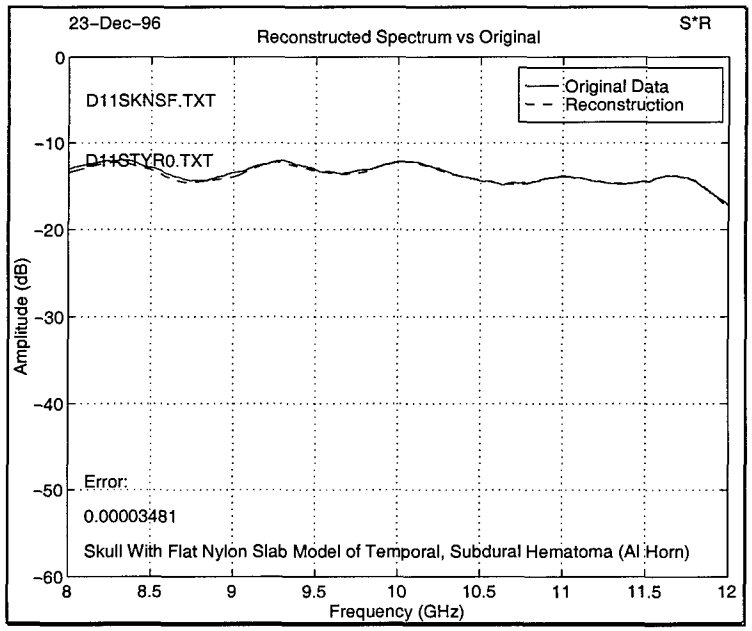

Figure 23: Reconstructed Spectrum vs. Original

4.2.2.4 Skull With Flat Nylon Slab After Subtraction

These plots are created from the data of Figures 15 through 23 using a signal subtraction technique. For Figures 24 through 26, the first scatterer has been removed from the processing. This was done as an attempt to "pull out" the nylon slab. Figure 24 now shows a separate peak at 25 cm for the slab. It is not known which interface of the slab is being shown or if this peak represents a combination of the two interfaces, but the slab is seen.

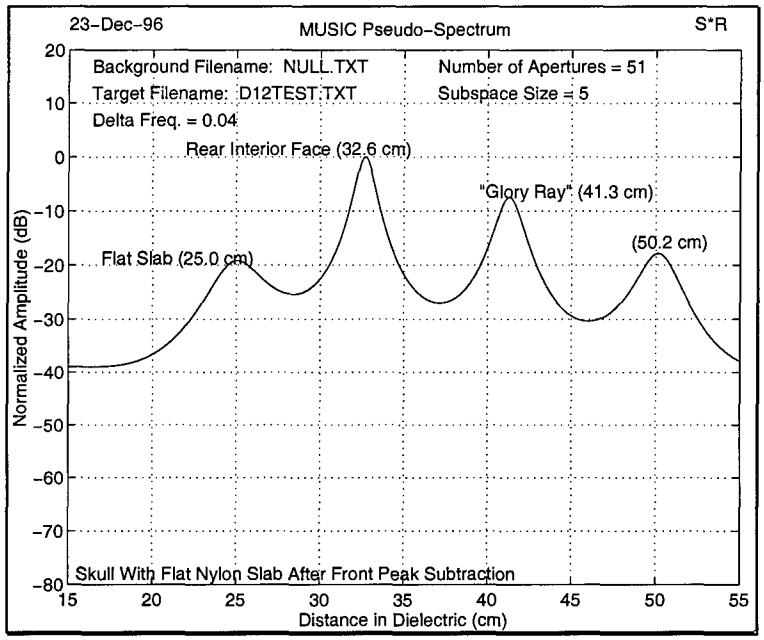

Figure 24: MUSIC Pseudo-Spectrum (Post Subtraction)

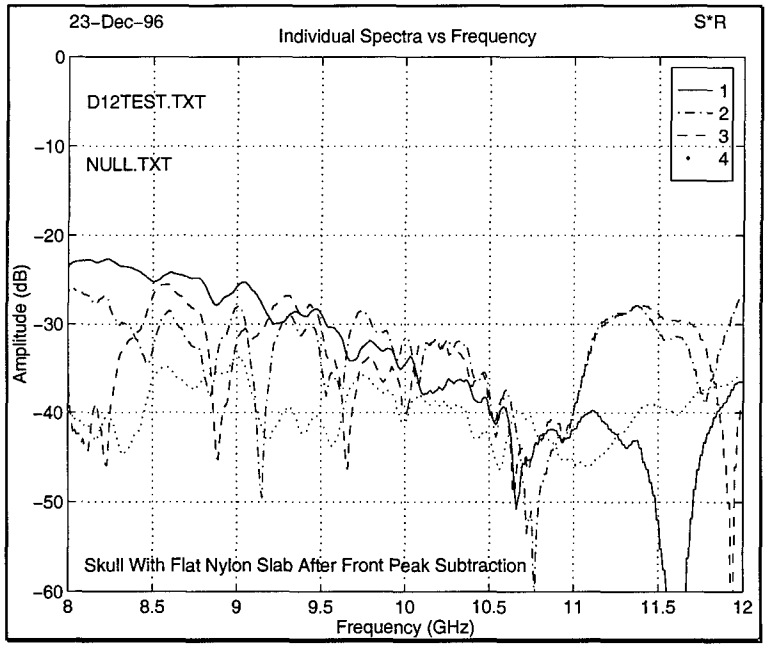

Figure 25: Individual Spectra vs. Frequency

Figure 24 shows that the first scatterer as seen in previous figures (16, 19 and 22) has now been eliminated. This allows for less prominent peaks to become more visible as Figure 24 illustrates.

4.2.3 Technical Results: Simulated Brain

4.2.3.1 Simulated Brain Tests

Separate tests using simulated brain material were performed using a mixture of silicon rubber compound (GE Silicones RTV-11) and carbon black (Cabot VXC72 GP-3587). This combination more closely resembles the lossy properties of human brain tissue. Figure 26 shows the test setup using two silicon rubber "pucks." One test was performed using silicon rubber pucks containing no carbon black (called simply "silicon rubber") with a slab of silicon rubber mixed with carbon black (called "simulated brain") placed in-between as the figure shows. Another test was performed using the opposite configuration—pucks made with carbon black enveloping a slab of silicon rubber with no carbon added. These test setups allowed for measurements to be made on exclusively lossy material.

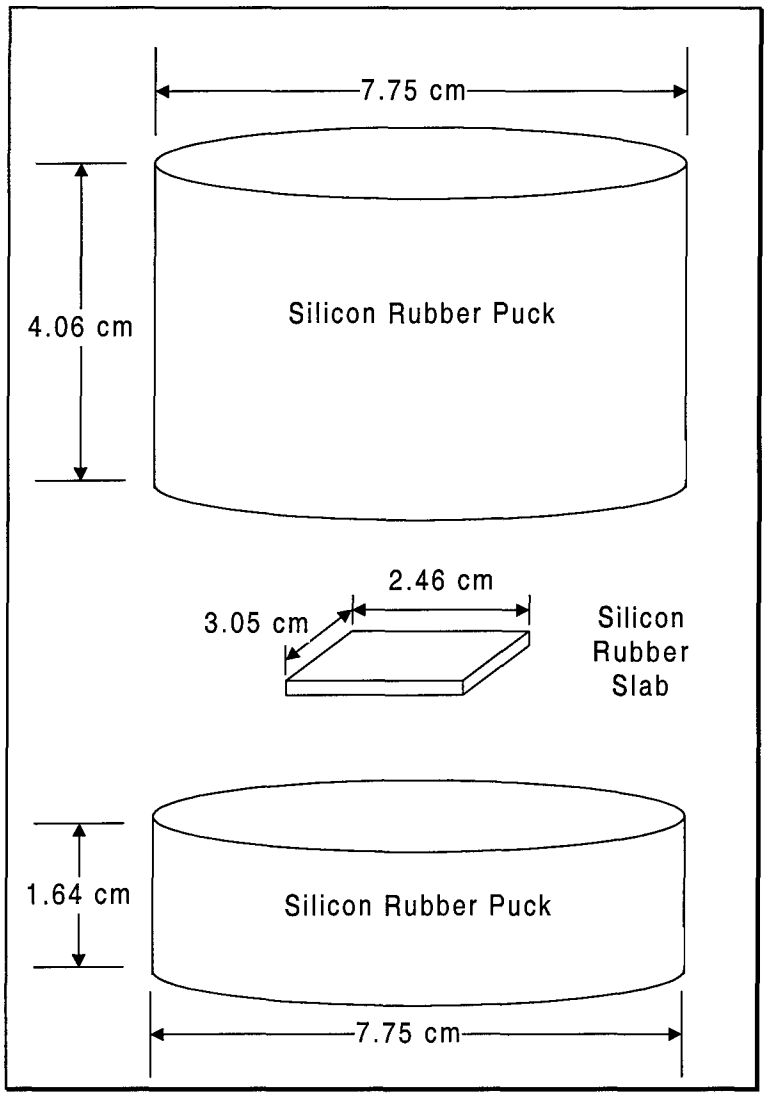

Figure 26: Exploded View of Silicon Rubber Puck Measurements. Test signal directed from either the top or the bottom of the stacked-puck target.

Initial test results show that the slab of contrasting silicon placed between the pucks (simulating a clot) can be seen by the MUSIC algorithm. Three clear peaks manifest themselves representing the front interface, the clot and the rear interface of the stacked-puck target.

Figure 27 shows the results of a test using pucks made of simulated brain material (silicon rubber with carbon black added) enveloping a slab of pure silicon rubber. The data clearly shows the front (43.6 cm) and rear (55.9 cm) interfaces of the target with a less prevalent peak between 45 and 50 cm representing the simulated clot. Figures 28 and 29 show the individual spectra vs. frequency and the reconstructed data vs. frequency for this data.

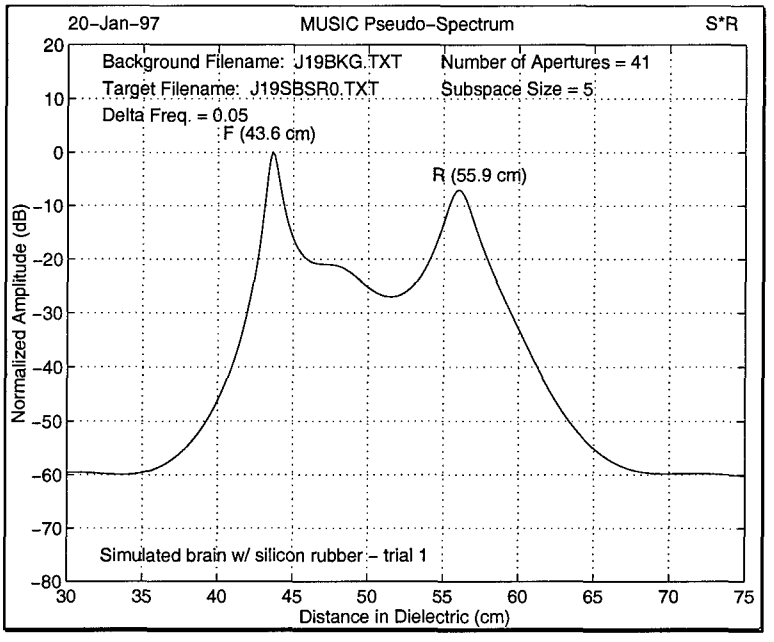

Figure 27: MUSIC Pseudo-Spectrum

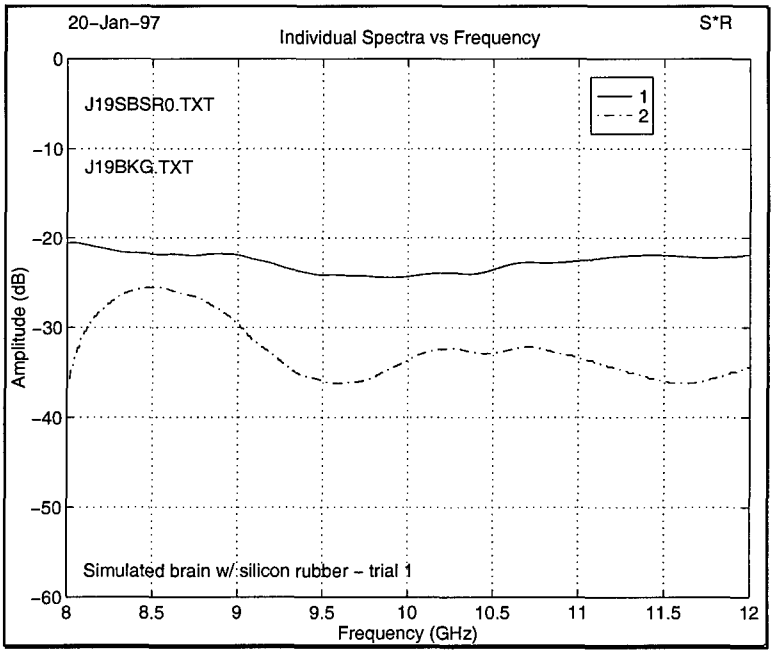

Figure 28: Individual Spectra vs. Frequency

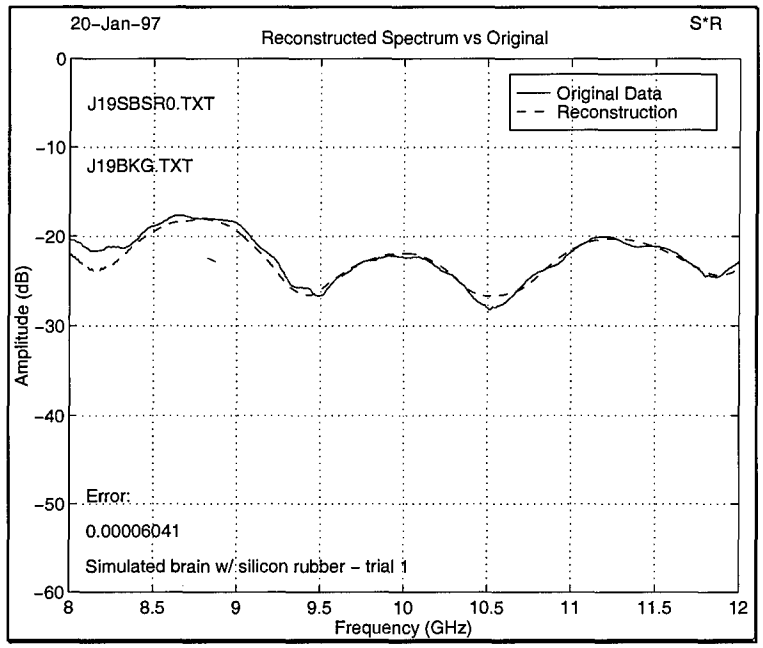

Figure 29: Reconstructed Spectrum vs. Original

Figure 30 shows the effect of analytically subtracting the first scatterer, which is in this case the front of the target. The location of the clot becomes clear now that the stronger front peak scatterer no longer influences its perceived location.

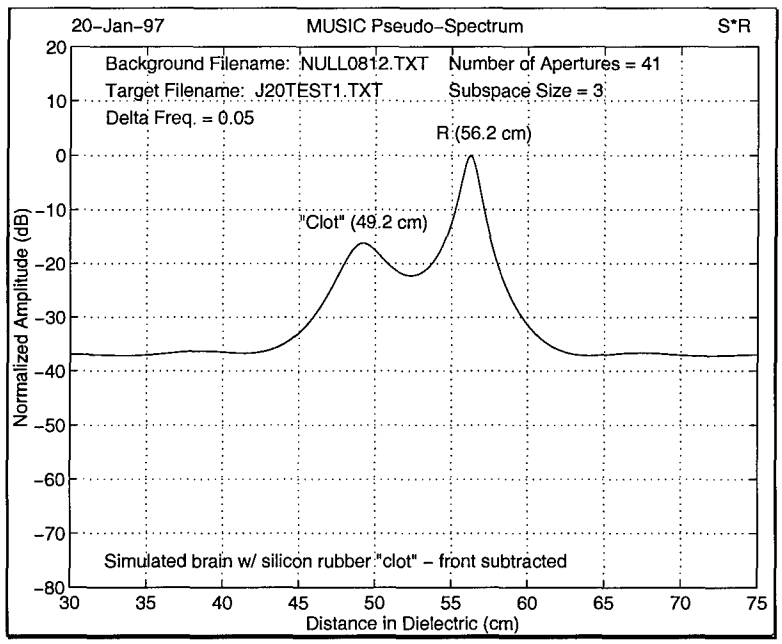

Figure 30: MUSIC Pseudo-Spectrum

Figure 31 represents the results for the opposite case—silicon rubber pucks enveloping simulated brain material. The front interface and the clot are easily identified. The rear is also discernible.

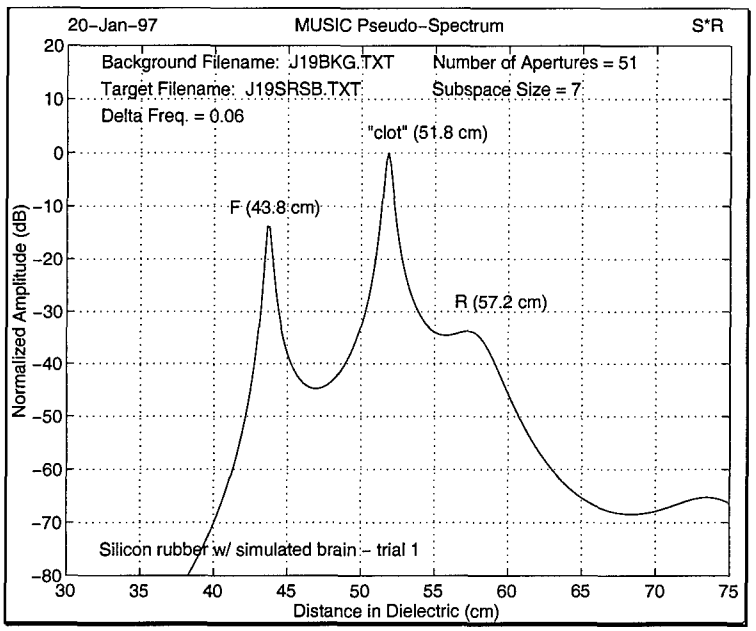

Figure 31: MUSIC Pseudo-Spectrum.

Figures 32 and 33 shows the individual spectra vs. frequency and the data reconstruction vs. frequency.

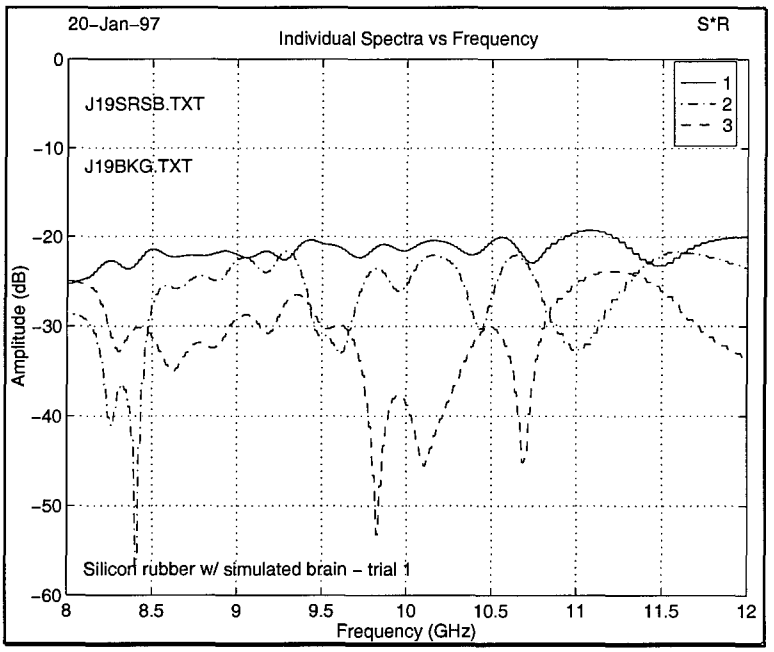

Figure 32: Individual Spectra vs. Frequency.

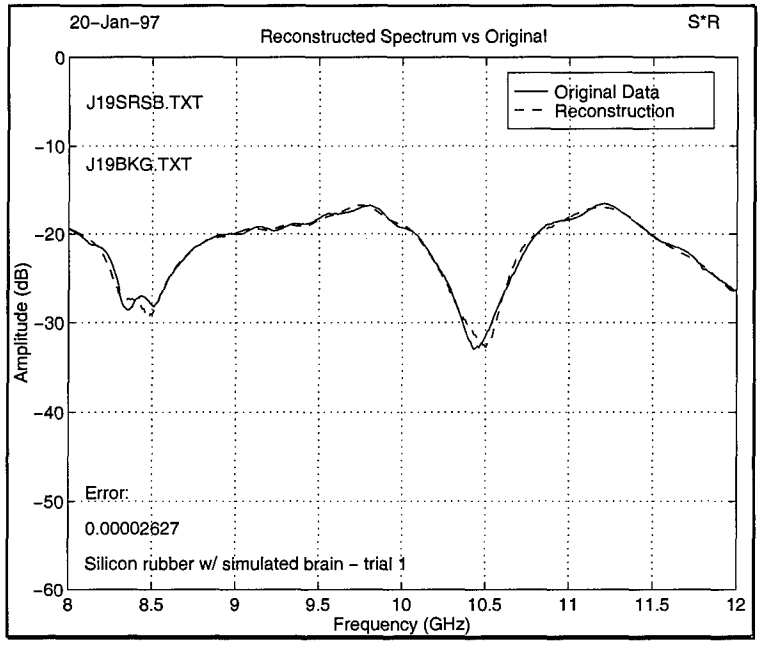

Figure 33: Reconstructed Spectrum vs. Original.

Figure 34 shows the results of subtracting the front scatterer from the above data. The simulated hematoma is easily located after subtraction.

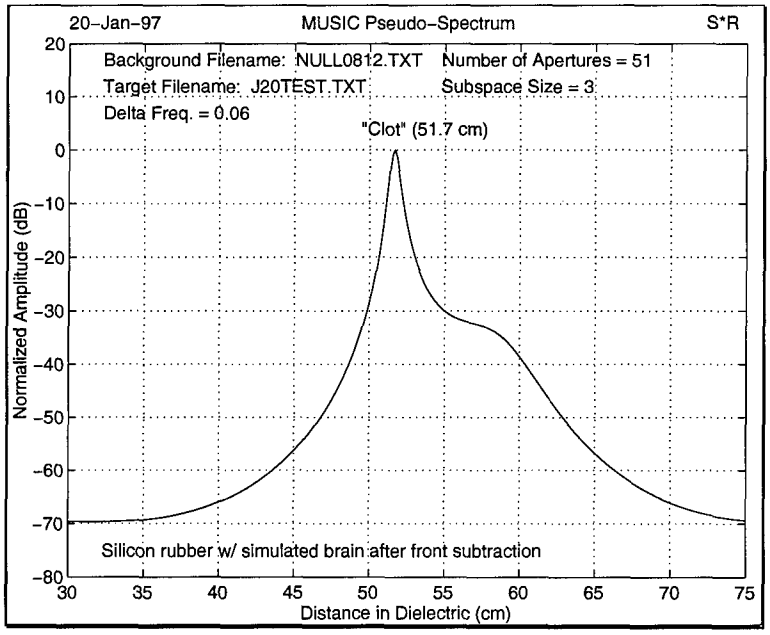

Figure 34: MUSIC Pseudo-Spectrum.

Figures 35, 36 and 37 show the results from a second trial of the above test setup.

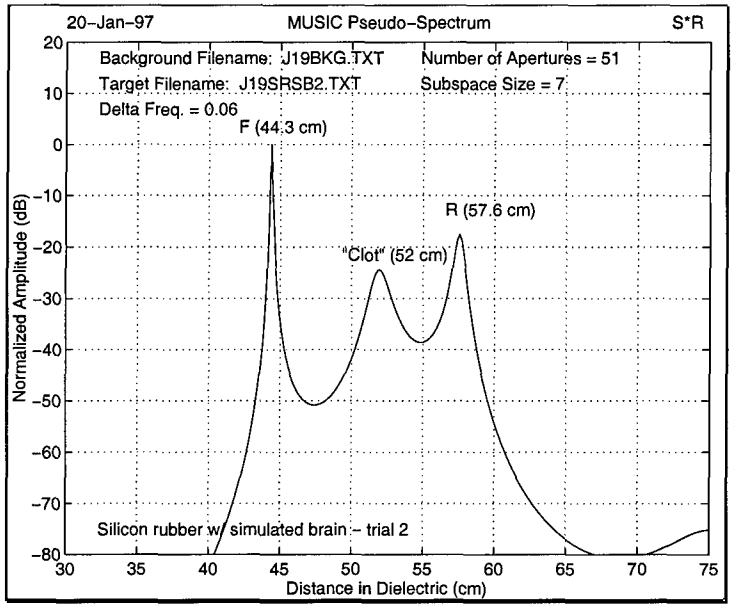

Figure 35: MUSIC Pseudo-Spectrum.

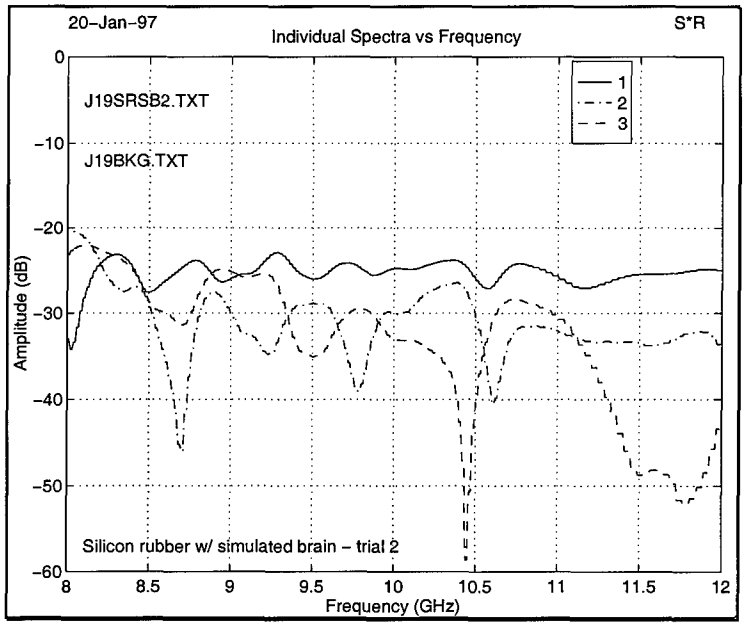

Figure 36: Individual Spectra vs. Frequency.

4.2.4 Second Series of Skull Measurements Using Full Size Simulated Brain

Once the measurements on the cylindrical simulated brain were complete, a full size brain was constructed to fit into the cranial cavity of the skull used in the earlier tests. The simulated gray matter we used had the same percentage by weight of carbon black as the material used in the cylindrical measurements presented earlier. Table 1 presents a measurement matrix for the skull and simulated brain.

Table 1. Skull Measurement Matrix

Measurement Number	Filename	Frequency Range	Ventricle model	View	Half Skull	Full Skull
1	j23skemp.txt	8 -12 GHz	Air	Posterior	x	
2	j23skab1.txt	"	Acrylic ball	"	x	
3	j23skgb1.txt	"	Glass ball	"	x	
4	j23sksb1.txt	"	Steel ball	"	x	
5	j23wskem.txt	"	Air	"		x
6	j23wskab.txt	"	Acrylic ball	"		x
7	j23wskmb.txt	"	Glass ball	"		x
8	j23wsksb.txt	"	Steel ball	"		x
9	j23pssem.txt	"	Air	Temporal	x	
10	j23pssab.txt	"	Acrylic ball	"	x	
11	j23pssgb.txt	"	Glass ball	"	x	
12	j23psssb.txt	"	Steel ball	"	x	
13	j23fsemp..txt	"	Air	"		x
14	j23fsab1.txt	"	Acrylic ball	"		x
15	j23wssmb.txt	"	Glass ball	"		x
16	j23wsssb.txt	"	Steel ball	"		x

The test matrix was chosen to illustrate the method and demonstrate the capability of the algorithm to identify and spatially locate the ventricles.

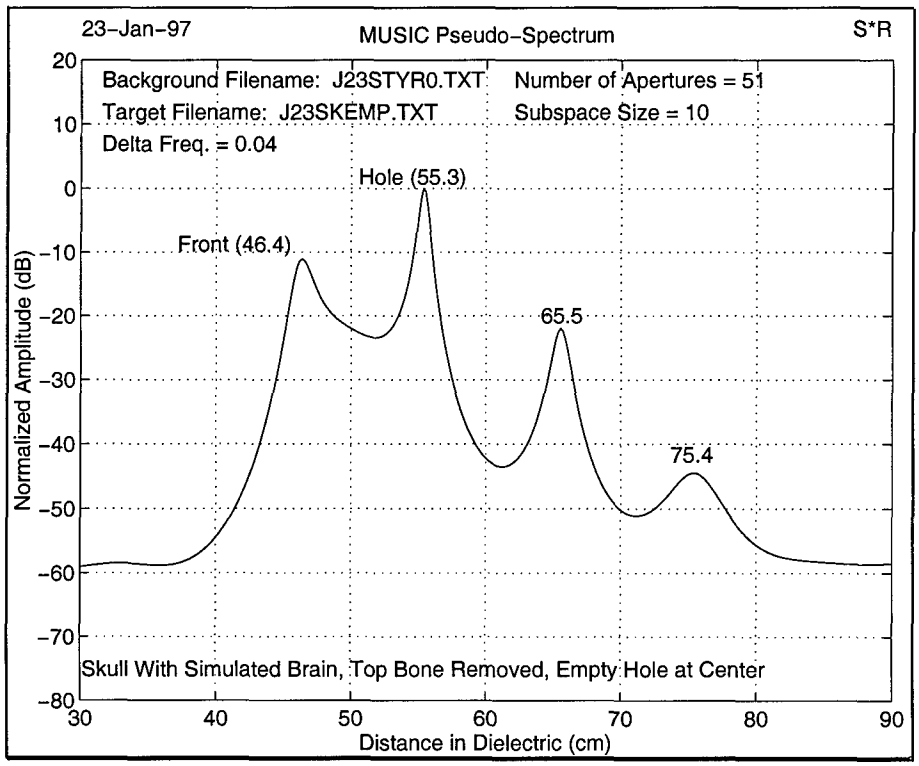

Figure 37: Empty Half Skull, Posterior View.

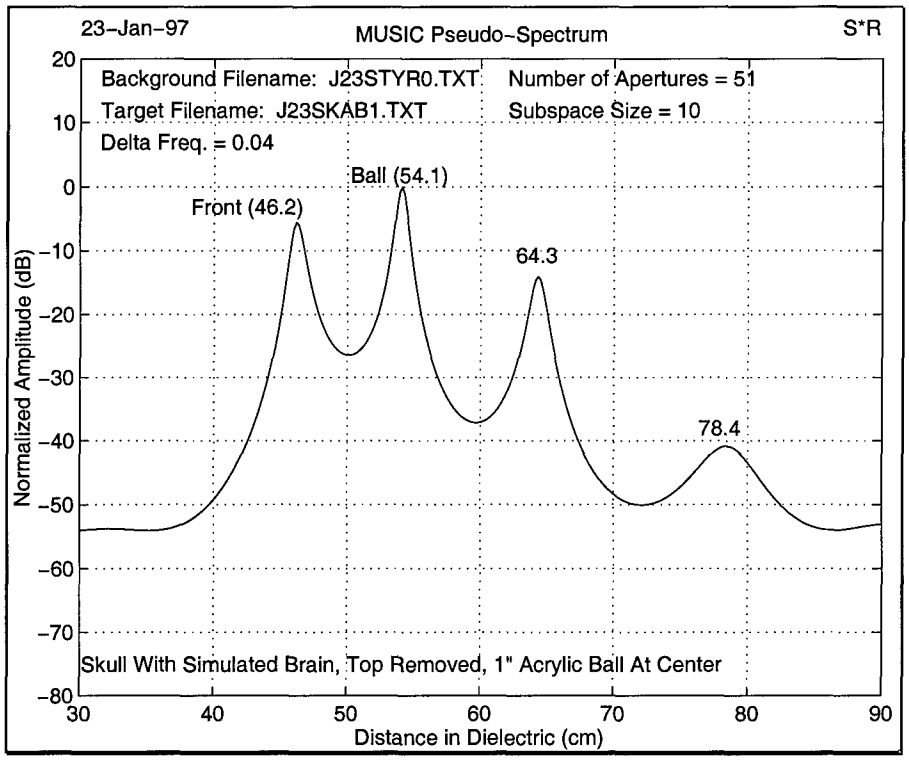

Figure 38: Half Skull With 1" Acrylic Ball at Ventricle Hole, Posterior View.

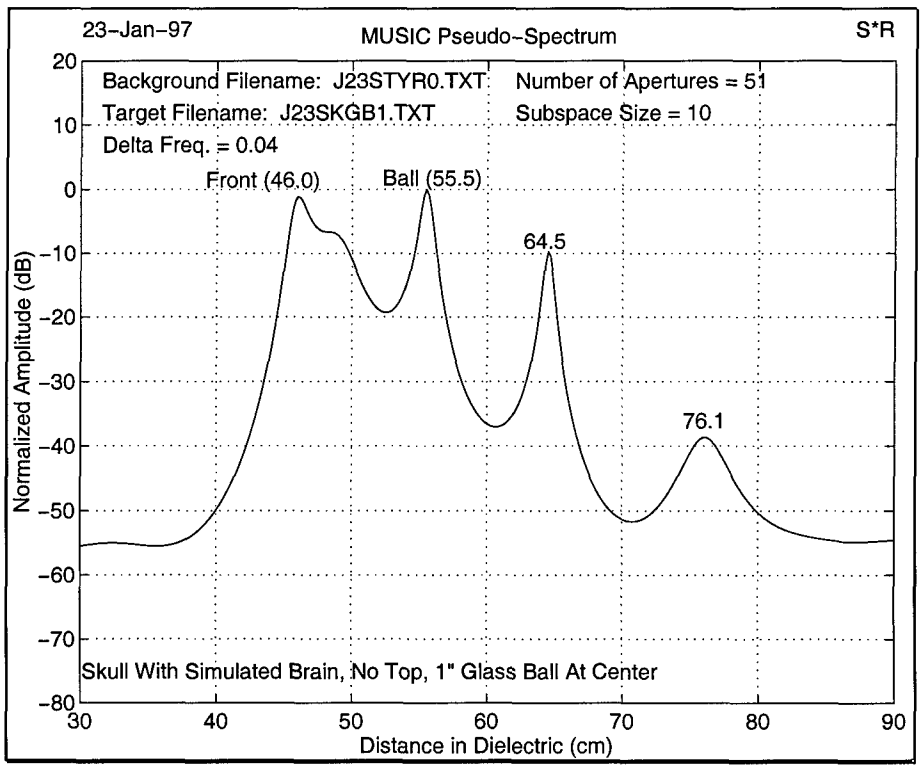

Figure 39: Half Skull With 1" Glass Ball at Ventricle Hole, Posterior View.

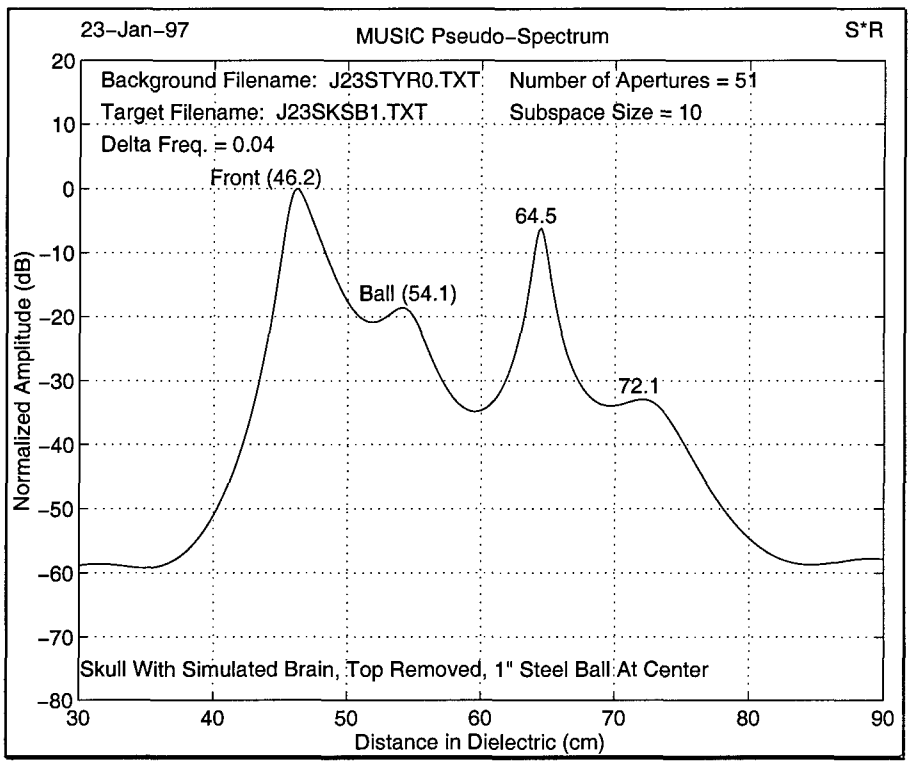

Figure 40: Half Skull With 1" Steel Ball at Ventricle Hole, Posterior View.

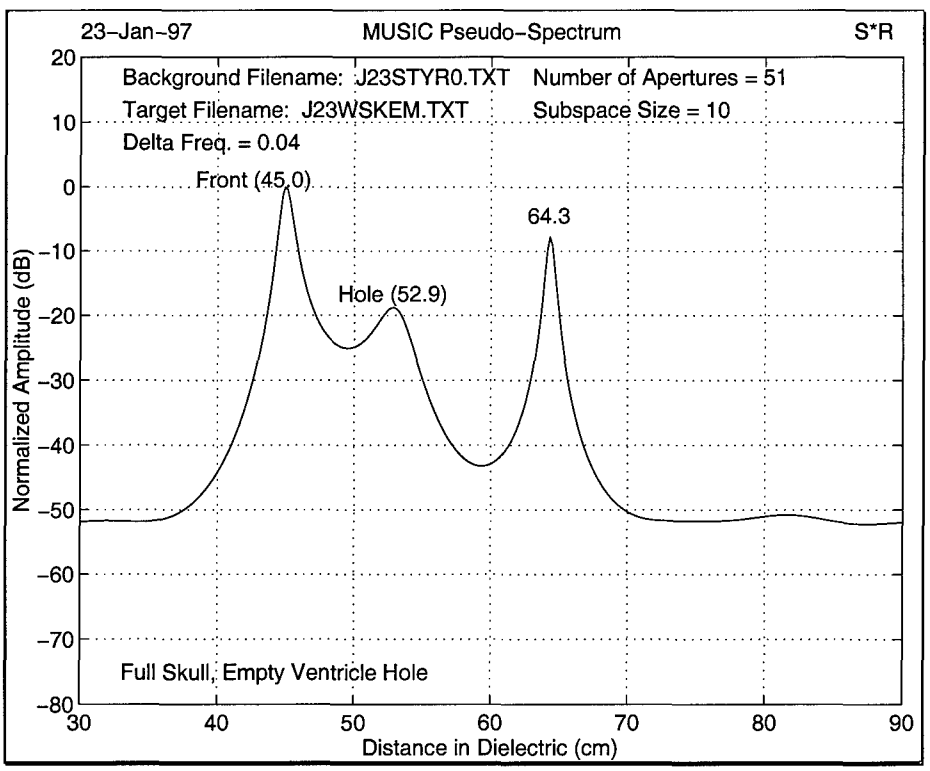

Figure 41: Whole Skull, Empty, Posterior View.

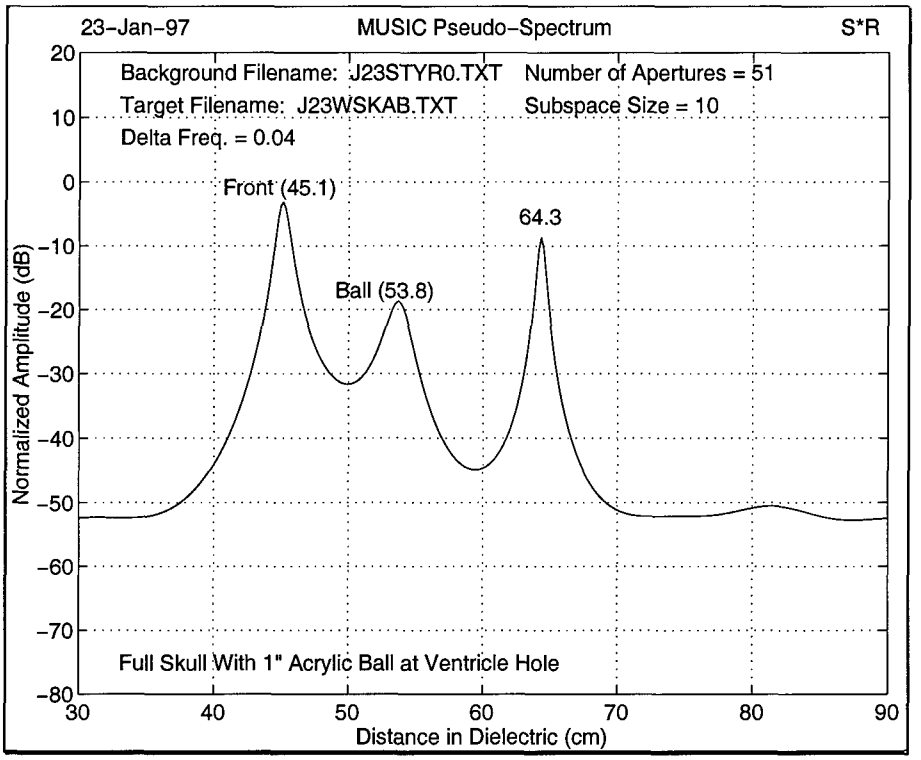

Figure 42: Whole Skull With 1" Acrylic Ball at Ventricle Hole, Posterior View.

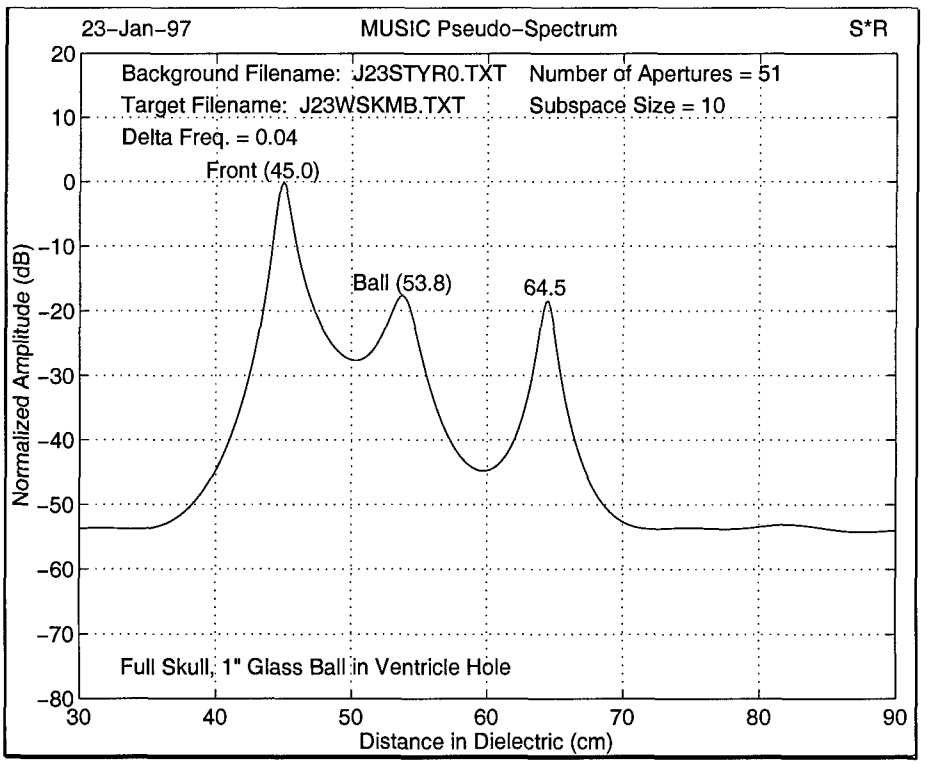

Figure 43: Whole Skull With 1" Glass Ball at Ventricle Hole, Posterior View.

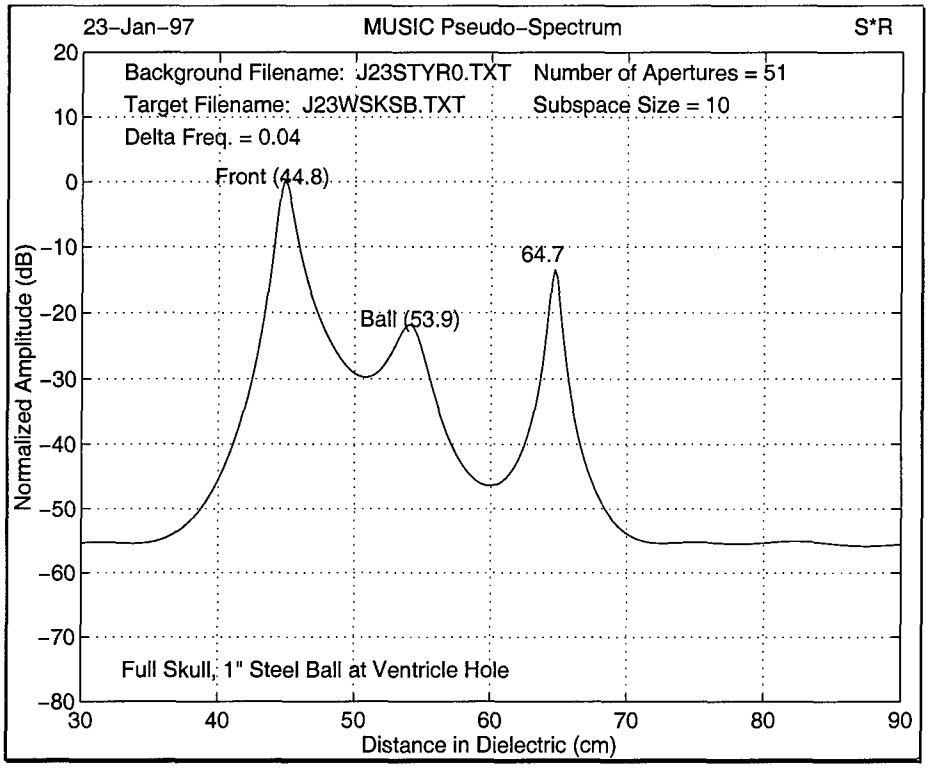

Figure 44: Whole Skull With 1" Steel Ball at Ventricle Hole, Posterior View.

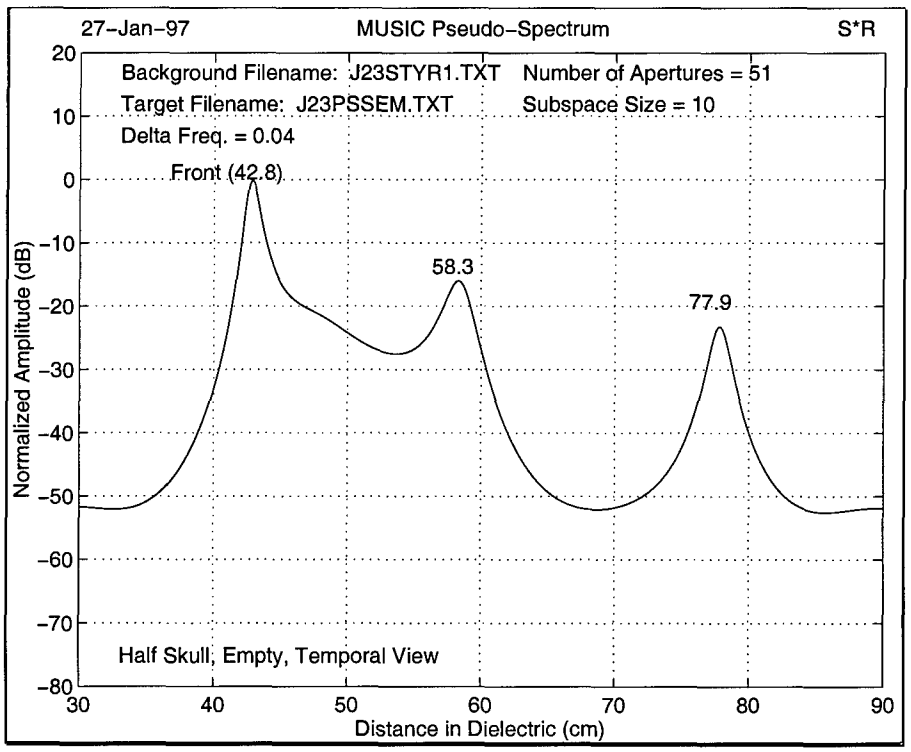

Figure 45: Half Skull, Empty, Temporal View.

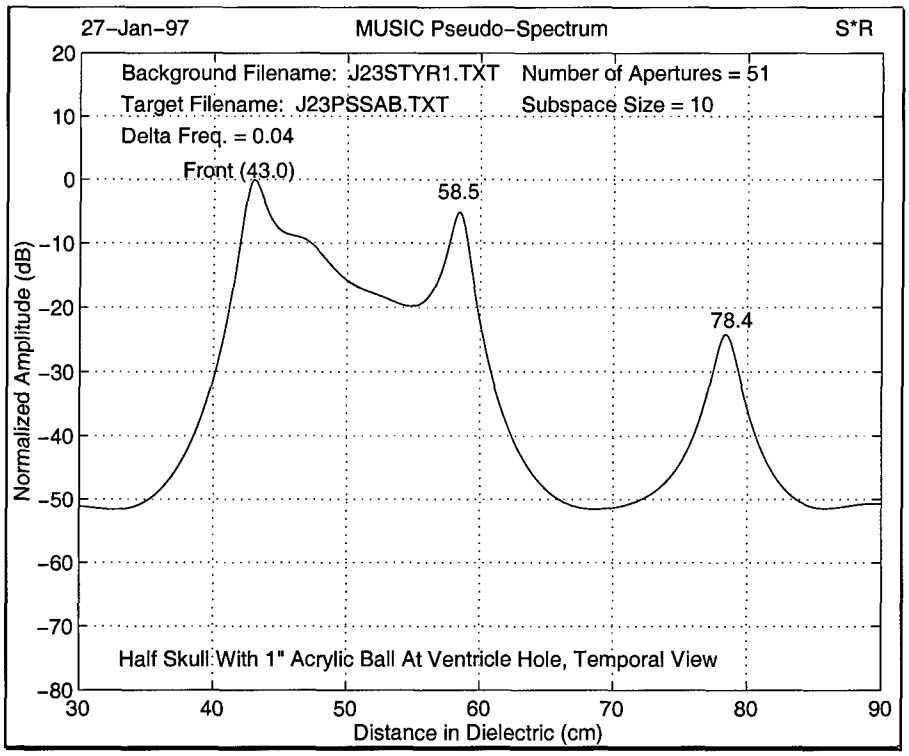

Figure 46: Half Skull With 1" Acrylic Ball At Ventricle Hole, Temporal View.

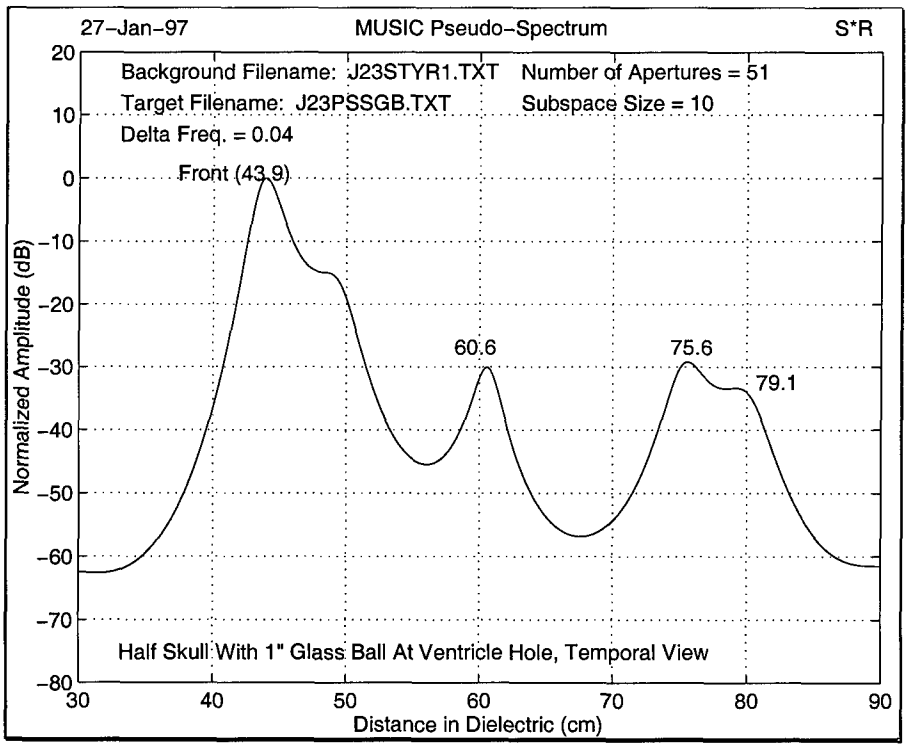

Figure 47: Half Skull With 1" Glass Ball At Ventricle Hole, Temporal View.

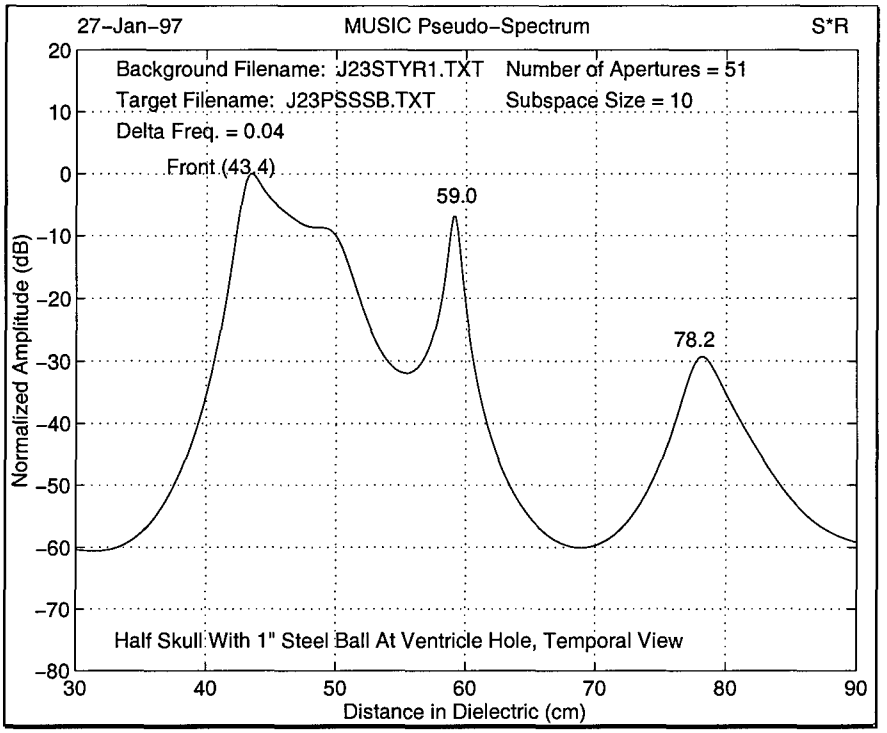

Figure 48: Half Skull With 1" Steel Ball At Ventricle Hole, Temporal View.

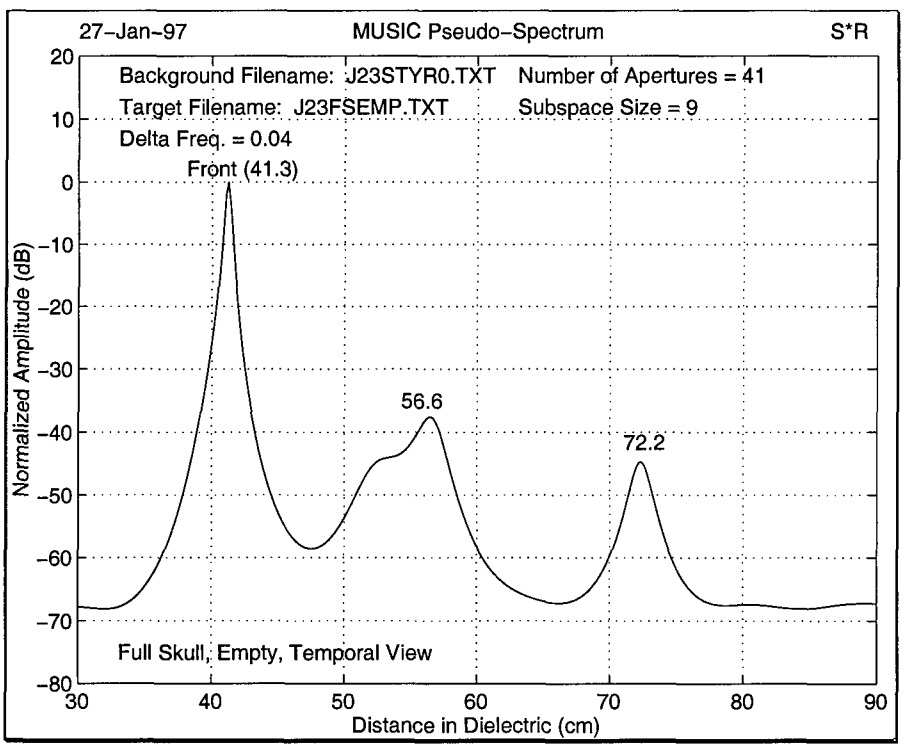

Figure 49: Whole Skull, Empty, Temporal View.

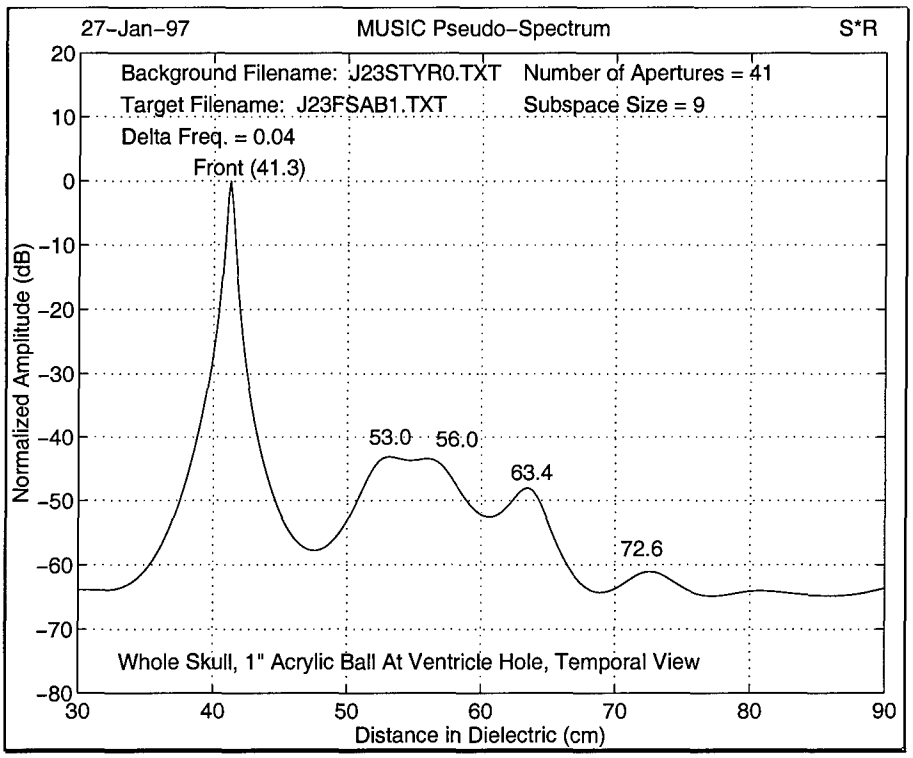

Figure 50: Whole Skull With 1" Acrylic Ball At Ventricle Hole, Temporal View.

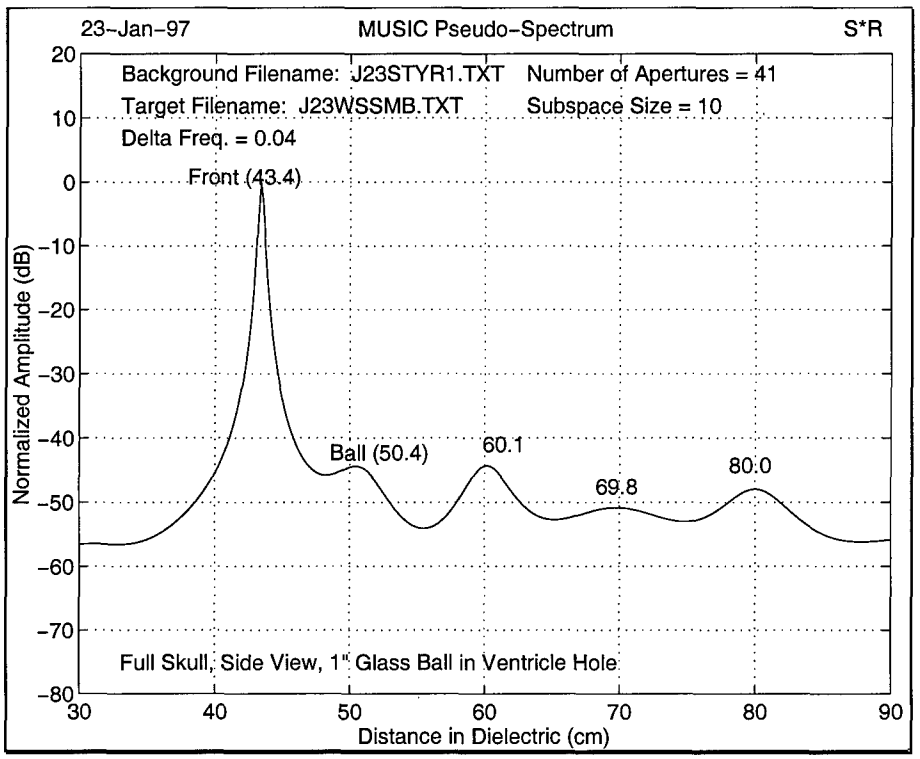

Figure 51: Whole Skull With 1" Glass Ball At Ventricle Hole, Temporal View.

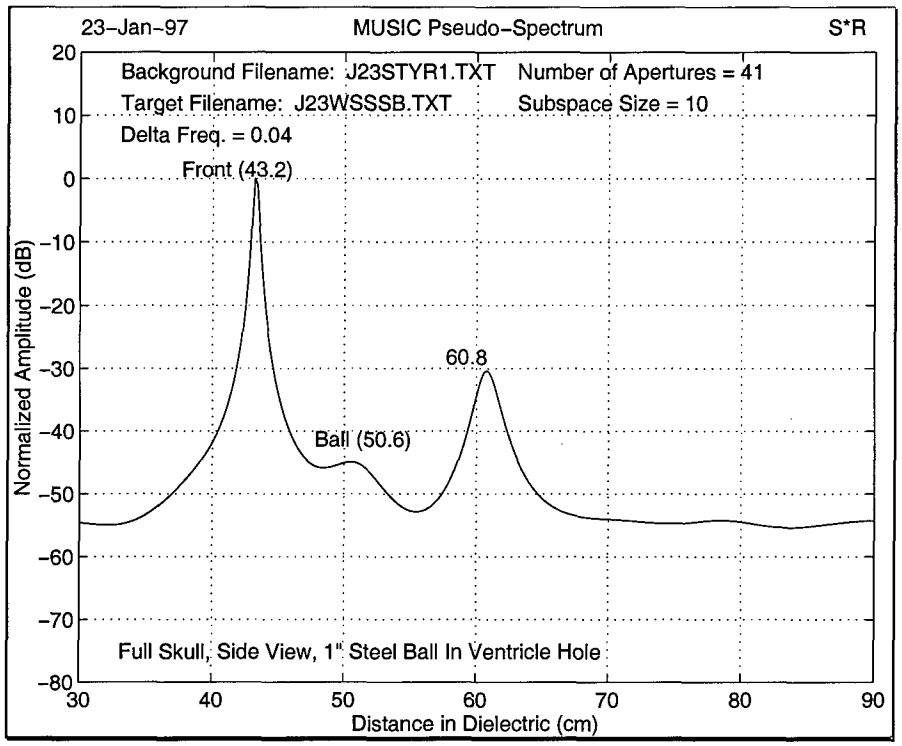

Figure 52: Whole Skull With 1" Steel Ball At Ventricle Hole, Temporal View.

4.4 Measurement Results for Porcine Brain

Measurements were made for a chemically fixed porcine brain placed against a human skull section to simulate the actual conditions under which the instrument would be used. The skull section was placed on the support as a bowl and two brains were placed into the bowl with minimal separation between the skull surface and the brain. The reflected signal was measured and processed to determine the interface signature. Figures 5 - 8 present the signature of the skull interface backed by two porcine brains compared with the signature of the interface of the skull backed by the two porcine brains containing an intervening layer of blood. Signature data are presented as, real part, imaginary part, amplitude and phase versus frequency.

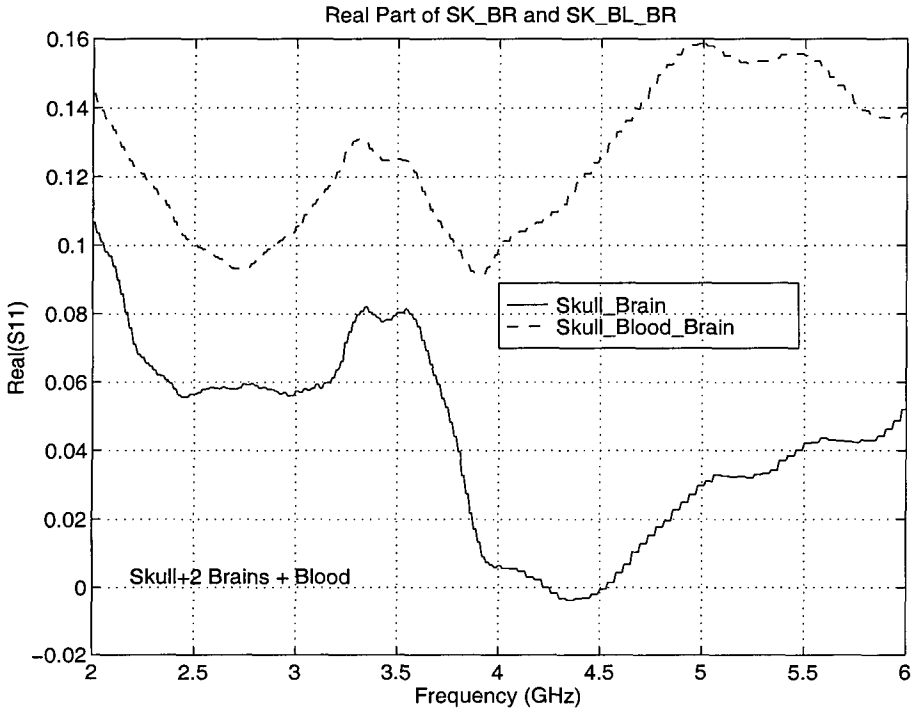

Figure 53. Real Part of Skull/ Skull-Brain Signature.

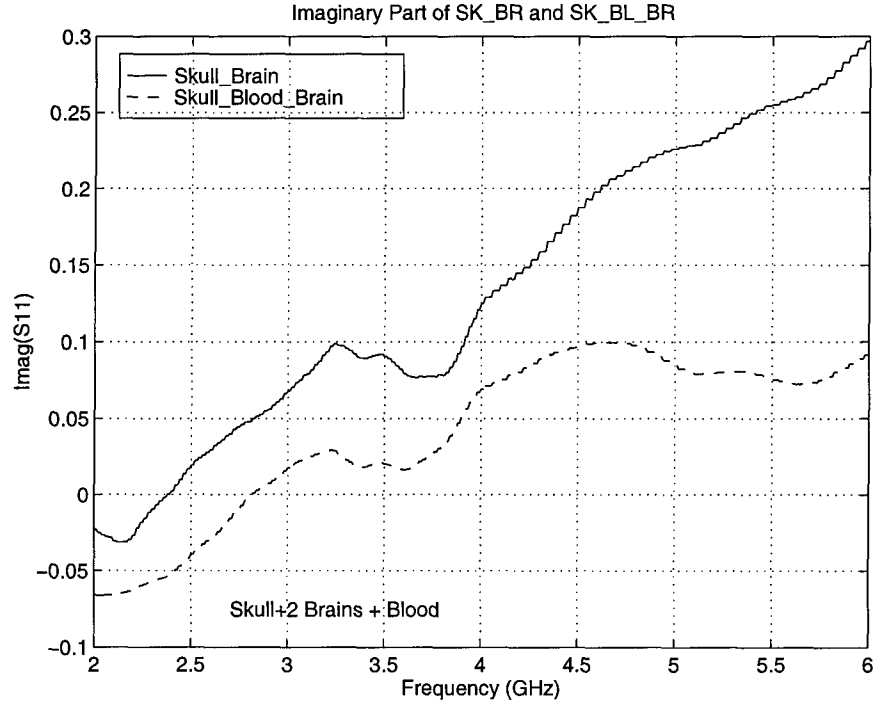

Figure 54. Imaginary Part of Skull/ Skull-Brain Signature.

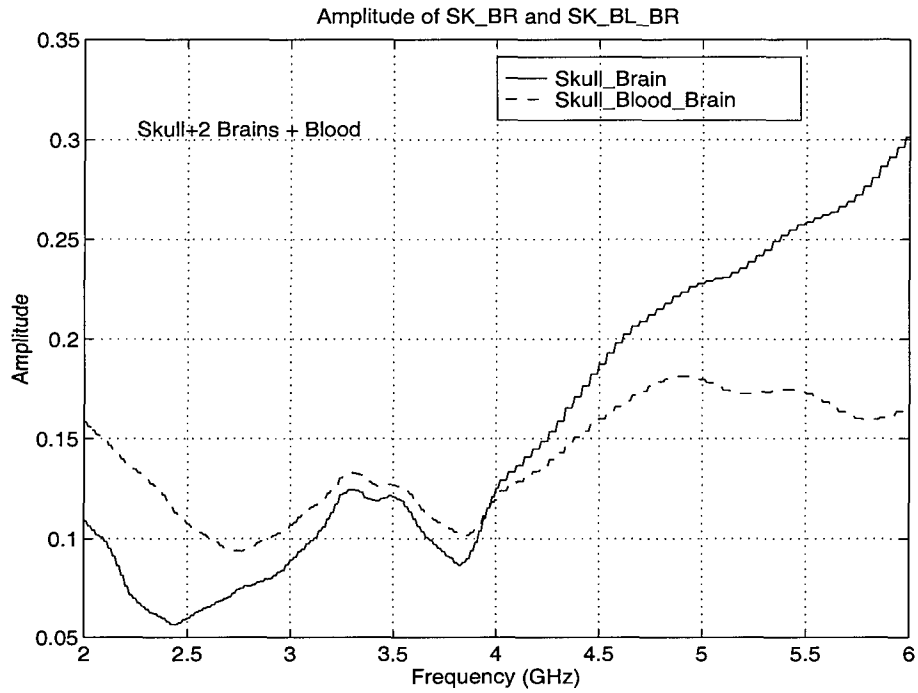

Figure 55. Amplitude of Skull/ Skull-Brain Signature.

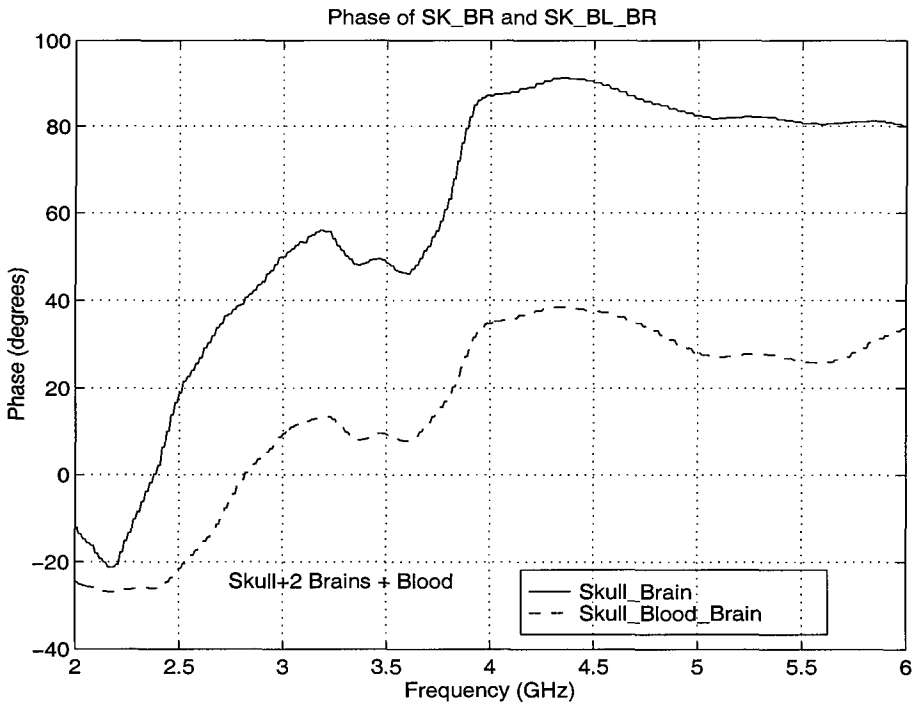

Figure 56. Phase of Skull/ Skull-Brain Signature.

Note that there are quite discernible differences between the signatures, indicating the effect of the presence of the brain on the reflected signal. It appears that obtaining the real and imaginary parts of the backscattered signal will be the most effective way of declaring the presence of blood behind the skull. It is this effect that presents an opportunity to detect the presence or absence of subdural hematomas. Employment of standard neural net algorithms will enhance the detection probability and reduce the human interface in the system. Current research is directed to the development of a more usable applicator and reducing the size and complexity of the hardware. Extensive additional measurements are to undertaken using other models to provide an adequate statistical sample to permit the definition of the appropriate neural net algorithms for later implementation.

5.0 CONCLUSIONS and RECOMMENDATION for FURTHER RESEARCH

Hemorrhage site location using microwaves offers an interesting new modality for "first responder" diagnosis and treatment of closed head injuries. Potentially, this can be extended to include both hemothorax and pneumothorax injuries making the instrument a major addition to the capability of the diagnostician. The important concepts and results: 1) The detection/location technique utilizes electromagnetic backscattering, 2) This backscatter is due to discontinuities in permittivity between interfaces in the body, 3) Blood/Brain interfaces have sufficiently high contrast ratios to be detected using this technique.

6.0 ACKNOWLEDGEMENT

This work was supported by the U. S. Army Medical Research and Materiel Command, Combat Casualty Care Research Branch, under Contract DAMD17-96-C-6074. We gratefully acknowledge the interest and support of Col. William Wiesmann, M.D. (Ret'd), and Major Stephen Bruttig, Ph.D (Ret'd) throughout this effort. Also the support of LTC Geoff Ling, M.D. is greatly appreciated.

7.0 REFERENCES

1. Johnson, C. C. and Guy, A. W., "Nonionizing Electromagnetic Wave Effects in Biological Materials and Systems," Proceedings of the IEEE, Vol. 60, No. 6, June, 1972, pp. 692-718.

2. Schepps, J. L. and Foster, K. R., "The UHF and Microwave Dielectric Properties of Normal and Tumour Tissues: Variation in Dielectric Properties with Tissue Water Content," Physics in Medicine and Biology, 1980, Vol. 25, pp. 1149-1159.

3. Pethig, R., "Dielectric Properties of Biological Materials: Biophysical and Medical Applications," IEEE Transactions on Electrical Insulation , Vol. EI-19, No. 5, October, 1984, pp. 453-474.

4. Campbell, A. M. and Land, D. V., "Dielectric Properties of Female Human Breast Tissue Measured *in vitro* at 3.2 GHz," Physics in Medicine and Biology, 1992, Vol. 37, No. 1, pp. 193-210.

5. Campbell, A. M. and Land, D. V., "A Quick Accurate Method for Measuring the Microwave Dielectric Properties of Small Tissue Samples," Physics in Medicine and Biology, 1992, Vol. 37, No. 1, pp. 183-192.

6. Chaudhary, S. S., et. al., "Dielectric Properties of Normal and Malignant Human Breast Tissues at Radiowave and Microwave Frequencies," Indian Journal of Biochemistry and Biophysics, Vol. 21, February, 1984, pp. 76-79.

7. Gandhi, O.P., and Chen, Jin-Yeun, "Electromagnetic Absorption in the Human Head from Experimental 6 GHz Handheld Transceivers," Transactions on Electromagnetic Compatibility, Vol. 37, No. 4, November, 1995, pp. 547-558

8. Wold, H., *A Study in the Analysis of Stationary Times Series*, Almqvist and Wiksell, Uppsala, Sweden.

9. Pisarenko, V. F., "The retrieval of harmonics from the covariance function," Geophysical Journal of the Royal Astronomical Society, Vol. 33, pp 276-290, 1973.

10. Schmidt, R. O., "Multiple Emitter Location and Signal Parameter Estimation," IEEE Transactions on Antennas and Propagation, Vol. AP-34, no. 3, pp. 276-280, March, 1986.

12. Schmidt, R. O., "Multiple Emitter Location and Signal Parameter Estimation," Proceedings of the RADC Spectrum Estimation Workshop, pp 243-258, Rome Air Development Center, 1979.

13. Shan, T-J., Wax, M., and Kailath, T., "On Spatial Smoothing for Direction-of-Arrival Estimation of Coherent Signals," IEEE Transactions on Acoustics, Speech, and Signal Processing, Vol. ASSP-33, No. 4, August, 1985.

14. Carrel, R., "The Design of Log-Periodic Dipole Antennas," IRE Convention Record, Part 1, pp. 61-75, 1961.

15. Campbell, C. K., et. al., "Design of a Stripline Log-Periodic Antenna," IEEE Transactions on Antennas and Propagation, Vol. AP-25, No. 5, September, 1975, pp. 718-721.

16. Pantoja, R. R., et. al., "A Microwave Printed Planar Log-Periodic Dipole Array," IEEE Transactions on Antennas and Propagation, Vol. AP-35, No. 10, October, 1987, pp. 1176-1178.

A.0 Appendix A. Details of the MUSIC Algorithm

A.1 Introduction

Spectra*Research has developed a technique applicable to hemorrhage detection that permits the user to detect, classify and identify hemorrhage sites. We have demonstrated experimentally and analytically the application of 1) Electromagnetic waves and 2) An existing signal processing technique, modified to improve performance of blood pool detection. This has led to the definition of a wide band electromagnetic signature for biological targets.

Our signal processing technique, a variation of the Multiple Signal Classification Algorithm (MUSIC) produces signatures that can be used to uniquely characterize targets. Target signatures have been measured in the laboratory. These signature results are the most important part of the technical work.

A.2 Physical Significance of Auto-correlation

Use of the Wold decomposition provides a means of applying methods from random process theory to analyze the performance of systems. Wold proved that any signal can be written in the following form:

$$s = r + \eta,$$

where r is the known signal and η is a Gaussian noise. Angle of Arrival (AOA) problems are of this kind, except that the known signal has a very specific form . AOA is concerned with two aspects of the problem, 1) Spatial location of the signal source, and 2) Signal identification. Since the sources of signals impinging on an aircraft are from radar, communications and electronic warfare systems, and such systems operate using known frequencies and modulations, the only major problem is spatial location, since the other signal properties can be determined by channelizing the receiver, and signal processing. Spatial location can be accomplished using an array of receivers with known properties, located in a known pattern. This concept is shown below.

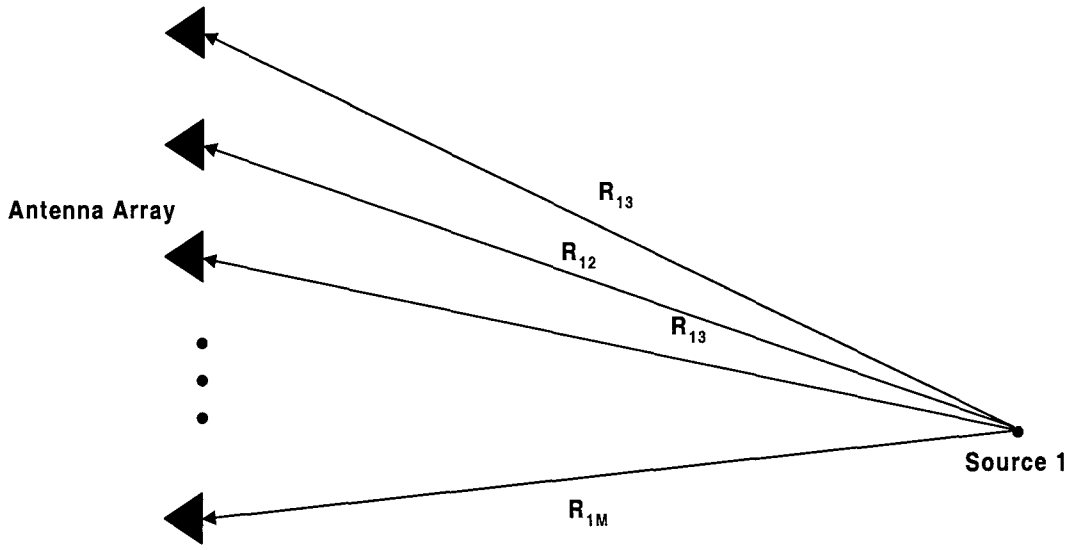

Figure A.1 Spatial Array MUSIC.

Another method for accomplishing the same result that offers a possible new electromagnetic imaging technique is to use a single antenna to transmit and receive, and operate the system over a wide band of frequencies. This obviously is not possible in the AOA problem, but for problems that involve the detection, location and identification of passive targets, this is an opportunity to accomplish a task that has significant importance in several communities. This system is shown in the diagram below.

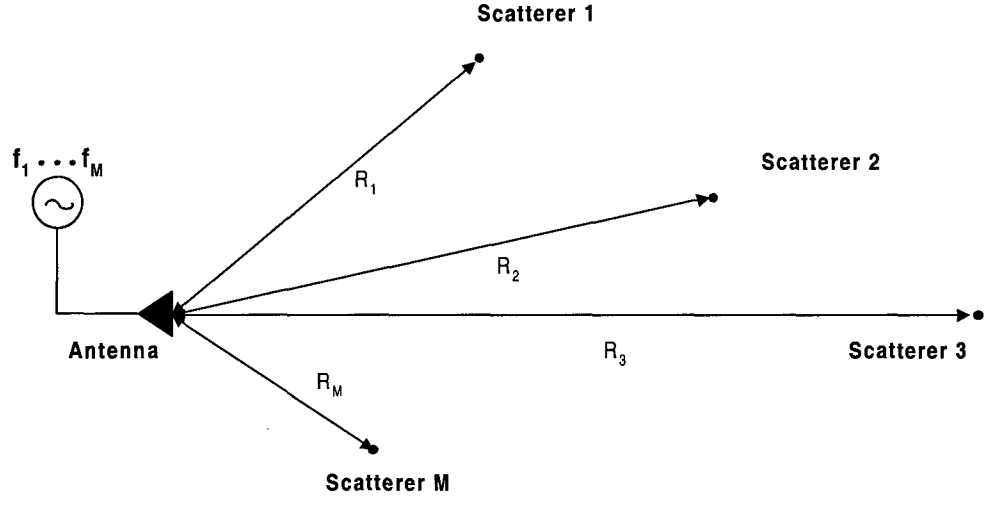

Figure A.2 Frequency Array MUSIC

A hemorrhage detection system (HDS) can be developed that operate over a relatively wide band of frequencies, stepping in frequency at some frequency step suitable for achieving the desired system performance. The choice of frequency band will be dictated by the physics of the

problem. For the hemorrhage detection problem, or medical detection, the frequency band will be centered at a frequency that optimizes the desired response with minimal degradation as the band edges are approached from above or below.

As an example, the case for hemorrhage detection, one would likely choose a frequency in the 0.5 - 2 GHz range to obtain the best possible tissue penetration. Using a high frequency such as X-band would be suitable for surface detection, but would have limited, if any, brain penetration. Thus the physics of the problem will drive the selection of the operating parameters for the system.

A.2.1 Auto-correlation of Continuous Signals

A concept from signal processing is that of the auto-correlation of a function. Auto-correlation for a continuous function is defined by the following expression,

$$R(\tau) = \int_{-\infty}^{\infty} f(x) f(x-\tau) dx ,$$

This is a measure of the "closeness" of the function and a shifted version of itself. The result is a function of the parameter τ . The function should be real valued since one would like to have some ability to compare two values of $R(\tau)$ and if the quantity is not real such comparisons cannot be made. Auto-correlation can be defined for complex valued functions as:

$$R(\tau) = \int_{-\infty}^{\infty} f^*(x) f(x-\tau) dx ,$$

The frequency domain properties of f are desired, hence the Fourier transform can be taken. It is of some interest to take the transform of $R(\tau)$ and consider this result. Taking this we obtain:

$$\Im[R(\tau)] = \int_{-\infty}^{\infty} R(\tau) e^{j\omega\tau} d\tau = |F(\omega)|^2 , \text{ where,}$$

$F(\omega)$ is the Fourier transform of the function f . This is "the power in the function f ." This can be seen if we consider the function as a voltage and the voltage be assumed to exist on a 1Ω resistor .

A.2.1.1 Auto-correlation of Stepped Frequency Signals

Thus the transformed auto-correlation contains information on which frequencies one would expect to have the greatest concentration of the signal power. This is of particular interest if one is measuring the reflected signals from scatterers. Figure 2 is an example of just this situation.

How one can use such information is directly dependent upon the excitation used. Suppose we have a situation where we have M scatterers and illuminate this constellation with a source having a signal that is of the form:

$$s(\omega) = e^{j\left(\frac{\omega}{c}\right)x}.$$

Let the radian frequency be $2\pi f$, and the resulting signal is:

$$s(\omega) = e^{j\left(\frac{2\pi f}{c}\right)x} = e^{j2\pi f\left(\frac{x}{c}\right)} = e^{2\pi ft}.$$

Letting the frequency become discrete leads to a set of frequencies that are used to interrogate the terrain, $\{f_1, f_2, \ldots, f_M\}$. Each frequency is permitted to exist for a finite duration during which the target region is illuminated. A frequency-time plot is presented below:

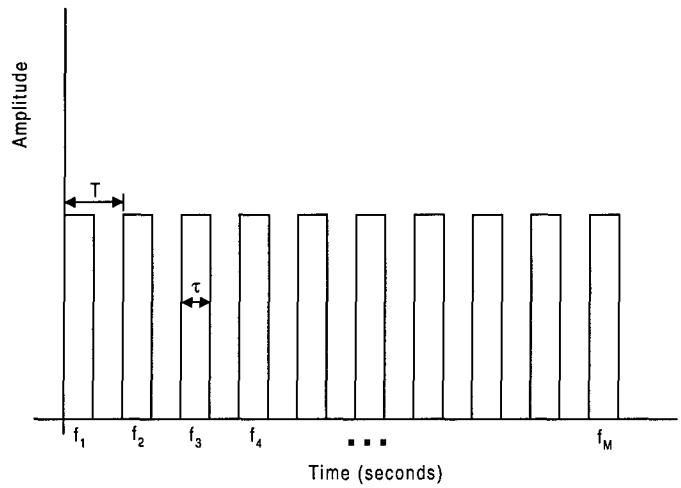

Figure A.3 Time-Frequency Plot.

The signal repeats every T seconds, and is of τ seconds in duration. This can be thought of as a set of individual signals, each a CW signal having time harmonic dependence. These signals are used to illuminate the terrain and the return is received and processed.

The reflected signal from the l^{th} scatterer is given by:

$$s_l(\omega) = \Gamma_l e^{j\left(\frac{\omega}{c}\right)x_l} = \Gamma_l e^{j2\pi ft_l},$$

Where f, is the cyclic frequency, and t_l is the two-way travel time from the source to the l^{th} scatterer and back, and Γ_l is the reflection coefficient for the l^{th} scatterer. The total signal is the vector sum of the M reflected signals from the scatterers in the illuminated region. This is just,

$$s_T(\omega) = \sum_{l=1}^{M} s_l(\omega) = \sum_{l=1}^{M} \Gamma_l e^{j2\pi f t_l}$$

We know that there will be additive noise present in the system and this will be frequency dependent also. This will modify the form above to,

$$s_T(f) = \sum_{l=1}^{M} \Gamma_l e^{j2\pi f t_l} + \eta(f)$$

This then is the signal with which the system will have to work.

A.2.2 Auto-Correlation of Discrete Frequency Signals

Since the signal is composed of desired and undesired components, we need to have some method of separating these out. A single frequency measurement cannot determine the desired information, more data must be obtained. The spatial measurement uses all of the antennas in the array to increase the information content in the measurement. The extension to the frequency domain case will require that one take data over N frequencies, and then perform some operation on this data to determine scatterer location. The resulting data will be of the form:

$$s_T(f_m) = \sum_{l=1}^{M} \Gamma_l e^{j2\pi f_m t_l} + \eta(f_m)$$

This equation is true for $m = 1,2,3\ldots,N$, and leads to the following set of equations:

$$\begin{aligned} s_T(f_1) &= \sum_{l=1}^{M} \Gamma_l e^{2\pi j f_1 t_l} + \eta(f_1) \\ s_T(f_2) &= \sum_{l=1}^{M} \Gamma_l e^{2\pi j f_2 t_l} + \eta(f_2) \\ &\vdots \\ s_T(f_N) &= \sum_{l=1}^{M} \Gamma_l e^{2\pi j f_N t_l} + \eta(f_N) \end{aligned}$$

This is a set of N equations in M unknowns, and the ability to obtain the solution will depend on the relationship between N and M. The system can be written in a matrix form by noting that the left hand side of the equation is a column vector and that the right hand side is the sum of a vector-matrix product (a column vector) and another column vector. This is conveniently written as:

$$\bar{s}_T = \overline{\overline{P}}\,\overline{\Gamma} + \overline{\eta}\,,$$

where matrix notation has been used to compress the space on the page. How the data is processed is the next question that must be answered. Since we are receiving the signals from a number of discrete sources, we would like some means of "separating" the various contributions. One method of accomplishing this is to investigate the auto-correlation of the backscattered signal. The resulting matrix will have an eigen-structure that will permit the desired information to be obtained. The next section will discuss the method used to accomplish this, the MUSIC algorithm.

A.2.3 MUSIC Algorithm

The original development of this algorithm was based on the early work of Pisarenko, and extended by Schmidt in the early 1980's. Schmidt's work was directed to the angle of arrival estimation problem and used the spatial array method. We propose to use multiple frequencies and measure the reflected signal.

Let there be M measurements made of the reflected signal, at the frequencies, $\{f_1, f_2, \ldots, f_M\}$. The auto-correlation matrix is given by the following expression,

$$\overline{\overline{C}} = E(\bar{s}_T \bar{s}_T^H), \text{ where,}$$

$\bar{s}_T = \overline{\overline{P}}\,\overline{\Gamma} + \overline{\eta}$,and all quantities are as previously defined.

This can be expanded using the definition of the total signal, the result, assuming that signals and noise are uncorrelated. This can be expanded in the following manner.

$$\overline{\overline{C}} = E(\bar{s}_d \bar{s}_d^H) + E(\eta\eta^H),$$

We have let the decomposition of the signal be in the form:

$$\bar{s}_d = \overline{\overline{P}}\,\overline{\Gamma},$$

the matrix contains the array properties, and the vector is the scattering properties of the various interfaces. The second term is the noise auto-correlation and can be treated, for the case of Gaussian noise, as a constant, σ_0^2 . Thus we can write,

$$\overline{\overline{C}} = E(\overline{\overline{P}}\,\overline{\Gamma}\overline{\Gamma}^H\overline{\overline{P}}^H) + \sigma_0^2\overline{\overline{I}}, \text{ where,}$$

$\overline{\overline{I}}$ is the identity matrix and σ_0^2 is the noise variance in the measurement. This matrix can lead to a significant result, that the measured signal vector space can be decomposed into two orthogonal subspaces as shown in Figure B.4. This is seen by simply considering the matrix-vector product,

$$\overline{\overline{C}}\,\overline{s}_d = E(\overline{\overline{P}}\,\overline{\Gamma}\overline{\Gamma}^H\overline{\overline{P}}^H)\overline{s}_d + \sigma_0^2\overline{\overline{I}}\overline{s}_d$$

Since the vector $\overline{s}_d$ is written in the following way: $\overline{s}_d = \overline{\overline{P}}\,\overline{\Gamma}$, using this in the equation above will yield:

$$\overline{\overline{C}}\,\overline{s}_d = E(\overline{\overline{P}}\,\overline{\Gamma}\overline{\Gamma}^H\overline{\overline{P}}^H)\overline{\overline{P}}\,\overline{\Gamma} + \sigma_0^2\overline{\overline{I}}\overline{s}_d$$

$$\overline{\overline{C}}\,\overline{s}_d = E[\overline{\overline{P}}\,\overline{\Gamma}(\overline{\Gamma}^H\overline{\Gamma})(\overline{\overline{P}}^H\overline{\overline{P}})] + \sigma_0^2\overline{\overline{I}}\overline{s}_d$$

$$\overline{\overline{C}}\,\overline{s}_d = E[(\overline{\Gamma}^H\overline{\Gamma})(\overline{\overline{P}}^H\overline{\overline{P}})\overline{\overline{P}}\,\overline{\Gamma}] + \sigma_0^2\overline{\overline{I}}\overline{s}_d$$

$$\overline{\overline{C}}\,\overline{s}_d = E[(\overline{\Gamma}^H\overline{\Gamma})(\overline{\overline{P}}^H\overline{\overline{P}})]\overline{\overline{I}}\overline{s}_d + \sigma_0^2\overline{\overline{I}}\overline{s}_d$$

$$\overline{\overline{C}}\,\overline{s}_d = [E((\overline{\Gamma}^H\overline{\Gamma})(\overline{\overline{P}}^H\overline{\overline{P}})) + \sigma_0^2)]\overline{s}_d = \lambda_C\overline{s}_d$$

This is a statement of the eigenvalue problem, a solution to which is easily obtained. The matrix $\overline{\overline{C}}$ has dimension M, thus if the matrix has full rank it will have M eigenvectors and eigenvalues. If it is not of full rank, then there will be some number of degenerate eigenvectors. A member of the set of degenerate eigenvectors has the same eigenvalue as the other members of the set. One can see that the smallest value that λ_C takes on is when the first term in brackets is zero. Thus we have a set of eigenvectors having as their eigenvalue, σ_0^2. These are the noise eigenvectors of the measured signal.

If there are N signals then there will be N signal eigenvectors if the individual signals are uncorrelated and thus $M - N$ noise eigenvectors. Since a priori knowledge of the actual number of signals in a measurement is not necessarily a known in advance, one can make an educated guess as to the number and then test the quality of the guess by plotting the eigenvalue spectrum.

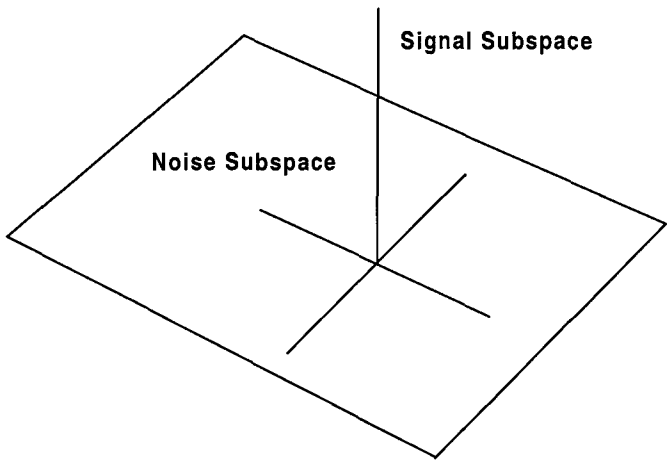

Figure A.4. Decomposition of Measured Signal Space into Two Orthogonal Subspaces.

A.2.4 A Decorrelation Technique

Signals used in the interrogation of a region are a sequence of single frequencies with known amplitude and phase relationships. At a frequency f signals are of the form,

$$s(f) = \Gamma_1 e^{j2\pi f t_1} + \ldots + \Gamma_M e^{j2\pi f t_M} + \eta(f).$$

Data are gathered at a number of frequencies and the resulting system of received signals is used to form the correlation matrix. If the signals (frequencies) are uncorrelated then one obtains the previous results and a distinct decomposition into the subspaces illustrated in Figure B.4 occurs. This procedure is also valid if the signals are partially correlated, the only real difficulty occurs if there is perfect correlation between the signals. Since the signal source for our interrogation is the swept source of the vector network analyzer, coherence of the signals is a problem and one must apply the method to achieve the performance expected from MUSIC.

Algorithm performance is greatly improved if the signals are more nearly uncorrelated than for correlated cases. Hence a method has been developed to "decorrelate" the signals. This method we refer to as "averaging" and is an integral part of the Hemorrhage Detection System signal processing algorithm. This section will describe the technique and its application to the problem. The technique can be best understood by considering a special case having a limited number of frequencies and scatterers. This will enable the reader to better understand the process and its importance.

Let the interrogated region contain two scatterers characterized by their respective reflection coefficients, Γ_1 and Γ_2. Let data be taken at four frequencies, f_1, f_2, f_3, f_4. One can view the data taken at the various frequencies as being taken over an array of antennas. The arrays are defined by the user and for this example, one can write:

$$\begin{aligned} r_1 &= \sum_{l=1}^{2} \Gamma_l e^{2\pi j f_1 t_l} + \eta(f_1) \\ r_2 &= \sum_{l=1}^{2} \Gamma_l e^{2\pi j f_2 t_l} + \eta(f_2) \\ &\vdots \\ r_4 &= \sum_{l=1}^{2} \Gamma_l e^{2\pi j f_4 t_l} + \eta(f_4) \end{aligned}$$

These relations, each defining a received signal in the frequency domain, can be written in matrix-vector form as:

$$\bar{s} = \bar{\bar{A}}\bar{\Gamma} + \bar{\eta},$$

where the quantities are as defined before. This form for the signal is representative of the entire data set, processed to find the eigenstructure. One can use this very simple case to illustrate the

application of the decorrelation scheme. Figure 6 shown below defines a set of arrays that can be used for processing.

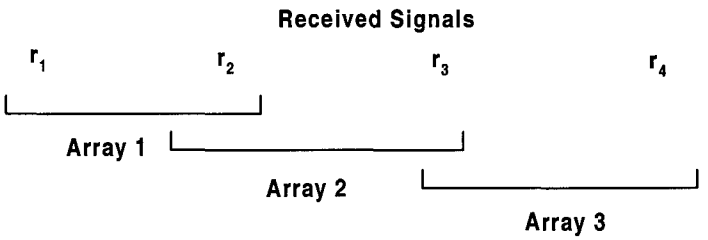

Figure A.5 Array Definition for Decorrelation Processing.

We assume the existence of received data r_k at four frequencies and form an overlapped set of subsets of the signals. Let array 1 be defined by:

$$\bar{r}_1 = \begin{bmatrix} r_1 \\ r_2 \end{bmatrix}, \text{ where,}$$

$$\begin{aligned} r_1 &= \sum_{l=1}^{2} \Gamma_l e^{2\pi i f_1 t_l} + \eta(f_1) \\ r_2 &= \sum_{l=1}^{2} \Gamma_l e^{2\pi i f_2 t_l} + \eta(f_2) \end{aligned},$$

This will permit us to write the above in the following compact form:

$$\bar{r}_1 = \bar{\bar{A}}\bar{\Gamma} + \bar{\eta}$$

Prior to further discussion, let us consider some results from matrix algebra. Let there be defined two matrices, $\bar{\bar{A}}$, and $\bar{\bar{D}}$. These are defined in the following way:

$\bar{\bar{A}} = \begin{bmatrix} a & b \\ c & d \end{bmatrix}$, and $\bar{\bar{D}} = \begin{bmatrix} \alpha & 0 \\ 0 & \beta \end{bmatrix}$. We will encounter products involving these two matrices in the course of this work.. Consider forming powers of $\bar{\bar{D}}$, e.g. $\bar{\bar{D}}^N$. Using matrix multiplication and induction on the exponent, we can prove that,

$$\bar{\bar{D}}^N = \begin{bmatrix} \alpha^N & 0 \\ 0 & \beta^N \end{bmatrix}.$$

Next consider the product, $\bar{\bar{A}}\bar{\bar{D}}$. This is just:

$$\overline{\overline{AD}} = \begin{bmatrix} \alpha a & \beta b \\ \alpha c & \beta d \end{bmatrix}.$$

This will enable us to write the products in terms that are formed in the development of the correlation matrix in a much simpler form. With these useful relationships the data will be processed as arrays, which has the effect of taking a moving average through the data. This process will remove many of the "small" signals that appear in the correlation matrix, leaving only the most important signals.

The other arrays are defined in a similar fashion, except that for the remainder of the arrays we must include a another matrix D, defined as:

$$\overline{\overline{D}} = \begin{bmatrix} e^{-2\pi j \Delta f t_1} & 0 \\ 0 & e^{-2\pi j \Delta f t_2} \end{bmatrix}, \text{ where,}$$

Δf is the frequency increment in the measurement system. This happens because each array is taken over a set of frequencies that differ by a one frequency increment. The result for the k^{th} array is:

$$\overline{r}_k = \overline{\overline{AD}}^{k-1}\overline{\Gamma} + \overline{\eta}\,.$$

The next step is to form the correlation matrix using each of the matrices formed from the sub-arrays. This leads to the following result for the k^{th} correlation matrix, R_k.

$$R_k = E\left[\overline{\overline{AD}}^{k-1}(\overline{\Gamma}\overline{\Gamma}^H)\overline{\overline{D}}^{k-1}\overline{\overline{A}}^H\right] + \sigma^2\overline{\overline{I}}\,, \text{ where,}$$

E denotes the expectation operator, and the superscript H denotes the hermitian conjugate of the matrix. The final step is to form the average of the various correlation matrices, the result is:

$$R_{avg} = \frac{1}{M}\sum_{k=1}^{M} R_k\,.$$

This is used to decorrelate the received signals removing the effects of coherence and producing a new correlation matrix with an eigenstructure having the most well-defined signal and noise subspaces. There being a finite group of signal eigenvectors, and a second finite group of noise eigenvectors.

The technique also assumes a reasonable guess at the number of signals is available. This will require skill on the part of the user to estimate the number of signals so as not to overwhelm himself with the interpretation of the results.

There are several techniques available to "remove" known scatterers from the problem, and these have proven to be very effective in producing results. We have identified one technique, background subtraction that can remove known scatterers leaving only signals of interest. A second technique known as "peak subtraction" can be used to remove selected signals from the received signal data, and a third which was not implemented in this study is the application of a constrained MUSIC algorithm. Later paragraphs will describe the first two techniques in detail. The principle of constrained MUSIC is briefly described in the next section.

A.2.5 Constrained MUSIC Algorithm

An alternative technique that significantly improves the estimation of the location and the frequency response of the unknown targets by reducing, if not eliminating, the effect of the known sources on the MUSIC algorithm. MUSIC algorithm essentially separates the data space into the noise subspace and the signal subspace and searches the "array manifold" to for those time delays steering vectors corresponding to which are orthogonal or nearly orthogonal to the noise subspace. The effect of sources at known locations may be reduced by introducing constraints into the MUSIC algorithm. Let us define the space of all the steering vectors corresponding to the time delays of known sources as:

$$C = \left[c_1, c_2, c_3, \ldots\ldots c_p\right],$$

where c_i are steering vectors corresponding to known sources. The noise subspace is now constrained to be orthogonal to **C.** This is accomplished by recognizing that the projection of the column space of X, the data space, into the orthogonal complement of the constraint space C, result in the projected columns of X being orthogonal to the noise subspace. The modified data space is now given by,

$$\hat{X} = X - P_C X.$$
$$P_C = C\left(C^H C\right)^{-1} C^H$$

MUSIC algorithm carried out with this modified data space which incorporates the known source locations will enhance the estimation of the unknown signal information.

A.2.6 Determination of Scatterer Frequency Dependence.

Scattering by a dielectric is dependent upon the properties of the medium in which the wave is propagating and on the material the wave interacts with. The geometry is shown below.

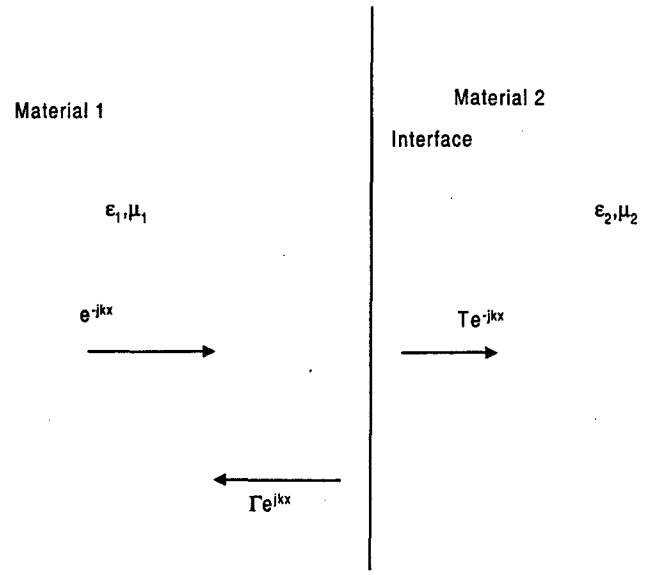

Figure A.6 Electromagnetic Propagtion at an Interface.

The situation is such that a wave impinges upon the interface and to satisfy the boundary conditions, a reflected wave is set up. The remainder is transmitted into the second material. The reflected wave is characterized by the coefficient Γ, the reflection coefficient. This coefficient is in general, complex and thus the amplitude of the reflection coefficient is the quantity of concern. The value of the reflection coefficient depends upon the wave impedance in each material. This dependence is,

$$\Gamma = \frac{Z_1 - Z_0}{Z_1 + Z_0}.$$

The wave impedance in turn, depends upon the constitutive parameters of the materials. i.e.

$$Z_k = \sqrt{\frac{\mu_k}{\varepsilon_k}}.$$

This dependence is the basis for the constitutive signature of biological materials. There is a second signature that is of importance, the geometrical signature. This characterizes the geometry of the interface and is used in imaging of the interface. The geometry of the interface can be simple, as depicted above or quite complex. This will render our brain image to be a functional image rather than an anatomical image.

We now consider the procedure for the determination of the scattering amplitude response at the p^{th} frequency $\Gamma_k(f_p)$, $k = 1,2,\cdots L$. Towards this end we consider a band of frequencies of width B_r and centered at f_p. Let there be $(N+1)$ samples of data over this band. The signal model corresponding to this band of frequencies is given by,

$$r_\ell = r(f_\ell) = \sum_{k=1}^{L} \Gamma_k(f_\ell)\, e^{-j2\pi f_\ell t_k}, \quad \ell = p - N/2, \cdots, p + N/2 .$$

Note that the scattering amplitudes are not assumed to be constant, and that the round trip time delays are assumed known and replaced by their estimates, t_k, previously determined. We assume a functional form for the k^{th} scattering amplitude function $\Gamma_k(f)$. These functional forms may be different for different values of k. For instance, it may be a polynomial of order q, as given by,

$$\Gamma_k(f) = \Gamma_{ko} + \Gamma_{k1} f + \Gamma_{k2} f^2 + \ldots + \Gamma_{kq} f^q .$$

Another possible functional form is a simple power rule:

$$\Gamma_k(f) = \Gamma_{ko} f^{\alpha} .$$

Biological materials have been measured over selected frequency ranges and the results are avilable in the literature. Such data has indicated that the dielectric properties are monotonically decreasing functions of frequency, e.g. $\varepsilon(f) = \alpha f^{-m}$. Since the reflection coefficient depends on the media involved in the scattering, we can use this *a priori* information to our advantage.

All the results presented in this report assume a polynomial functional form, and the order of the polynomial could be different for different values of k. The problem of obtaining the dispersion characteristics for the target may now be formulated as the determination of parameters $\Gamma_{k\ell}$, $k = 1,2,\cdots L$ *and* $\ell = 0,1,2\cdots q$, that results in the best match between the measured data and the signal model in a least squares sense.

Details of the formulation are best explained by considering a particular case with $L = 2$ and $q = 1$. The formulation may then be generalized for arbitrary L and q. For this case, the functional forms for $\Gamma_1(f)$ and $\Gamma_2(f)$ are given by,

$$\Gamma_1(f) = \Gamma_{10} + \Gamma_{11} f, \ \textit{and} \ \ \Gamma_2(f) = \Gamma_{20} + \Gamma_{21} f$$

The signal model, then, is given by,

$$\begin{aligned} r_o &= (\Gamma_{10} + \Gamma_{11} f_0)\, e^{-j2\pi f_0 t_1} + (\Gamma_{20} + \Gamma_{21} f_0)\, e^{-j2\pi f_0 t_2} + \varepsilon_0 \\ &\vdots \\ r_N &= (\Gamma_{10} + \Gamma_{11} f_0)\, e^{-j2\pi f_N t_1} + (\Gamma_{20} + \Gamma_{21} f_N)\, e^{-j2\pi f_N t_2} + \varepsilon_N . \end{aligned}$$

Note that, for notational convenience, the frequencies f_ℓ, $\ell = p - N/2$ *to* $p + N/2$ are renumbered from f_0 *to* f_N. The ε_k here represent the modeling errors. The measured signal at the k^{th} frequency, r_k, may be expressed, compactly, as,

$$r_k = \overline{\overline{W}}_k^H \overline{\Gamma} + \varepsilon_k, \qquad k = 0,1,\ldots,N$$

where,

$$\overline{\Gamma} = [\Gamma_{10}\, \Gamma_{11}\, \Gamma_{20}\, \Gamma_{21}]^T$$

$$W_k^H = [W_{k1}^H \; W_{k2}^H], \quad k = 0,1,\ldots\overline{N}$$

$$W_{kj}^H = [e^{-j2\pi f_k \hat{t}_j} \;\; f_k e^{-j2\pi f_k \hat{t}_j}], \quad j = 1,2.$$

The measurement vector, $\bar{r} = [r_0\; r_1 \ldots r_{\overline{N}}]^T$ may now be expressed as the sum of a matrix-vector product and an error term as,

$$\bar{r} = \mathbf{W}^H \overline{\Gamma} + \vec{\varepsilon}\,, \text{ where,}$$

$$\mathbf{W} = [W_0\; W_1 \ldots W_N], \text{ and}$$

$$\bar{\varepsilon} = [\varepsilon_0, \varepsilon_1, \ldots \varepsilon_N]^H$$

Our results continue to be valid for the L scattering centers and the $\Gamma_k(f)$ assumed to be represented by q^{th} order polynomials, with,

$$\vec{W}_k^T = [\vec{W}_{k1}^T\, \vec{W}_{k2}^T \ldots \vec{W}_{kL}^T]$$
$$\vec{W}_{kj}^T = [e^{-j2\pi f_k \hat{t}_j} \;\; f_k e^{-j2\pi f_k \hat{t}_j} \ldots f_k^q e^{-j2\pi f_k \hat{t}_j}], \quad j = 1,2,\cdots,L$$

$$\overline{\Gamma} = [\Gamma_{10} \ldots \Gamma_{1q}, \Gamma_{20} \ldots \Gamma_{2q}, \ldots, \Gamma_{L0} \ldots \Gamma_{Lq}]^T \quad .$$

The optimum parameter vector $\overline{\Gamma}_{opt}$ may now be determined by requiring the error power $J = \|\vec{\varepsilon}\|^2$ to be the least possible. Then,

$$J = \bar{\varepsilon}^H \bar{\varepsilon}$$

$$= (\bar{r} - \overline{\overline{W}}^H \overline{\Gamma})^H \; (\bar{r} - \overline{\overline{W}}^H \overline{\Gamma})$$

$$= \bar{r}^H \bar{r} - \bar{r}^H \overline{\overline{W}}^H \overline{\Gamma} - \overline{\Gamma}^H \overline{\overline{W}} \bar{r} + \overline{\Gamma}^H \overline{\overline{W}}\, \overline{\overline{W}}^H \overline{\Gamma}$$

Taking the gradient of the error power, J, with respect to $\overline{\Gamma}$ and setting the result to zero yields,

$$\nabla_{\overline{\Gamma}} J = -\overline{\overline{W}} \Gamma + \overline{\overline{W}}\, \overline{\overline{W}}^H \overline{\Gamma} = 0$$

Therefore, the optimum parameter vector, $\overline{\Gamma}_{opt}$ is given by,

$$\overline{\Gamma}_{opt} = (\overline{\overline{W}}\,\overline{\overline{W}}^{H})^{-1}\overline{\overline{W}}\,\overline{\Gamma}$$

Once this parameter vector is defined, the amplitude frequency responses evaluated at $\Gamma_k(f_p), k = 1,2,\ldots,L$, are readily determined. The frequency, then, is incremented from f_p *to* $f_p + \Delta f$ and the procedure is repeated to determine the frequency response at this new frequency. The frequency response over the entire band may be determined in this fashion, except for small bands of width $B_r/2$ at the edges of the band. Considerations for the proper choice of B_r and other parameters are discussed in the following paragraph.

The results obtained depend upon the choices made for the regression bandwidth, B_r, the frequency increment, Δf, and the number of subapertures, M, used to decorrelate $\overline{\overline{R}}$. The condition number of $(\overline{\overline{W}}\,\overline{\overline{W}}^{H})$ depends upon B_r. The condition number, defined as the ratio of the largest eigenvalue to the smallest eigenvalue, is high if B_r is too small and the system becomes ill-conditioned resulting in degraded estimates of scattering center frequency responses. The regression bandwidth corresponding to the first minimum of B_r as a function of the condition number of $(\overline{\overline{W}}\,\overline{\overline{W}}^{H})$ is the optimal choice. The choice of Δf determines the rate of sampling of the scattered fields in the frequency domain and as such dictates the range of time delays that are not aliased. The Δf must be chosen so that the expected range of time delays corresponding to the scattering centers on the target lie between $-1/2\Delta f$ and $1/2\Delta f$ Our results indicate that choosing the number of sub-apertures, M to be greater than one-half of the number frequency data points processed, decorrelates $\overline{\overline{R}}$ to a sufficient extent to permit the most significant scatterers to be located.

APPENDIX B: LOG-PERIODIC ANTENNA/APPLICATOR DESIGN

B.1 INTRODUCTION

A significant system member is the antenna/applicator. Initially a COTS antenna was used in the data collection. The antenna was an American Electronics Corporation wideband single ridged horn antenna. This device operates over the frequency range, 2 - 18 GHz and was chosen to offer the largest possible bandwidth. Since the constitutive properties of biological materials degrades the penetration as the frequency increases, it was determined that an antenna operating in the range 0.5 GHz to 2 GHz would be desirable. Such an antenna is the log-periodic dipole array (LPDA). As the program is ending, the antenna design remains in flux, with a final design as yet not available. This Appendix will briefly describe the operation of the LPDA and the relevant design methods.

B.2 OPERATION

The LPDA is a member of the class of antennas known as frequency independent antennas. These antennas operate over several octaves with nearly constant gain and voltage standing wave ratio (VSWR) over the band. The most commonly used antenna is the half-wave dipole. This antenna is easily constructed but has a very narrow bandwidth. This is due to the fact that the antenna has a physical length equal to one-half wavelength, and this is valid at a single frequency. This fact does not preclude the use of such a device but degraded gain and VSWR performance out-of-band is severe enough that data collection will also be degraded.

Rumsey has shown that an antenna that is designed using angle as the characteristic dimension, will be frequency independent. This occurs since the antenna does not radiate as a single length object, but the part of the object corresponding to a particular frequency radiates while the remaining part is quiescent. This allows one to design a radiator that can be compact yet operate over significantly increased bandwidths.

As an example, consider the operating range of the HDS, 0.5 GHz - 2 GHz, for a half wave dipole antenna, it would require a physical length of 60 cm (twice the half wave length dimension to include both arms of the antenna) at 0.5 GHz. Such a length is impractical for this application. Not only is this a problem, but the antenna operates efficiently only at this frequency, and its performance at the higher frequency would be diminished.

B.3 DESIGN

A solution to this problem was presented by Carrel. He proposed that an array of dipoles fed by a common transmission line be designed. The array would have a number of dipole elements determined to provide gain over a wide frequency range. A typical LPDA configuration is shown in Figure B1. The LPDA has the property that the longest element is one-half wavelength at the lowest frequency in the band of interest, and the shortest is one half wavelength at the highest frequency.

The elements between act to radiate the frequencies in the band and are related in the following way. If we define an angle α as shown in Figure B1. And use the apex of the angle as a measurement reference, then we can use the n^{th} dipole length and distance from the apex to write,

$$tan\left(\alpha/2\right) = \frac{(L_n/2)}{R_n}$$

similarly, on can write an expression for the $(n+1)^{st}$ ratio,

$$tan\left(\alpha/2\right) = \frac{(L_{n+1}/2)}{R_{n+1}}.$$

Thus, one has the result that

$$\tau = \frac{R_{n+1}}{R_n} = \frac{L_{n+1}}{L_n}.$$

The ratio τ is the scale factor for the LPDA, and the ratio of successive element positions is the same as the ratio of successive element lengths. The spacing factor of the LPDA, σ is defined by the ratio,

$$\sigma = \frac{d_n}{2L_n}.$$

With these two parameters and knowledge of the operating bandwidth, one can use the design curves presented in Figure B2. To obtain the desired gain for a given set of σ and τ.

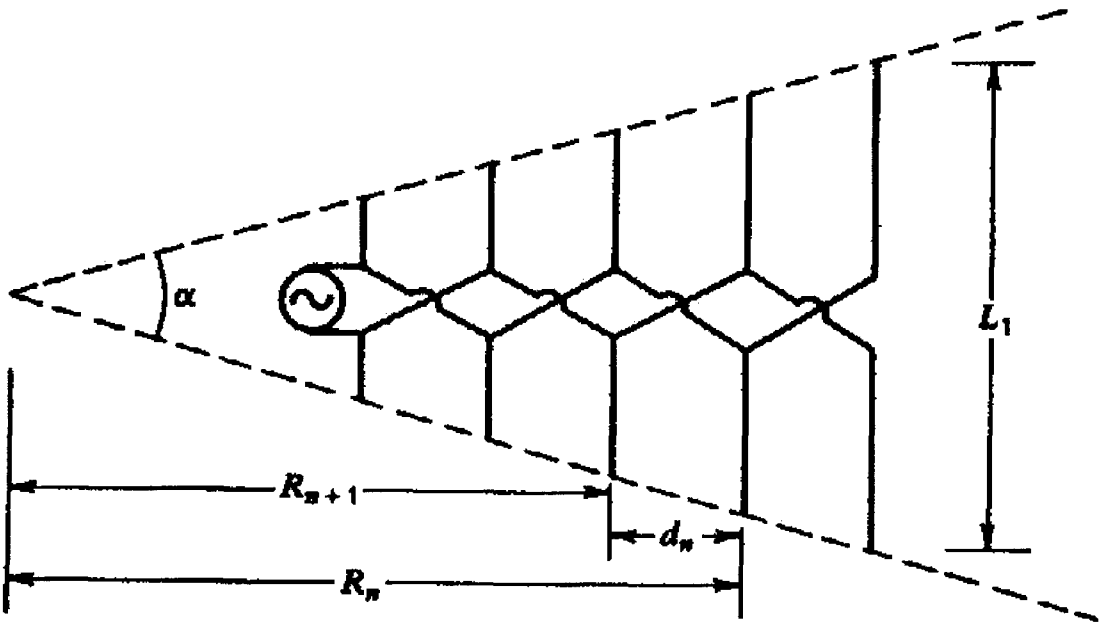

Figure B1. Typical LPDA Configuration.

The design for such an antenna will produce a physically large structure for operation in the low frequency region required for HDS. Thus we require a method whereby one could reduce the physical size of the antenna while maintaining the electrical performance.

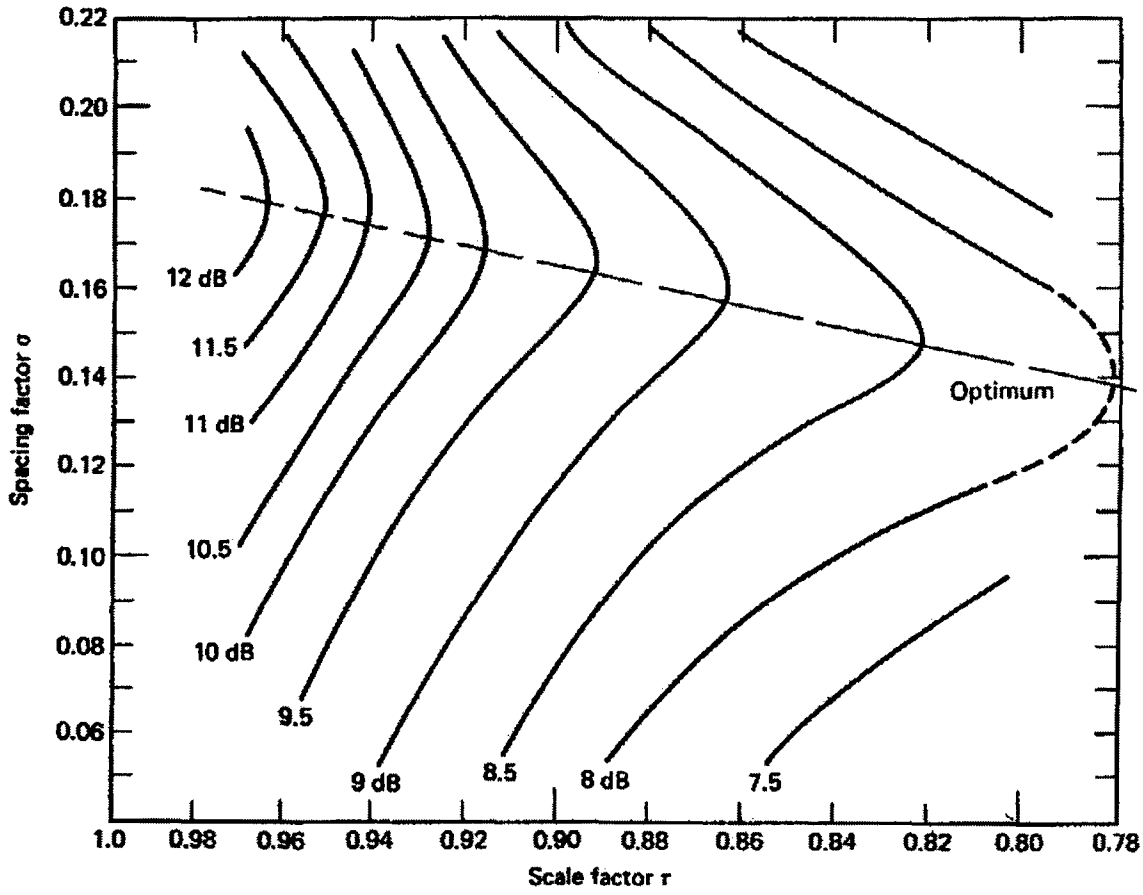

Figure B2. Graphical Design Curves for LPDA.

A solution to this problem is to operate in a region where the dielectric properties are different from those of free space. The advantage in doing this is the fact that the wavelength in the dielectric region is reduced relative to the free space wavelength. The relationship is,

$$\lambda_m = \frac{\lambda_0}{\sqrt{\varepsilon_r}}, \text{ where,}$$

λ_m is the wavelength in the material, and λ_0 is the free space wavelength, and ε_r is the relative permittivity of the region. This will reduce the electrical dimensions of the log-periodic antenna by the same factor. Design techniques for a log-periodic are presented in the literature by Campbell, and Pantoja.

Two designs have been fabricated for LPDA's to be used as applicator/antennas. These are realized in a material from Glasteel Industrial Laminates (GIL) with a dielectric constant of $\varepsilon_r = 3.05$. Figure B3 presents the design for the high band applicator, operating in the 1 - 2 GHz range.

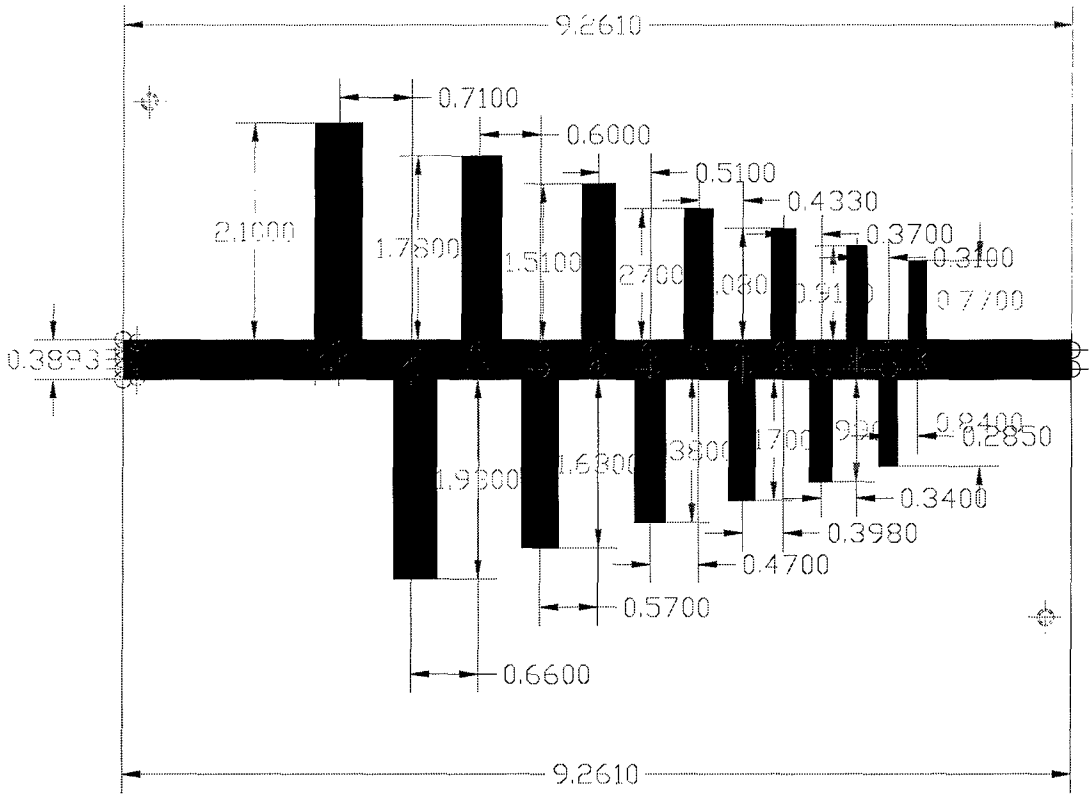

Figure B3. High Band LPDA Design for HDS Applicator (All Dimensions in Inches).

Details of the design are available in the referenced paper. One of the advantages of this design is the fact that it is "flat" having a thickness of 0.120 inches. The unit will be approximately the size of a clipboard, and will be capable of being stored on the underside of the portable unit. Testing of this design has not been accomplished due to the program ending.

There are a number of issues of importance in this implementation of the design, not the least is the impedance conversion inherent in the design. This conversion process is required because the characteristic impedance of the feeding line is a value that is not compatible with the coaxial line that feeds the unit. This will require careful design to reduce the mismatch at this junction. Further work in this area will await funding.

APPENDIX C: RF SAFETY ISSUES

C.1 SAFETY ISSUES FOR MICROWAVE SYSTEMS IN MEDICINE

C.1.1 INTRODUCTION

Safety questions arise whenever microwaves are proposed for use in medicine. This document will review some of the pertinent information regarding human exposure to electromagnetic waves. The data presented is based upon research and approximations to the actual problem. RF or microwave energy interactions with biological systems has only recently (in the past twenty years) been studied in depth. The results of this research have led to several sets of exposure standards, one in the U.S., one in Western Europe, and another in Eastern Europe. U.S. standards are presented in two formats, as a specific absorption rate (SAR), or as a power density (e.g. watts per unit area). European standards are usually presented as power density, electric field strength (V/m), or magnetic field strength (A/m).

There are two parameters of concern in the exposure area, the quantity of electromagnetic energy and the time of exposure to the energy. Use of the specific absorption rate involves the exposure time, while standards in terms of field strengths do not implicitly include the exposure time, but include the time of exposure explicitly.

C.1.2 U.S. MICROWAVE STANDARDS

Standards that have been promulgated for the United States are set for frequency bands and not for a well defined, fixed exposure time. The use of the specific absorption rate (SAR) as a measure for human exposure is based upon research conducted using laboratory animals. Results of this research have indicated that "behavioral incapacitance" occurred for exposure times under ***one hour*** and for a ***power per unit mass of nearly 0.4 W/kg***. Based upon these results ANSI adopted this as the standard for humans as well as animals. The symptoms of the so-called behavioral incapacitance are not well defined and appear to be somewhat subjective. The ANSI standard is also stated in other terms as: exposure to electromagnetic radiation in the frequency range 10 MHz to 100 GHz shall not exceed 10 mW per square cm averaged over 0.1 hr.

The frequency dependence of electromagnetic interactions with the body becomes apparent when one thinks of the body as an antenna. The maximum response occurs at those frequencies corresponding to electrical lengths of approximately $\lambda/2$. Thus the maximum absorption frequency for an adult will differ somewhat from that for an infant.

The absorption frequency for an adult based upon the maximum dimension of the scatterer parallel to the electric field vector will be 30 MHz , while that for an infant is 300 MHz. The geometry of the interaction is also important, since the effect of a person standing on a ground plane will differ from that for a person not on a ground plane. A SAR level of 0.4 W/kg is the standard set for frequencies in the resonance region, therefore, since different individuals will have their resonant frequencies at different values each will absorb different amounts of EM energy. Also, different body parts, such as the head will have different resonant frequency

associated with the adult head is 400 MHz while that associated with the infant head is 700 MHz. The incident field in all cases is assumed to be a plane wave.

The use of SAR as a standard can be misleading, since we are not dealing with a homogenous structure, regions of high field strength can be set up within the body, as was illustrated by Shapiro et. al. for the human head, and by others for different regions in the body. Such regions can have significantly higher local fields than that incident on the body. Thus what appears to be a safe level, is in reality not safe at all.

The skin effect leads to a similar result, i.e. the maximum EM energy is absorbed in the epidermal layer creating an effect that gives rise to the sensation of warmth reported in the literature. The skin effect is frequency dependent, with the penetration depth or "skin depth" decreasing as frequency increases. This implies that at higher frequencies such as employed in military radars most of the energy incident on the skin is absorbed there. Thus if thermal effects on the internal organs is the concern, then at high frequency the problem is reduced significantly. This is the reason for the higher permissible exposure limits in the high frequency regions.

The uncertainty of the location of the "hot spots" created within the body is the primary reason hyperthermia researchers perform sophisticated analytical studies and perform experimental studies on animals, prior to exposure of human subjects to therapeutic levels of microwave energy.

The use of power as the standard implies the existence of an exposure time. The U.S. standard is based on an averaged time of exposure of one tenth of an hour. Others use different times and confusion has been the result, with no commonly accepted time by the community. Still the time factor must enter since the body is acting as an absorber of EM energy. The times are also based upon the assumption that the whole body is being exposed to the EM field, not a particular body part or region.

The U.S. government, in 1968, established by PL 90-602, a microwave oven RF emissions standard. This standard limited RF emissions from microwave ovens to 10 mW / cm^2 at a distance of 5 cm from any point on the surface of the unit. This was revised to a more stringent standard of 1 mW / cm^2 at delivery and 5 mW / cm^2 at the end of the unit's working life at the same distance from the unit as the previous standard.

The U.S. military has an interest in the safety question as well and has set up organizations to set exposure standards for the services. The USAF School of Aerospace Medicine periodically publishes an RF Dosimetry Handbook with various SAR values presented and the standards explained in detail. The U.S. Army has supported studies at Walter Reed Medical Center on the biological effects of electromagnetic radiation in recent years also. Information on any programs sponsored by the U.S. Navy in this area is not readily available, although one would expect that such studies have been conducted considering that the flight deck of an aircraft carrier represents one of the most hostile electromagnetic environments for both biological system and electronic systems, exposing these systems to almost the entire EM spectrum at relatively close ranges.

The standardization effort is continuing, with NIOSH, EPA and USDHHS seeking a new legal exposure standard based upon a SAR level defined for each frequency band. These standards are based on the mass of the subject and exposure of the entire body to the EM radiation. This type of standard may be inappropriate for application to a microwave hemorrhage detection system.

Summarizing, the U.S. standards are considered by most to be adequate in all respects, but others, notably the Eastern Europeans feel that the U.S. standard is 10-20 dB to high.

C.1.3 EAST EUROPEAN MICROWAVE STANDARDS

The most rigid standards on microwave exposure are set by the Polish and former Soviet Union, now Russian governments, and have been adopted by the old COMECON countries. The concern of these governments is based upon research in these countries that indicates effects upon behavior when humans are exposed to certain levels of microwave radiation, or to high electric or magnetic fields. They have also identified certain modulations that appear to contribute to the reported anomalous behavior patterns. We present the standards in the following paragraphs.

The Polish microwave exposure standard can be presented in tabular form shown in Table 1. A power density of 0.1 mW / m^2 W/m and 1.0 mW / m^2 W/sq m are equivalent to 0.01 mW / cm^2 and 0.1 mW / cm^2 respectively. These levels are 20 dB and 10 dB below the U.S. levels respectively, in the frequency region where the standards can be directly compared. Soviet standards for exposure of personnel to microwave radar signals are presented in tabular format as shown in Table 2.

The maximum and minimum power densities have to do with rotating and stationary radar sources respectively. These standards are set for specific frequencies rather than power level since the general population is not likely to have a high probability of exposure to the radiation from such systems. Exposure to radar emissions from lower power units such as those found small water-craft and general aviation aircraft. These standards are included for completeness.

Table C.1 Polish Microwave Exposure Standards.

Frequency Range (MHz)	**Power Density (W / m^2) or Electronic Field (V/m)**
ELF	10 kV/m
0.1-10 MHz	20 V/m
10-300 MHz	7 V/m
300 MHz-300 GHz	0.1 W / m^2 (Stationary Source) 1 W / m^2 (Rotating Source)

Table C.2 Former Soviet Union Microwave Radar Exposure Standards.

Radar Type	Frequency Range (GHz)	Maximum/Minimum Power Density (W / m^2)
Meteorological	37.5	140/10
Meteorological/Similar Units	60	10
	3	20
	1.76	24/12
Aviation Radars	3	15
	1.3	20
	0.86	25

C.1.4 West European Standards

The Western Europeans also have addressed the issue although the standards are set by individual nations. We briefly present the standards for those countries that have them.

Finland

The basic Finnish standards are shown in the Table D.3. The values are time averaged over any six minute period during the day. Table D.4 shows the maximum permissible field strength values and Table 5 shows the limits for workers located within 10 cm of a ground plane.

Table C.3. Finnish Microwave Exposure Standards.

Frequency (MHz)	Electric Field (V/m)	Magnetic Field (A/m)
3-30	140	0.4
30-300	60	0.16
0.3-300 GHz	60	-

Table C.4. Finnish Microwave Exposure Standards (Maximum).

Frequency (MHz)	Electric Field (V/m)	Magnetic Field (A/m)
3-300	300	0.8
0.3-300 GHz	300	-

Table C.5. Finnish Microwave Exposure Standards (Workers 10 cm from a Ground Plane).

Frequency (MHz)	Electric Field (V/m)	Magnetic Field (A/m)
3-30	47	0.13
30-60	20	0.05
3-60 GHz	100 (Max)	0.27 (Max)

United Kingdom

The UK has two standards, based upon the exposure time for the subject, the first, presented in Table C.6 is for exposures not exceeding two hours per day. The second shown in Table C.7 governs exposures not to exceed five hours per day. This differs from the European exposure times. The values are to be determined using the formula in the table, the value used for "f" is the frequency in MHz.

Table C.6. UK Microwave Exposure Standards (not to exceed 2 hours per day).

Frequency (MHz)	Power Density (W / m^2)	Electric Field (V/m)	Magnetic Field (A/m)
30-100	10	60	0.16
100-500	f/10	$6.0\sqrt{f}$	$0.016\sqrt{f}$
0.5-300 GHz	50	135	0.36

Table C.7. UK Microwave Exposure Standards (not to exceed five hours per day).

Frequency (MHz)	Power Density (W / m^2)	Electric Field (V/m)	Magnetic Field (A/m)
30-300	4	38	0.1
300-1.5	$f / 75$	$2.2\sqrt{f}$	$0.006\sqrt{f}$
1.5-300 GHz	20	85	0.23

Another country having its own set of standards is Canada. Canadian standards are presented with the Western European countries. Table C.8 illustrates Canadian occupational standards. When the values are to be determined using a formula, use the value of the frequency in MHz.

Table C.8. Canadian Microwave Exposure Standards (averaged over six minutes).

Frequency (MHz)	Electric Field (V/m)	Magnetic Field (A/m)	Power Density (W / m^2)
30-100	60	0.16	-
100-300	60	0.16	10
300-1500	$3.45\sqrt{f}$	$0.0093\sqrt{f}$	-
1500-300,000	140	0.36	50

The previous tables demonstrate that there is no universal standard for microwave exposure. A choice of standard based upon location of the experiment seems logical, hence we will adopt and use the U.S. standard of 10 mW / m^2 averaged over 0.1 hour for the purposes of RF/HDS experimental work.

C.1.5 Estimated Power Density for RF/HDS Experimental Equipment

S*R experimental equipment is shown in Figure C.1 below.

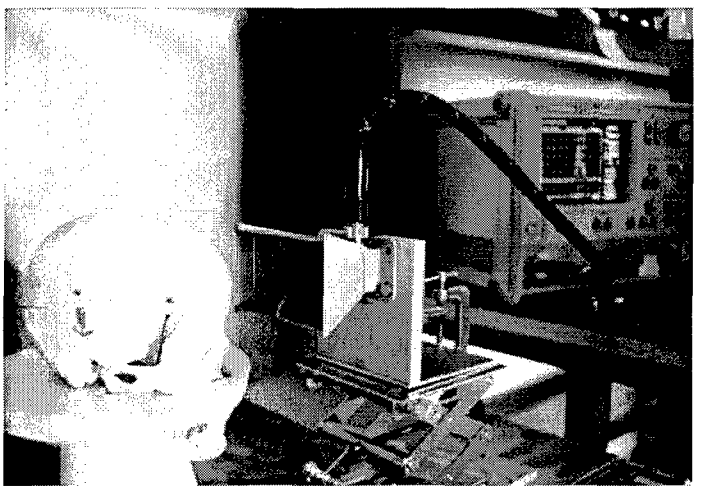

Figure C.1. S*R Experimental Equipment

The photograph shows a human skull used in a previous set of measurements supported on a styrofoam pedestal. The antenna is an AEL Industries H-1798 wide band ridged horn. The antenna is fed by a Gore coaxial cable that is "matched" to the network analyzer, a Wiltron 37267B, vector network analyzer (VNA). The unit operates over the frequency range, 40 MHz to 20 GHz. The Wiltron VNA output power was measured using an HP-435B Power Meter. The output power is approximately 0 dBm (1 mW). Data for the unit is presented in Table 9 versus frequency. The last column is the effective radiated power (ERP) given by the product of the output power and the antenna gain (the sum of these quantities in dB). Thus the ERP is approximately 10 mW. The fact that we are operating at a distance of 10 cm from the target reduces the ERP. The result is shown in the graph following Table 9.

Table C.9. System Operating Parameters

Frequency (GHz)	Output Power (dBm)	Gain (dB)	ERP (dBm)
2	-0.4	7.8	7.4
3	-0.5	8.0	7.5
4	-0.5	10.0	9.5
5	-0.6	10.7	10.1
6	-0.9	9.1	8.2
7	-0.7	11.0	10.3
8	-0.8	11.0	10.2

The simplest way in which to express the predicted data is graphically. Power density is given by the expression:

$$P_D = \frac{P_T G_T}{4\pi R^2},$$

The product $P_T G_T$ is the ERP listed in the table above, and R, is the range to the target (10 cm in this case).

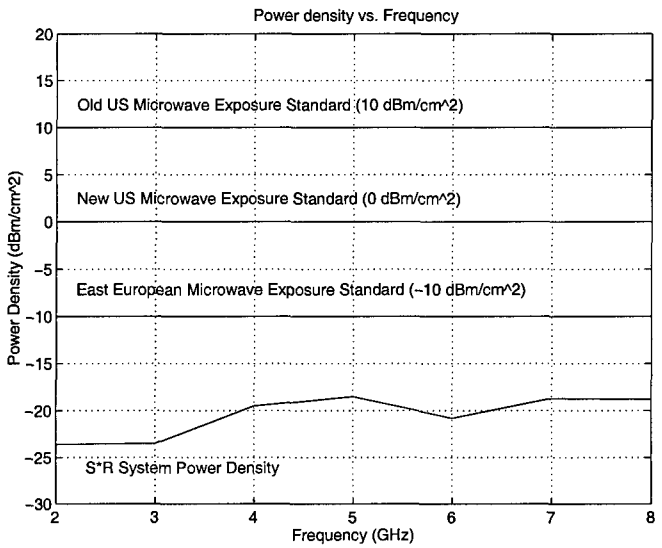

Figure C.2 Power Density vs. Frequency for S*R Experimental Set-up.

C.2 TISSUE HEATING

We have mentioned the US safety standard and didn't go very far beyond that. The standard is rather loosely defined and has been the source of consternation for many, especially in the light of recent litigation concerning development of brain cancers allegedly caused by prolonged use of cellular telephones. The cell phone operates in the 800 MHz region of the EM spectrum. This is well below the proposed operating frequencies for the HDS, and the key word in the sentence regarding cancer is, ***prolonged***. S*R proposes that an HDS measurement involve a patient exposure to EM energy of 90 seconds or less.

Testimony in the case above indicated that the victim had used a cell phone for periods of time in excess of one hour. Cellular telephones have output powers measured in watts, 1000 times the minimum power the proposed HDS is expected to require and approximately 400 times more exposure time than we expect to require. Thus we should not compare these two types of systems since they are dissimilar in most respects. The exposure time stated in the US safety standard is five minutes. This is approximately three times the exposure expected an HDS measurement.

Obviously time is a critical parameter in this discussion. Recall that power is dimensionally equivalent to energy per unit time. The watt is 1 joule per second, so to determine the amount of energy deposited in a region we must multiply the power by the number of seconds the person is exposed. The US standard is a power density (w/sq m) so to obtain the energy, multiply the standard value by time in seconds and by the area over which the power is distributed.

If we use the US safety level, and assume a circular applicator of diameter 0.75 in (1.905 cm) and an exposure time of 0.005 s we obtain an energy of 0.0023 J. We assume this energy to be 100% converted into heat and consequently this heat energy will cause an increase in the ambient temperature of the brain. The increase in temperature can be determined from the usual relation between heat and temperature change,

$$\Delta T = Q / mc \text{, where}$$

Q is the heat energy in calories, m is the brain mass in grams, and c is the specific heat of the material.

If we use nominal values of 1 kg for the mass and 1.0 (water) for the specific heat respectively, we can see that the temperature increase will be quite small ($\approx 0.0023\,^{\circ}C$). This analysis does not include the dissipation due to the blood flow in the brain, which would also help to further reduce the increase in temperature. Thus, it is evident that concern over possible brain tissue heating is unfounded for the HDS system.

C.3 RECENT RADIOFREQUENCY INTERFERENCE (RFI) STANDARDS

A new set of RFI standards was described in a recent issue of the IEEE Engineering in Medicine Magazine. These are not set up for human exposure, but for potential effects on various medical instruments in use in the clinical environment. The more important problem may be from potential interference between HDS and other medical devices.

The following is quoted from this issue. "*The prevailing standard for the RTF immunity of medical devices is the 1993 revision of the International Electrotechnical Commission (IEC) Standard IEC60601-1-2. This standard sets a minimum immunity level of 3 V/m in the 26-1000 MHz frequency range. For non-life supporting devices, testing is required only at the specific frequencies of 27.12, 40.68, and 915 MHz.*" Since the HDS operating frequency band is proposed to be 0.5 - 2.0 GHz, validation of the non-interference of the unit with other equipment at 0.915 GHz must be accomplished.